THE ROLE OF THE OCEAN IN THE ATMOSPHERIC BUDGETS OF

METHYL BROMIDE, METHYL CHLORIDE AND METHANE

A Dissertation

by

LEI HU

Submitted to the Office of Graduate Studies of
Texas A&M University
in partial fulfillment of the requirements for the degree of

DOCTOR OF PHILOSOPHY

August 2012

Major Subject: Oceanography

The Role of the Ocean in the Atmospheric Budgets of Methyl Bromide, Methyl Chloride

and Methane

THE ROLE OF THE OCEAN IN THE ATMOSPHERIC BUDGETS OF

METHYL BROMIDE, METHYL CHLORIDE AND METHANE

A Dissertation

by

LEI HU

Submitted to the Office of Graduate Studies of
Texas A&M University
in partial fulfillment of the requirements for the degree of

DOCTOR OF PHILOSOPHY

Approved by:

Chair of Committee,	Shari A. Yvon-Lewis
Committee Members,	John D. Kessler
	Robert Rhew
	Gunnar W. Schade
Head of Department,	Piers Chapman

August 2012

Major Subject: Oceanography

ABSTRACT

The Role of the Ocean in the Atmospheric Budgets of Methyl Bromide, Methyl

Chloride and Methane. (August 2012)

Lei Hu, B. S., Ocean University of China

Chair of Advisory Committee: Dr. Shari A. Yvon-Lewis

The ocean is both a source and a sink for atmospheric methyl bromide (CH_3Br) and methyl chloride (CH_3Cl). It plays a significant role in their global biogeochemical cycling. In response to the Montreal Protocol, the atmospheric CH_3Br is declining and the saturation state of CH_3Br in the surface ocean is becoming more positive. Results from two large-scale transect studies in the eastern Pacific and the eastern Atlantic suggest that the ocean became near equilibrium with atmospheric CH_3Br in 2010. Results from a "top-down" two-box model indicate that, if the remaining anthropogenic emissions are eliminated, atmospheric CH_3Br is likely to drop to the pre-industrial level and the ocean would become a net source to atmospheric CH_3Br.

This study also represents an effort to improve current understanding of the oceanic and atmospheric budgets of CH_3Cl. The global net sea-to-air flux of CH_3Cl was estimated at 335 (210 – 480) Gg yr^{-1} with improved parameterizations on the solubility, seasonal saturation anomaly – (sea surface temperature, wind speed) relationships and the use of an updated parameterization on gas transfer velocity. For the first time, we estimated the gross oceanic emission and gross oceanic uptake rates of CH_3Cl in the

surface ocean, which was 700 (490 to 920) Gg yr^{-1} and -370 (-440 to -280) Gg yr^{-1}, respectively. The ocean accounts for 10 - 19 % in the global CH_3Cl emission and 6 - 9 % in its global sinks.

Methane (CH_4) is a potent greenhouse gas, which has a warming potential 72 times that of carbon dioxide over a 20 year time horizon. Gas hydrates are the largest CH_4 reservoir in the planet. How much CH_4 is transported from marine gas hydrates to the atmosphere is under debate. In this study, we investigated CH_4 fluxes over three deepwater hydrocarbon seeps in the northern Gulf of Mexico using continuous air-sea flux measurements. Extrapolating the highest daily flux from this study to other deepwater seeps in the northern Gulf of Mexico suggests that CH_4 fluxes to the atmosphere from the deepwater hydrocarbon seeps in this region are an insignificant source to atmospheric CH_4 budget.

ACKNOWLEDGEMENTS

I would like to thank all the people who have helped and inspired me during this study. I would like to thank my advisor, Dr. Shari A. Yvon-Lewis, for giving me the opportunity to pursue my Ph.D. at Texas A&M University. I learned greatly from Shari about instrumentation, modeling and scientific writing. I remembered how scared I was when she asked me to cut the injector of a new GC for the first time. But when I saw how the change we made to turn a manual injection into an automated injection, I realized how amazing it was. For my research, Shari left me a lot of freedom to decide the direction I like. She always paid attention to have me do and think things independently, which fostered my ability to conduct scientific research independently. She is not just a great mentor but also a great friend. During the several trips with her on a ship, we watched movies together, had fun at the Equator, and ate chocolates together. She showed me how to calm down under stressed environment. I feel so lucky to work with her.

I would like to thank my committee members, Drs. John D. Kessler, Robert Rhew and Gunnar W. Schade. I went to two cruises with John and coauthored several papers with him. He gave me a lot of help and inspiration for methane study. He also inspired me a lot about his passion to science. He recommended me very strongly when I was applying the postdoc fellowships. When I was facing the difficulty to choose, he gave a lot of inspiring advice. I always considered John as my second mentor. Rob gave me lots of help on the study of methyl bromide and methyl chloride. I feel very lucky to

have him in my committee. He also helped me on the writing of a research proposal during a fellowship application and wrote me a nice host letter. I felt very grateful for his help. I took atmospheric chemistry class with Gunnar. During this class, I learned a lot and became very interested in atmospheric chemistry. Very luckily, I got the opportunity to do more work on atmospheric chemistry and modeling for my postdoc. In addition, Gunnar gave me tremendous help for my postdoc fellowship applications.

I also would like to thank all the coauthors in my papers which were eventually part of my dissertation, Ms. Yina Liu, Dr. Thomas S. Bianchi, Dr. James H. Butler, Dr. Stephen A. Montzka, Dr. Joseph E. Salisbury, Dr. Ian R. MacDonald, Dr. Jürgen M. Lobert, Dr. Daniel B. King, and Ms. Julia O'Hern. Without their contribution, I couldn't complete this study. In addition, Steve, Jim and Tom provided me lots of help and advice on my career as well. I would like to thank Yina, not just for her being a coauthor in my paper, but also for a lot of things, i.e., watching out my instrument, helping me inject samples and troubleshooting with me when the instruments had problems etc. These things seem small on a daily basis, but they are a lot in terms of these five years.

I would like to extend my gratitude to Drs. John Pohlman, Carolyn Ruppel, David Valentine, and Daniel Thornton for their help on my research, graduate study and career. Last but not the least; I would like to thank my family, lab mates, and friends for their support, especially my husband, Yu, for his unwavering love, support, encouragement and devotion.

TABLE OF CONTENTS

LIST OF FIGURES

FIGURE   Page

LIST OF TABLES

1. INTRODUCTION

1.1. Background

Global warming and stratospheric ozone depletion are two priority environmental problems, which are mainly caused by increased greenhouse and ozone depleting gases from human activities. Since the 1900s, the global surface air temperature (SAT) has increased by about 0.8 ^{o}C [*Le Treut et al.*, 2007]. Multi-model results suggest that, for non-mitigation scenarios, the global mean SAT is likely to be further increased by 1.8 − 3.4 ^{o}C by the end of the 21st century [*Meehl et al.*, 2007]. Methane (CH_4), a potent greenhouse gas, has the second largest radiative forcing after carbon dioxide in the Long-Lived Green-House Gases (LLGHG) [*Ramaswamy et al.*, 2001]. The atmospheric abundance of CH_4 has increased by about a factor of 2.5 since the pre-industrial era [*Ehhalt et al.*, 2001]. CH_4 is also involved in both tropospheric and stratospheric chemistry. Due to its important role in global radiative forcing and atmospheric chemistry, quantifying the sources and sinks of CH_4 has been a major research focus over the past several decades. However, substantial uncertainties remain.

Stratospheric ozone depletion has been observed since the late 1970s. Halogenated compounds are transported to the stratosphere and destroy ozone catalytically. In response to the Montreal Protocol and its amendments, most long-lived

---

This dissertation follows the style of *Journal of Geophysical Research.*

halogenated compounds that originate from anthropogenic sources are declining in the atmosphere [*World Meteorological Organization (WMO)*, 2011], resulting in an increasing in the relative importance of natural halocarbons in stratospheric ozone depletion.

Methyl bromide (CH_3Br) and methyl chloride (CH_3Cl) are the most abundant brominated and chlorinated gases in the troposphere. They contributed about 34% of the total bromine and 17% of the total chlorine to the stratosphere in 2008 [*WMO*, 2011]. CH_3Br and CH_3Cl originate in large part from natural sources such as the ocean, biomass burning, tropical rainforests, salt marshes, wetlands and fungus. Despite tremendous efforts made in the past several decades to quantify the sources and sinks of CH_3Br and CH_3Cl, knowledge of their atmospheric budgets is limited. An imbalance between their total known sources and their total known sinks calls for further studies on their "missing sources".

1.2. Statement of problems

1.2.1. Methyl bromide

The total known sinks of atmospheric CH_3Br exceed the total known sources by ~35 Gg yr^{-1} in its pre-industrial, pre-phaseout and phaseout budgets [*Montzka and Reimann et al.*, 2011; *Saltzman et al.*, 2004; *Yvon-Lewis et al.*, 2009]. Measurements in the firn air and ice core air bubbles from the Antarctic suggested that the atmospheric increase in the Southern Hemisphere during the 20th century could not be explained by the increase in anthropogenic emissions alone [*Reeves* 2003; *Saltzman et al.*, 2004], suggesting emission rate of CH_3Br from fumigation – agriculture uses might be

underestimated or there was an increase in natural emissions or a decrease in the atmospheric sinks during this period. Global atmospheric observations from NOAA/ESRL Global Monitoring Division indicate that the decline in the atmospheric CH_3Br mixing ratio from the mid-1990s to the mid-2000s was larger than what was expected [*Montzka et al.*, 2003], which also implies that there might be an underestimate of the anthropogenic emission, or an overestimate of the overall sinks. *Yvon-Lewis et al.* [2009] suggested that the enhanced decline of CH_3Br from the end of 1990s to the beginning of the 2000s could be explained by elevated CH_3Br mixing ratios in the atmosphere at 1998 due to decreased hydroxyl radical (OH) concentrations or enhanced biomass burning emissions. They also suggested that the anthropogenic emissions were slightly underestimated, and the emission fraction from the fumigation - non-Quarantine and Pre-Shipment (non-QPS) uses should be increased from 50% to 60%. However, the increase in the anthropogenic emission cannot completely close the gap between the total emissions and total uptake rates in the CH_3Br budget.

The ocean, the largest source and the second largest sink of atmospheric CH_3Br, plays a significant role in the global CH_3Br cycling. In the early 1980s, the surface ocean was mis-interpreted to be highly supersaturated with respect to atmospheric CH_3Br [*Singh et al.*, 1983]. Improvements in the analytical technique and extended open ocean measurements allowed *Lobert et al.* [1995] to more accurately assess the CH_3Br saturation anomaly in surface ocean. Their results suggested that the surface ocean was undersaturated with respect to atmospheric CH_3Br and established a global net sea-to-air flux of -13 Gg yr^{-1}. Observations in the surface ocean over the following several years

provided a more comprehensive picture of surface seawater CH_3Br distribution in the global ocean [*Groszko and Moore*, 1998; *King et al.*, 2000, 2002; *Lobert et al.*, 1995, 1996; *Yvon-Lewis*, 2002, 2004]. Due to the implementation of the Montreal Protocol and its amendments, atmospheric CH_3Br is declining, which should lead to open-ocean surface seawater CH_3Br becoming less undersaturated than that before the phaseout [*Yvon-Lewis et al.*, 2009]. Results from ice core air bubble measurements [*Saltzman et al.*, 2004] suggest that the ocean was a net small source to the atmospheric CH_3Br in the pre-industrial era, which raises the question of whether or not it is possible that the ocean would become a net small source again if all the anthropogenic sources were eliminated.

In contrast to the open ocean, the coastal ocean was observed to be highly supersaturated [*Groszko and Moore*, 1998; *King et al.*, 2000; *Lobert et al.*, 1995; *Sturrock et al.*, 2003]. Since the coastal ocean is highly influenced by human activities, river runoff and coastal terrestrial ecosystems, CH_3Br emission rates could vary significantly among different coastal regions. It is necessary to make more coastal measurements in order to better characterize CH_3Br emissions and uptake rates in the coastal ocean.

1.2.2. Methyl chloride

CH_3Br and CH_3Cl have similar chemical properties. It was reported that these two gases share a number of common sources, i.e., the ocean [*Hu et al.*, 2010; *Moore et al.*, 1996; *Yvon-Lewis et al.*, 2009], biomass burning [*Lobert et al.*, 1999; *Yvon-Lewis et al.*, 2009], fungus [*Lee-Taylor and Holland*, 2000; *Mead et al.*, 2008; *Watling and Harper*, 1998], salt marshes [*Rhew et al.*, 2000], wetlands [*Dimmer et al.*, 2001; *Varner*

et al., 1999], rice paddies [*Lee-Taylor and Redeker*, 2005], mangroves [*Manley et al.*, 2007] and tropical rainforest [*Blei et al.*, 2010]. They also share common sinks, i.e. reaction with hydroxyl radicals [*World Meteorological Organization (WMO)*, 2003, 2007, 2011], uptake by the surface ocean [*Moore*, 2000; *Moore et al.*, 1996], photolysis in the stratosphere [*World Meteorological Organization (WMO)*, 2011] and uptake by soils [*Keene et al.*, 1999; *Keppler et al.*, 2005; *Shorter et al.*, 1995]. Since atmospheric CH_3Cl shares many common natural sources and sinks with atmospheric CH_3Br, understanding the variability in atmospheric CH_3Cl may provide insights into the natural emissions of CH_3Br.

The ocean is both a source and a sink to atmospheric CH_3Cl. The global net efflux of CH_3Cl from the warm waters to the atmosphere was estimated at $470 – 508$ Gg yr^{-1} whereas the net influx from the atmosphere to the cold waters was estimated at $90 – 150$ Gg yr^{-1} [*Moore*, 2000; *Yoshida et al.*, 2004]. Although the warm water is a net source to the atmospheric CH_3Cl, it could also be a sink as well because the removal processes including hydrolysis and biological degradation may be ubiquitous in the surface ocean [*Elliott and Rowland*, 1995; *Tokarczyk et al.*, 2003]. For cold waters, there is likely to be production of CH_3Cl from the phytoplankton and thereby emissions from cold water to the atmosphere. To have a complete understanding on the role of the ocean in the atmospheric CH_3Cl budget, it is necessary to provide separate estimations on the gross emission and gross uptake rates for the global surface ocean.

One of the key parameters for determining the oceanic emission and oceanic uptake rates is the solubility coefficient. *Elliott and Rowland* [1993] first determined the

solubilities of CH_3Cl in distilled water and seawater at 0 ^{o}C and 22 ^{o}C. Later, *Moore et al.* [1995] reported solubilities of CH_3Cl at 0 – 6 ^{o}C in seawater. *Moore* [2000] improved the solubility parameterization by measuring the solubilities of CH_3Cl in seawater for a temperature range from 5 – 25 ^{o}C. His results suggest that the solubility expressions from *Elliott and Rowland* [1993] and *Moore et al.* [1995] tend to overestimate the solubilities of CH_3Cl. Although an improvement was made by *Moore* [2000], he did not include the salinity dependence in the solubility function. Applying the solubility expression from *Moore* [2000] in coastal areas could result in underestimation on the net sea-to-air fluxes.

Emissions of CH_3Cl from the coastal ocean to the atmosphere are poorly quantified. Since the coastal ocean is highly influenced by anthropogenic activities and river runoff from terrestrial ecosystems, the CH_3Cl emissions from coastal ocean could be very different from those in the open ocean.

1.2.3. Methane

CH_4 originates from both natural and anthropogenic sources. The total atmospheric sources and sinks of CH_4 were estimated at 580 Gg yr^{-1} [*Denman et al.*, 2007]. Methane clathrate hydrates, a crystalline solid consisting of water and mostly methane gas, are buried in the seafloor of continental margins and the Arctic permafrost. The total abundance of methane reserved in the form of gas hydrates is about 2 X 10^6 Tg in a global inventory [*Boswell and Collett*, 2011]. It is comparable to about 400 times the total mass of atmospheric methane [*Ehhalt et al.*, 2001]. Although the methane clathrate hydrate is an enormous methane reservoir, little is known about methane emissions from

this reservoir to the atmosphere and how the emission rate responds to the climate change.

The ocean is a small source of methane to the atmosphere, contributing about 1 – 15 Tg yr^{-1} of methane to the atmosphere [*Houweling et al.*, 2000; *Rhee et al.*, 2009; *Wuebbles and Hayhoe*, 2002]. The interest in methane from marine environment is not due to the oceanic production of methane, but to understand the processes involving enormous methane additions from marine sediments to the water column and eventually to the atmosphere [*Reeburgh* 2007]. It is not clear how much methane reaches the atmosphere after it is emitted from the deep seafloor.

1.3. Hypotheses

The goal of this study is to improve the current understanding on the role of the ocean in the atmospheric budgets of methyl bromide, methyl chloride and methane. According to problems discussed above, we attempted to achieve our goal through the following aspects: 1) characterizing emissions of methyl halides from coastal ocean to the atmosphere; 2) quantifying the global net sea-to-air flux of methyl bromide after the fumigation – non-Quarantine and Pre-Shipment (non-QPS) phaseout; 3) including the salinity dependence into the solubility expression of methyl chloride and estimating its global oceanic emission and oceanic uptake rates; 4) finding out the origin of the "missing sources" of methyl halides and estimating the contribution of the ocean to their atmospheric budgets; and 5) improving our knowledge about deepwater gas hydrates as a source to the atmospheric methane budget.

Hypothesis I is that emissions of methyl bromide and methyl chloride from the coastal ocean to the atmosphere might be significant and they might contribute to the "missing sources" of atmospheric methyl bromide and methyl chloride. Emission rates or uptake rates of methyl bromide and methyl chloride in coastal ocean are different from those in the open ocean [*Lobert et al., 1995*; *Moore et al.*, 1996; *Tokarczyk et al.*, 2001, 2003a, 2003b]. When estimating the global oceanic emission and uptake rates [*King et al.*, 2002; *Yvon-Lewis et al.*, 2009], the coastal-ocean area was not separated from the open-ocean area. Since methyl bromide is supersaturated in the coastal ocean [*Lobert et al., 1995*; *Moore et al.*, 1996; *Sturrock et al.*, 2003] whereas it is undersaturated in the open-ocean area, emission rates of methyl bromide in the coastal ocean could be higher than those in the open ocean. For methyl chloride, concentrations in the coastal ocean may be influenced by coastal salt marshes, which are a significant source for atmospheric methyl chloride [*Rhew et al.*, 2000]. Thus, emissions of methyl chloride in coastal ocean may be higher than those in open ocean. However, the total global emissions of methyl bromide and methyl chloride from coastal area are not well quantified. It is possible that the coastal ocean may contribute to their "missing sources".

Hypothesis II is that saturation anomalies of methyl bromide are likely to become more positive at the end of the fumigation - non-QPS phaseout. In response of the fumigation - non-QPS phaseout, the atmospheric mixing ratio of CH_3Br has been declining. This should lead to an increase in the saturation state of CH_3Br in the surface ocean, assuming annual surface oceanic production rates, and biological, chemical and eddy degradation rate constants remain the same as they were before the phaseout

[*Butler*, 1994; *Yvon-Lewis et al.*, 2009]. Since chemical and eddy degradation rate constants are a function of salinity, sea surface temperature (SST), thermocline temperature and mixed layer depth, it is easy to assume that they have not changed significantly since 1994. Annual production rates and biological degradation rate constants are unlikely to have changed since 1994, but this is less certain.

Hypothesis III is that both warm waters and cold waters play dual roles in the atmospheric budget of CH_3Cl. CH_3Cl is consumed in aquatic environment via hydrolysis [*Elliott and Rowland*, 1995] and bacteria degradation [*Tokarczyk et al.*, 2003a, 2003b]. It is also produced by phytoplankton [*Sœmundsdóttir and Matrai*, 1998; *Scarratt and Moore*, 1996, 1998]. Since production and consumption of CH_3Cl are ubiquitous in the ocean, warm waters and cold waters should be both a source and a sink for atmospheric CH_3Cl. However, there is no estimate about the gross emission and gross uptake rates of CH_3Cl from warm and cold waters.

Hypothesis IV is that the "missing sources" of CH_3Br and CH_3Cl are likely to be located in tropical terrestrial ecosystems. *Warwick et al.* [2006] evaluated the possible origins for the "missing sources" of CH_3Br using a global three-dimensional chemical transport model. Based on their results, it suggests that the "missing sources" of CH_3Br are likely either from tropical vegetation source or a double-strength biomass burning source. *Blei et al.* [2010] estimated a global net flux of CH_3Br from tropical rainforests using their field measurements, which is about 20 Gg yr^{-1}. Adding this source to the atmospheric budget of CH_3Br will reduce the gap between its total sources and sinks. However, it cannot fully explain the imbalance in the CH_3Br budget. It is possible that

the gross emissions of CH_3Br from tropical rainforests are higher than the range they reported since the gross emission is equal to the sum of the net flux and the gross consumption rate. For CH_3Cl, the gap between its total annual emission and its annual uptake rate was suggested to be closed by emissions from tropical plants and tropical leaf litter [*Clerbaux and Cunnold et al.*, 2007; *Xiao et al.*, 2007; *Yoshida et al.*, 2004]. However, an imbalance in the atmospheric budget of CH_3Cl was raised again due to a suggested higher soil uptake rate [*Keppler et al.*, 2005]. It is possible that gross emissions of CH_3Cl from terrestrial ecosystems are much higher than the prior estimates because of a higher uptake rate. Due to limited gross emission measurements from terrestrial ecosystems, there is no estimate on the total gross emission from terrestrial ecosystems currently.

Fluxes of methane from deepwater hydrocarbon seeps are highly uncertain. They ranged from -6.6 to 10,500 μmol m^{-2} d^{-1} (e.g., *Bange et al.,* 1994; *Bange et al.,* 1996; *Reeburgh et al.,* 2006; *Schmale et al.,* 2005; *Solomon et al.,* 2009). Fluxes reported in deepwater hydrocarbon plume area in the northern Gulf of Mexico [*Solomon et al.,* 2009] were about three orders of magnitude higher than those reported from the previous studies from the Black sea [e.g., *Reeburgh et al.,* 2006; *Schmale et al.,* 2005]. Since *Solomon et al.* [2009] used a submersible to collect water-column samples adjacent to bubble plumes, this technique might be more capable to capture the hydrocarbon plumes compared to the traditional method - shipboard hydrocasts. Our hypothesis V is that using the traditional sampling technique (shipboard hydrocasts) may result in an underestimated methane fluxes from deepwater hydrocarbons seeps.

Sections 2 – 6 present our efforts to address those hypotheses and section 7 summarizes the main findings of this dissertation.

2. COASTAL EMISSIONS OF METHYL BROMIDE AND METHYL CHLORIDE ALONG THE EASTERN GULF OF MEXICO AND THE EAST COAST OF THE UNITED STATES*

2.1. Introduction

CH$_3$Br and CH$_3$Cl are the most abundant brominated and chlorinated gases in the troposphere [*Khalil et al.*, 1999; *Schauffler et al.*, 1993; *Schauffler et al.*, 1999]. The global averaged mixing ratio of CH$_3$Br is 7.9 ppt (parts per trillion) [*World Meteorological Organization (WMO)*, 2007], representing > 50 % of total organic bromine in the troposphere [*Schauffler et al.*, 1999], and the global averaged mixing ratio of CH$_3$Cl in the troposphere is ~ 540 ppt, accounting for over 15 % of organic chlorine in the total tropospheric burden [*Butler*, 2000]. Both trace gases originate in large part from natural sources, and are transported to the stratosphere, releasing bromine and chlorine, which then destroy ozone catalytically. In the past twenty years, a lot of work has been done to quantify their sources and sinks. However, large uncertainties in their budgets remain.

The ocean, as one of the major sources and one of the major sinks [*Butler and*

Rodriguez, 1996; *Yvon-Lewis and Butler*, 1997] for CH_3Br, plays a significant role in its atmospheric budget. While the open ocean is a net sink for CH_3Br with a net flux of -18 (±4) Gg yr^{-1} [*Groszko and Moore*, 1998; *King et al.*, 2002; *King et al.*, 2000; *Lobert et al.*, 1995; *Lobert et al.*, 1996; *Moore et al.*, 1996; *Yvon-Lewis et al.*, 2004], the coastal ocean exhibited significant supersaturations during previous studies [*Groszko and Moore*, 1998; *King et al.*, 2000; *Lobert et al.*, 1995; *Low et al.*, 2003; *Sturrock et al.*, 2003]. However, there were only a few samples collected in the coastal ocean during the previous investigations, resulting in a limitation of the data to represent the global coastal-ocean area.

Until 1996 the largest source of CH_3Cl to the atmosphere was thought to be the oceans [*World Meteorological Organization (WMO)*, 2003]. However, most field studies and modeling work in recent years indicate that terrestrial plants in tropical regions are probably the largest source of CH_3Cl and that the ocean source was overestimated [*Li et al.*, 2001; *World Meteorological Organization (WMO)*, 2007; *Yoshida et al.*, 2004] . The global net flux from the ocean to the atmosphere was estimated to be in the range of 320 to 400 Gg yr^{-1} by *Moore* [2000]. Recalculation on the CH_3Cl net sea-to-air flux was reported to be 350 Gg yr^{-1} by *Yoshida et al.* [2004], using the empirical relationship between saturation anomaly and sea surface temperature and the Comprehensive Ocean-Atmosphere Data Set (COADS) $2^{o} \times 2^{o}$ grid of physical properties. The net sea-to-air flux of CH_3Cl is higher in the tropics than in the mid-latitudes, and the ocean is a net sink in the cold waters beyond the latitude of 50° [*Khalil et al.*, 1999; *Moore*, 2000; *Yvon-Lewis et al.*, 2004]. In recent years, the coastal environment has received

increasing attention. Large sources of CH_3Cl to the atmosphere were observed in coastal salt marshes and tropical coastal lands [*Rhew et al.*, 2000; *Yokouchi et al.*, 2002]. However, the coastal oceanic emission of CH_3Cl has not been investigated.

In this study, CH_3Br and CH_3Cl results are presented from continuous underway measurements in the atmosphere and surface seawater and from depth profile measurements along the eastern coast of Gulf of Mexico and the east coast of the U. S. during the period from July to August, 2007. The measurements are used to calculate the CH_3Br and CH_3Cl production rates in and subsequent emission from the coastal ocean, and to assess the contribution of the coastal region to the global atmospheric CH_3Br and CH_3Cl budgets.

2.2. Methods

Measurements of CH_3Br, CH_3Cl and a suite of other halocarbons were made during the Gulf of Mexico and the East Coast Carbon (GOMECC) Cruise. The ship departed from Galveston, Texas on 10 July 2007, sailing east to Florida and then north along the east coast of U.S., arriving in Boston, Massachusetts on 4 August 2007. The cruise consisted of a series of 9 depth profile transects orthogonal to the coastline and a comprehensive set of underway measurements during the entire cruise (Figure 2.1). However, because of difficulties with the instruments, our measurements began five days after the departure of the ship.

The analytical methods for CH_3Br and CH_3Cl were described in detail by *King et al.* [2000] and *Yvon-Lewis et al.* [2004] (Appendix A). Air samples were pumped
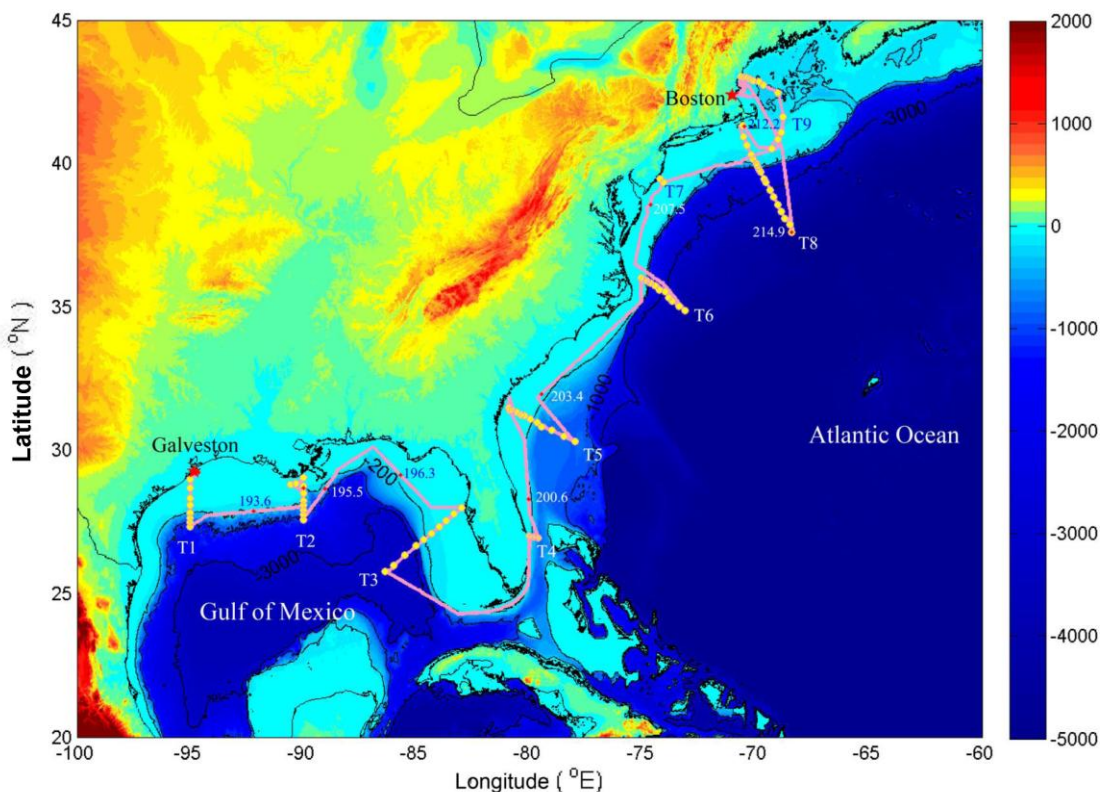
Figure 2.1. Cruise track of GOMECC cruise, 10 July – 4 August, 2007. Colored surface of the map indicates the elevation of the land and the bottom depth of the ocean. Contours with 200m, 1000m and 3000m water depths were labeled in the map. Region within 200m bottom depth was regarded as coastal ocean in our study; all the bathymetric data were downloaded from NOAA National Geophysical Data Center (http://www.ngdc.noaa.gov/mgg/bathymetry/relief.html). Red dots mark Julian days along the cruise track and the numbers beside them are Julian days. Sampling stations on transects (T1-T9), are labeled with yellow dots.

continuously at ~ 6 L min^{-1} through 0.63cm ID Synflex tubing (Motion Industries, TX) mounted on the mast and running from the bow of the ship to the laboratory. Surface seawater was sampled by pumping it continuously through a Weiss-type equilibrator in which the recirculated headspace was periodically sampled. Both air and equilibrated headspace samples were dried through a Nafion dryer, then cryo-trapped, cryo-focused, and injected into a 60 m DB-VRX (J&W) column configured for back-flushing, followed by a mass spectrometer analysis. Air and equilibrator samples were analyzed alternately, ~ 40 min per sample. Calibration gas standards were analyzed after every fourth sample to calibrate the system. Calibration standards were whole air standards calibrated against standards from NOAA/ESRL Global Monitoring Division.

Discrete seawater samples at different depths in each transect were collected from Niskin bottles into ground glass syringes, and then loaded to the volume calibrated glass bulbs. They were measured by a Gas Chromatography and Mass Spectrometry (GC-MS) system similar to the one described above for the saturation anomaly measurements (Appendix D). This instrument has a custom-built purge system that attaches to a Nafion dryer, with the rest of the analysis occurring as described above. The difference between the sequences in the saturation anomaly measurements and those in the depth profile measurements are the blanks which were included after every third sample to monitor the system when measuring the discrete samples.

Continuous underway chlorophyll-a, chromophoric dissolved organic matter (CDOM) and dissolved oxygen (DO) measurements were made in a black 80-liter tank continuously flushed with the ship's scientific seawater, in which the analytical

instruments were submerged. A Wetlabs "Ecopuck" instrument was used to measure stimulated fluorescence of chlorophyll-a (μg L^{-1}; λ_{ex}=470nm, λ_{em} =695nm) and CDOM as calibrated by quinine sulfate (QSU; λ_{ex}=370 nm, λ_{ex} = 460nm). The instrument was factory calibrated prior to the cruise. DO was measured by an Aanderaa Optode sensor. The "Optode" underwent a 4-point calibration prior to deployment using Winkler titrations.

2.3. Results and Discussion

2.3.1. Air mixing ratios and sea surface concentrations

The mean atmospheric mixing ratio of CH_3Br is 10.1 ppt with a range of 5.6 – 37.3 ppt, and the mean CH_3Cl mixing ratio is 517 ppt, with a range of 406 - 1211 ppt (Figures 2.2a and 2.2b). The background mixing ratios in northern hemisphere were 8.3 ppt for CH_3Br and 529 ppt for CH_3Cl during July and August 2007 (*Montzka et al.* [2003] and updates in ftp://ftp.cmdl.noaa.gov/hats/methylhalides). The mean atmospheric CH_3Br from GOMECC is 22% higher than the hemispheric mean, but for CH_3Cl the atmospheric mean from GOMECC is 2% lower than hemispheric mean. This along with the fact that the wind direction was predominately oceanic, suggests that the coastal ocean may be a significant source for CH_3Br but it does not have a great impact on CH_3Cl concentrations in the overlying air.

Surface seawater concentrations reported here are from the measured partial pressures of surface seawater flowing through the equilibrator and corrected for any warming. Concentrations of CH_3Br fell within 0.8 - 5.0 pM, representing saturation anomalies of – 45 % to 236 %. Enhanced concentrations were located at 28°N - 29°N
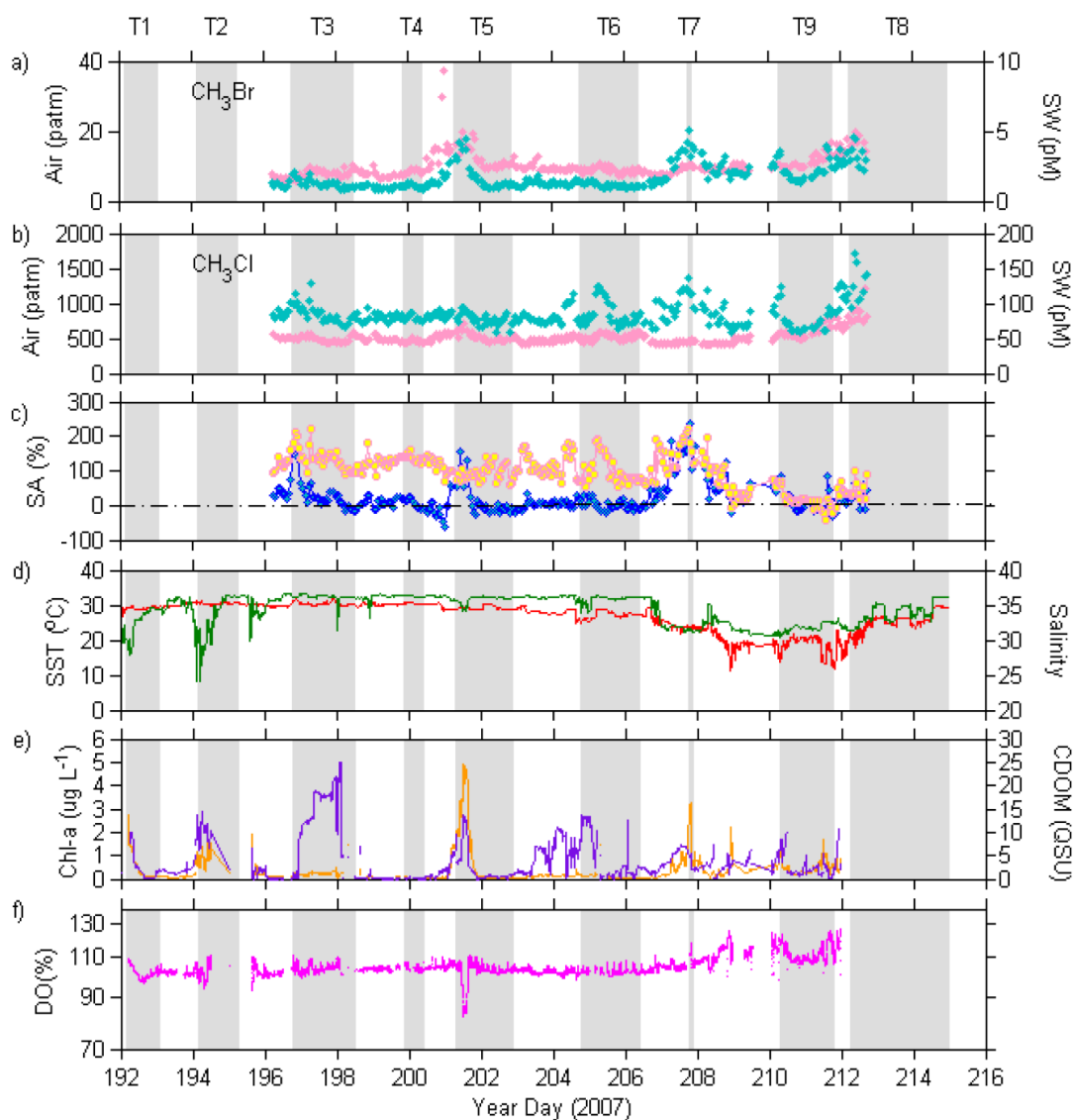
Figure 2.2. Underway measurements of CH₃Br and CH₃Cl in the air (●) and sea surface waters (◆) (a and b); (c) saturation anomalies of CH₃Br (—◆—) and CH₃Cl (—●—); the dash dot line indicates the saturated state; (d) sea surface temperature (SST) (—) and salinity (—); (e) stimulated fluorescence of chlorophyll-a (—) and chromophoric dissolved organic matter (CDOM) (—); and (f) dissolved oxygen (%) in logarithmic scale for y-axis; dark shadows indicate the transects.

along the west coast of Florida, 31° N - 32° N along the Georgia coast, and along the coast of New Jersey, Massachusetts and Rhode Island (Figures 2.1 and 2.2a). *King et al.* [2000] observed that the averaged saturation anomaly of CH_3Br in the southern Gulf of Mexico and Caribbean Sea was – 31 %, suggesting a net sink in these waters. We also found undersaturation at the end of transect 3, which is close to the location of the *King et al.* [2000] study (Figure 2.2c). In contrast to the sink term in open ocean, the mean saturation anomaly along the eastern coast of the Gulf of Mexico is 31 %. This agrees with the conclusion of the previous study of *Saemundsdottir and Matrai* [1998] that species which are strictly coastal or more abundant in coastal areas appear to be stronger producers of CH_3Br than species that are more abundant in the open ocean.

During GOMECC, most regions with elevated CH_3Br also displayed increased stimulated fluorescence of chlorophyll-a and CDOM (Figure 2.2e). CDOM in coastal waters is primarily terrestrial in origin [*Blough and Del Vecchio*, 2002] and may indicate a source of CH_3Br associated with the transport from wetland or salt marshes. However, not all regions with elevated CDOM displayed elevated dissolved CH_3Br concentrations, making it difficult to correlate CH_3Br with the terrestrial transport. Only the regions where the elevated CDOM coincided with elevated stimulated fluorescence of chlorophyll-a exhibited elevated dissolved CH_3Br concentrations. A linear correlation (R=0.71) between the stimulated fluorescence of chlorophyll-a and sea surface concentrations of CH_3Br exists along the east coast of the U.S., suggesting that CH_3Br in this region comes from *in situ* biological processes. During transect 5, there was a dramatic drop in DO, corresponding with the large spikes in the stimulated fluorescence

of chlorophyll-a and the CH_3Br concentration (Figures 2.2a, 2.2e and 2.2f). This suggests that CH_3Br might be produced and/or released as a phytoplankton bloom ages.

The CH_3Cl concentrations in surface seawater ranged from 61.5 to 179 pM, with a mean of 88.4 pM. Elevated seawater concentrations of CH_3Cl were observed in the regions with elevated CH_3Br, except for the outer banks of North Carolina during year days 204 to 206 (Figures 2.1 and 2.2b). This suggests that CH_3Cl and CH_3Br share some common sources, but they may also have their own specific producers. Differences may also be due, in part, to the different lifetimes for the two gases in seawater. The corresponding lower salinity, lower temperature and elevated CDOM observed outside of outer banks of North Carolina suggest that the CH_3Cl enhancement in this region might be due to the terrestrially influenced freshwater input and sea surface cooling (Figures 2.2b, 2.2d and 2.2e). The saturation anomalies of CH_3Cl fluctuated around 100% until year day 208. Then, as the seawater concentration decreased and the air mixing ratio slightly increased, the saturation anomaly declined.

In terrestrially influenced regions where the stimulated fluorescence of chlorophyll-a is also high, dissolved CH_3Br concentrations are elevated, while CH_3Cl concentrations appear slightly to substantially elevated in all terrestrially influenced regions as indicated by elevated CDOM. While CH_3Cl and CH_3Br both have wetland and salt marsh sources [*Rhew et al.*, 2000; *Varner et al.*, 1999], the degradation rate for CH_3Br is faster than that for CH_3Cl which may explain the lack of corresponding elevation in CH_3Br where only CH_3Cl and CDOM are elevated. The elevated CH_3Br is observed where the stimulated fluorescence of chlorophyll-a is also elevated suggesting

that in situ production of CH_3Br occurred in these regions but not in the other terrestrially influenced regions. This does not preclude *in situ* CH_3Cl production from occurring in the same regions, but we cannot separate the terrestrial influence from the possible *in situ* production for CH_3Cl with the available data.

2.3.2. Water column distribution

The calculated mixed layer depths using the method of *Brainerd and Gregg* [1995] were less than 50 meters in this cruise. Vertical distributions of CH_3Br and CH_3Cl show that the highest concentrations were in the subsurface water just below the mixed layer in transects 4, 5, 6 and 8 (Figures 2.3 and 2.4). This may result from enhanced chemical degradation and lower solubility due to the higher temperatures near the surface. The SST decreased from $\sim 30^o$ C to $\sim 20^o$ C from transect 4 to transect 9, reducing the degradation rate, increasing the solubility and allowing for higher dissolved concentrations to persist at the surface during transect 9 (Figures 2.2d, 2.3 and 2.4). The intensity and width of near surface maxima varies with different transects, depending on their localized sources and mixing conditions.

The vertical distributions of CH_3Br show higher concentrations in the coastal ocean than in the open ocean, except for transect 6, where elevated concentrations are present in both (Figure 2.3). This observation further supports the conclusion that production rates are higher in the coastal ocean than in the open ocean. For CH_3Cl, it is elevated in open ocean regions (Figures 2.4a, 2.4b and 2.4c), which raises the question of whether phytoplankton communities in the open ocean might be more efficient at producing CH_3Cl, compared to those of coastal waters.
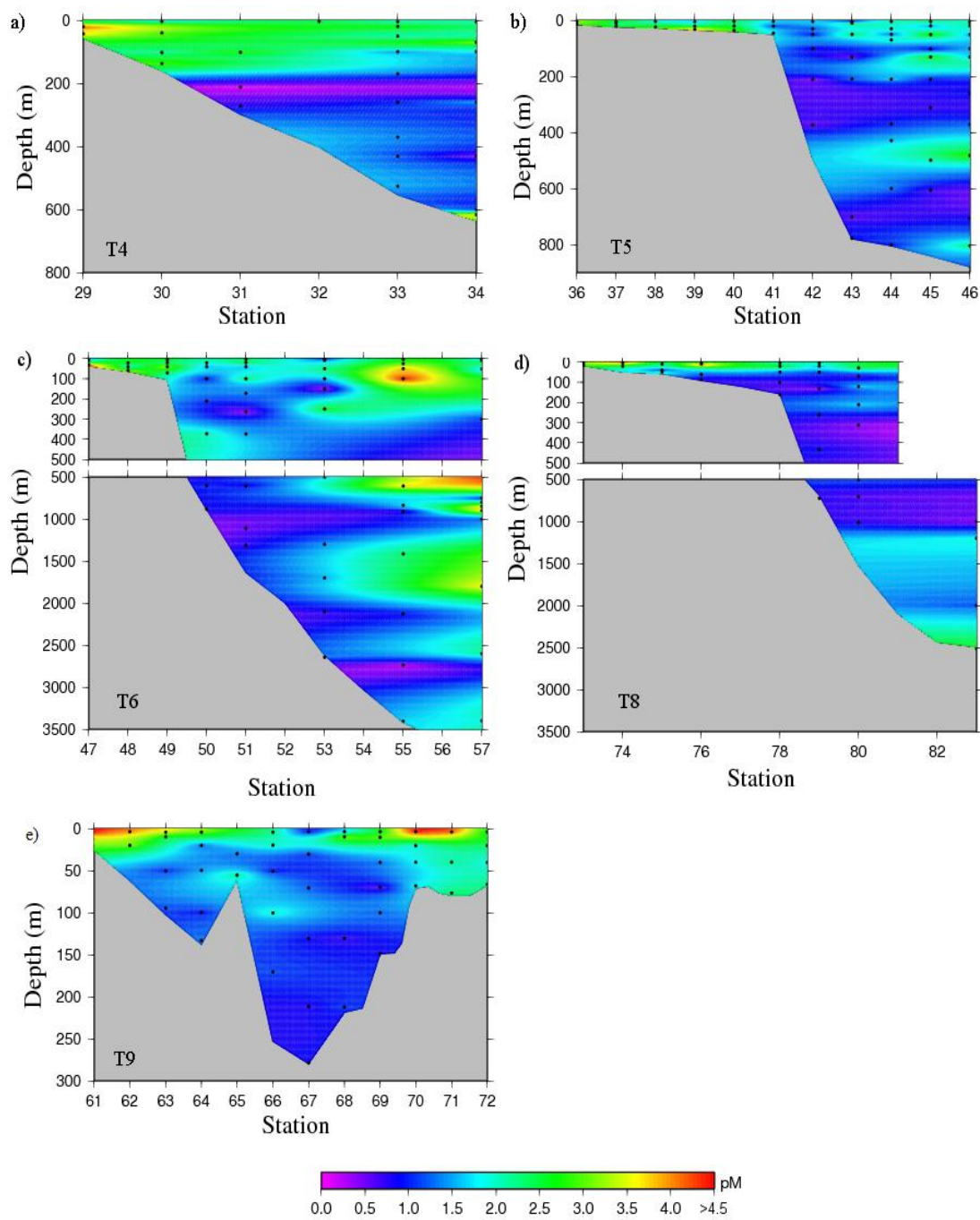
Figure 2.3. Vertical distributions of CH$_3$Br in transects 4, 5, 6, 8 and 9.
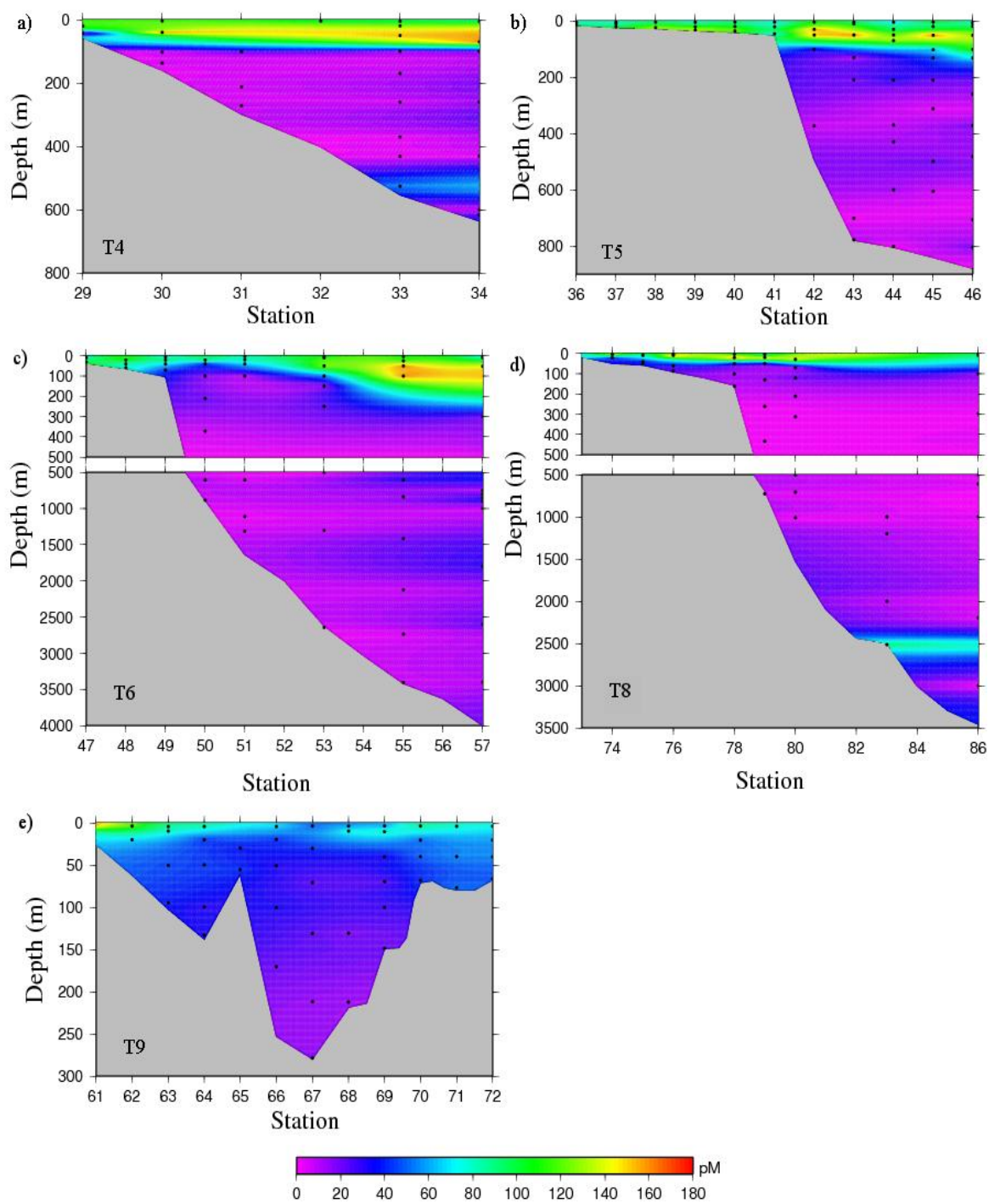
Figure 2.4. Vertical distributions of CH₃Cl in transects 4, 5, 6, 8 and 9.

2.3.3. Flux and production

The net sea-to-air flux (F, nmol m^{-2} d^{-1}) was calculated by the following equation:

$$F = k_w (\frac{p_w}{H} - \frac{p_a}{H}) \tag{2.1}$$

where k_w is gas transfer velocity, H is solubility (m^3 atm mol^{-1}), p_w and p_a are the partial pressures (atm) in the surface water and atmosphere. Wind speeds were measured with an anemometer at a height of 19m above the sea level, then normalized to a height of 10m using the equation of *Large and Pond* [1982] and *Erickson* [1993] to calculate the gas transfer velocity [*Wanninkhof*, 1992]. The solubilities of CH$_3$Br and CH$_3$Cl were calculated following the method of *De Bruyn and Saltzman* [1997] and *Moore* [2000]. The net fluxes of CH$_3$Br and CH$_3$Cl are in the range of -3.5 to 10.8 nmol m^{-2} d^{-1} and -5.9 to 348 nmol m^{-2} d^{-1}. The CH$_3$Br flux is controlled by the saturation state of the seawater, while the variation in the flux of CH$_3$Cl appears to be driven mainly by variations of wind speeds (Figures 2.2c, 2.5a and 2.5b).

Assuming the ocean is at a steady state, the production rate should be equal to the rate needed to balance the sum of the degradation rate and the net flux. However, the ocean does not achieve thermal equilibrium in most situations. Surface cooling or warming would affect the saturation anomaly and the production calculation. Therefore, the saturation anomaly of CFC-11 was used to correct the thermal effect *Yvon-Lewis et al.* [2004] and the net production rate was calculated by the corrected net flux and degradation rate, as shown below:

$$P = \frac{k_w}{z} \frac{[\Delta - \Delta_{CFC-11}] p_a}{100H} + (k_{chem} + k_{bio}) C_w \tag{2.2}$$

where P is production rate (mol m^{-3} d^{-1}); Δ is saturation anomaly of CH$_3$Br or CH$_3$Cl; Δ_{CFC-11} is saturation anomaly of CFC-11; z is mixed layer depth (m); C_w is surface seawater concentration; k_{chem} and k_{bio} are the chemical and biological degradation constants (d^{-1}). The rest of the parameters are defined above. Chemical degradation of CH$_3$Br and CH$_3$Cl, varying from 0.03 to 0.53 d^{-1} and 0 to 0.05 d^{-1} in this study, were calculated using the equations from *King and Saltzman* [1997] and *Mabey and Mill* [1978]. Biological degradation constant of CH$_3$Br was from King and Saltzman [1997], 0.11 d^{-1} off the coast of Florida during the summer. For CH$_3$Cl, the biological degradation constant, 0.085 d^{-1}, was from the averaged biological degradation rate constant in July in the study of [*Tokarczyk et al.*, 2003], which is the only study on the biological degradation off the coast.

The distributions of calculated CH$_3$Br and CH$_3$Cl production rates appear similar except for the spike in CH$_3$Cl production before transect 6 (Figure 2.5c), where terrestrial transport, as discussed earlier, may have influenced the CH$_3$Cl concentrations. A linear regression analysis of the production rates shows a linear fit through the data with correlation coefficient of 0.47 (n=287) indicating correlation within 95% confidence levels [*Emery and Thomson*, 2001]. This correlation coefficient increases to 0.75 after we removed the spike in CH$_3$Cl production extending from year day 202.8 to 204.9. *Scarratt and Moore* [1998] tested nine phytoplankton species, most of which are common in the open ocean, and found that CH$_3$Cl and CH$_3$Br were produced in all cultures, except CH$_3$Br was absent in cultures of *Tetraselmis sp.* and *Isochrysis sp.* This good correlation between the calculated production rates of CH$_3$Br and CH$_3$Cl in our
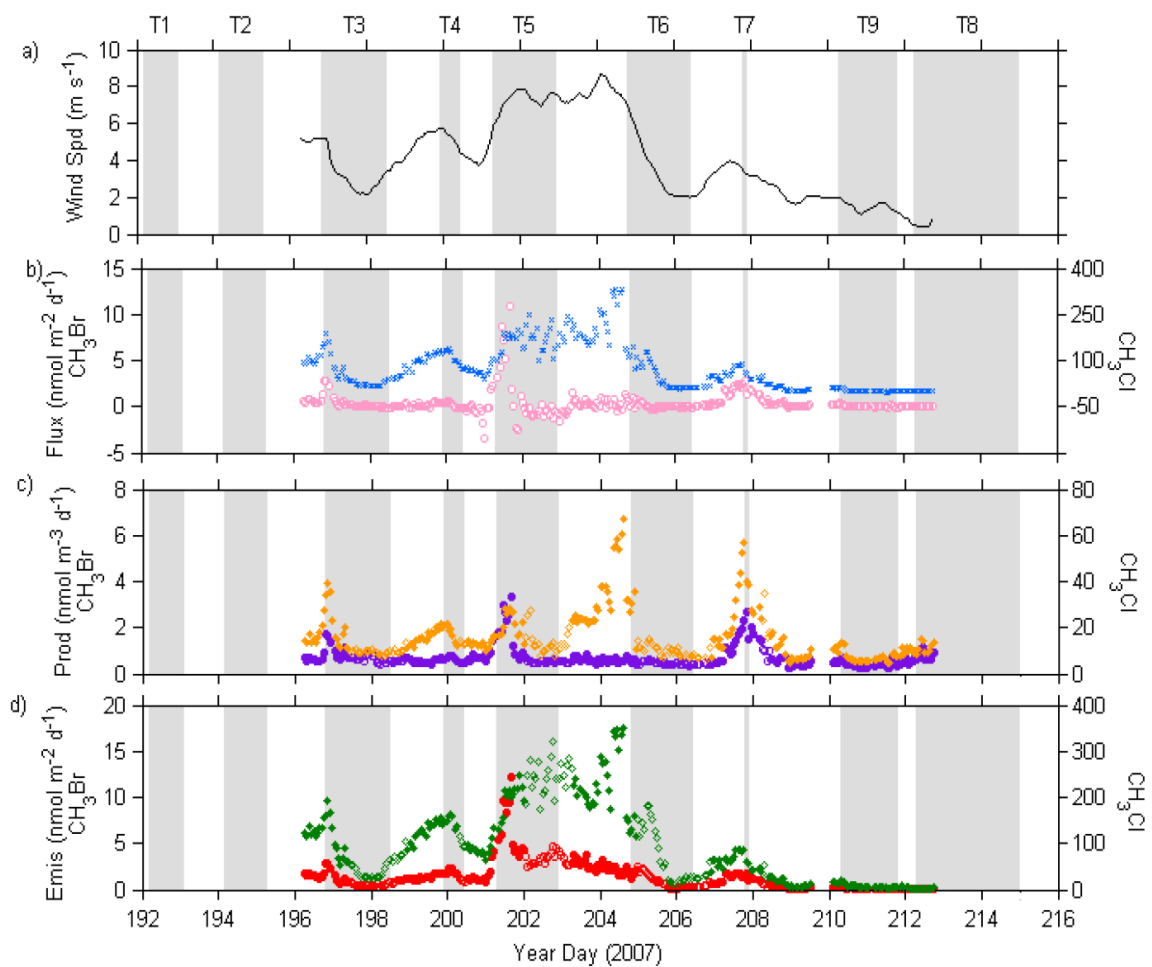
Figure 2.5. (a) 24-h averaged wind speed at 10m before sampling; (b) calculated sea-to-air fluxes of CH$_3$Br (o) and CH$_3$Cl (x); (c) calculated production rates of CH$_3$Br in the coastal ocean (●) and the open ocean (○), and calculated production rates of CH$_3$Cl in the coastal ocean (◆) and the open ocean (◇); (d) calculated emissions for CH$_3$Br in the coastal ocean (●) and the open ocean (○), and calculated emissions for CH$_3$Cl in the coastal ocean (◆) and the open ocean(◇).

study suggests that CH_3Br and CH_3Cl also have some common sources in the coastal ocean.

2.3.4 Estimating total coastal emissions

The area of the coastal ocean, defined as the area with bottom depth less than 200m, was determined from bathymetric data from the NOAA National Geophysical Data Center (http://www.ngdc.noaa.gov/mgg/bathymetry/relief.html). The mean value of the calculated production rates of CH_3Br for the coastal oceans in this study is 0.76 nmol m^{-3} d^{-1}, which is much higher than the global open ocean production rate, 0.15 nmol m^{-3} d^{-1} [*Yvon-Lewis and Butler*, 2002]. The calculated coastal CH_3Cl production rate ranges from 4.5 to 67nmol m^{-3} d^{-1} with a mean value of 18 nmol m^{-3} d^{-1}.

Emission is defined as the amount of gas which is produced in the ocean and emitted to the atmosphere. It is calculated from the following equation:

$$E = P_{uncorr}(1-R)z \qquad (2.3)$$

where E is emission from the ocean (mol m^{-2} d^{-1}); P_{uncorr} is uncorrected production rate, which is calculated from equation (2.2) using the uncorrected saturation anomaly; and R is the fraction of gas entering the water that is destroyed before exiting to the atmosphere [*Butler*, 1994].

The entire cruise track was divided into four regions, each spanning five degrees of latitude, to capture the regional variations. Regionally averaged emissions were enhanced within the 30° N - 35° N area (Table 2.1). The calculated emission from the entire GOMECC coastal region ranged from 0.01 to 0.06 Gg yr^{-1} for CH_3Br and 0.3 to 1.6 Gg yr^{-1} for CH_3Cl (Table 2.1). The global coastal-ocean area is approximately

$27.123 \times 10^6 \, \text{km}^2$, accounting for 7.4 % of global ocean area [*Menard and Smith*, 1966].

Assuming that the GOMECC area is representative of the global coastal-ocean region, the extrapolated global coastal-oceanic emissions range from 0.5 to 3.6 Gg yr^{-1} for CH$_3$Br and from 19 to 98 Gg yr^{-1} for CH$_3$Cl. Using the same method, the extrapolated global coastal-ocean fluxes are estimated to be in the range of -0.9 to 3.4 Gg yr^{-1} and 12 to 94 Gg yr^{-1} for CH$_3$Br and CH$_3$Cl. For CH$_3$Cl, the global open-oceanic emission ranges from 1284 to 1364 Gg yr^{-1} as calculated from the global net flux of 320 to 400 Gg yr^{-1} [*Moore*, 2000], the partial atmospheric lifetime with respect to oceanic loss of 4.1 years [*Tokarczyk et al.*, 2003] and its averaged global atmospheric mixing ratio, 536 ppt, from NOAA/ESRL Global Monitoring Division (ftp://ftp.cmdl.noaa.gov/hats/methylhalides). For CH$_3$Br, it is more complicated. With the decline in atmospheric concentrations since the implementation of the Montreal Protocol, the global net flux of CH$_3$Br has likely changed since the previous global estimates of net flux were determined [*Yvon-Lewis et al.*, 2009]. Comparing the extrapolated coastal-ocean net fluxes determined in this study to the pre-phaseout global ocean net fluxes is not a valid comparison. However, the oceanic production rate and emission are not functions of the atmospheric concentration and should not have changed. Therefore, the global oceanic emission of 42 Gg yr^{-1} determined by *Yvon-Lewis et al.* [2009] remains the best estimate. Including the coastal-oceanic emissions of CH$_3$Br and CH$_3$Cl will increase the global oceanic emissions by 1% - 9% and 1% - 8%, respectively.

Table 2.1. Estimated coastal emissions of CH_3Br and CH_3Cl.

Region	Area (km^2)	CH_3Br		CH_3Cl	
		Emission (nmol m^{-2} d^{-1})	Annual Emission (Gg yr^{-1})	Emission (nmol m^{-2} d^{-1})	Annual Emission (Gg yr^{-1})
I (Latitude <30°N)	1.82×10^5	1.5 (0.9-2.8)	0.01 (0.004-0.02)	119 (52-192)	0.4 (0.2 - 0.6)
II (Latitude 30~35°N)	8.50×10^4	3.7 (0.9-12)	0.01 (0.003-0.04)	202 (63-349)	0.3 (1.0-5.4)
III (Latitude 35~40°N)	6.58×10^4	1.4 (0.6-2.5)	0.003 (0.001-0.006)	95 (38-351)	0.1 (0.04-0.4)
IV (Latitude > 40°N)	1.18×10^5	0.2 (0-0.5)	0.001 (0-0.002)	8.3 (1.1-28)	0.02 (0-0.06)
GOMECC coastal total	4.52×10^5	-	0.02 (0.01-0.06)	-	0.8 (0.3-1.6)
Global coastal ocean	27.123×10^6	-	1.4 (0.5-3.6)	-	50 (19-98)

The GOMECC data represent a much larger coastal area than the few previous coastal studies covered [*Baker et al.*, 1998; *Sturrock et al.*, 2003]. For CH_3Br, the results presented here fall within the range of data reported in the other studies (Table 2.2). However, the saturation anomalies of CH_3Br off the coast of Tasmania [*Sturrock et al.*, 2003] were substantially higher than those in our study which suggests that coastal emissions may have significant regional variability and limit the ability to extrapolate the emission from any one region. In addition, there has been no investigation of the coastal-ocean emissions from high latitudes. Our knowledge of the seasonality of CH_3Br and CH_3Cl emissions from the coastal ocean is limited. *Baker et al.* [1999] observed a seasonal cycle in coastal waters of the southern North Sea for CH_3Br but no seasonal pattern was observed in the Tasmanian data of *Sturrock et al.* [2003]. *Khalil and Rasmussen* [1999] found seasonal variation at various latitudes in the atmosphere for CH_3Cl, but there was no seasonal study of CH_3Cl in seawater. Therefore, large uncertainties in these estimated global coastal emissions arise from the limited spatial and temporal coverage of our dataset and are difficult to quantify using the current data.

2.4. Conclusions

The coastal ocean is a highly productive region for CH_3Br, and it may also be highly productive for CH_3Cl based on its large range of calculated production rates. Elevated concentrations of CH_3Br might be due to enhanced biological processes, and elevated CH_3Cl in seawater might be associated with biological processes and terrestrial transport. The vertical distributions showed that the waters with elevated CH_3Br and CH_3Cl in the investigated transects were located in the subsurface, just below the mixed

Table 2.2. Comparison of CH$_3$Br measurements in different coastal regions.

Region	Time	Atmospheric Mixing Ratio (ppt)	Seawater Concentration (pM)	Saturation Anomaly (%)	Reference
GOMECC (Coastal)	10 Jul- 4 Aug, 2007	10.5 (5.6-37.3)	1.9 (0.8-5.0)	30 (-45-236)	This study
Coastal Nova Scotia	Oct-Nov, 1995	11.4-13.0	1.5-2.5	9	Groszko and Moore, 1998
Coastal Water of the North Sea	Feb, 1996 – Feb,1997	9.5-25.5	2-8.7	-60-200	Baker et al., 1999
Subtropical/ temperate NE Pacific (coastal)	7 May -7 Jul, 2000	12.16	2.66	30	King et al., 2000
Coastal waters off Tasmania	Mar, 2000 -Sep, 2002	6-24	0-26	-50-1200	Sturrock et al., 2003

layer, which may be due to more rapid degradation in the surface layer. Evidence from the correlation of calculated production rates indicates that some common sources for CH_3Br and CH_3Cl exist in the coastal ocean. Including the emissions of CH_3Br and CH_3Cl from the coastal area of the ocean may increase the estimates for global oceanic emissions of these gases by 1% - 9% and 1% - 8%. Although there are substantial uncertainties in the global coastal estimates due to the limited amount of data representing global coastal regimes and a lack of information on seasonal variation, these results provide an initial approximation of the contribution of the coastal ocean to the budgets of these gases. More investigations in coastal ocean regions including seasonal variations for CH_3Br and CH_3Cl are needed in order to obtain a more accurate assessment of their coastal emissions.

3. THE OCEAN IN NEAR EQUILIBRIUM WITH ATMOSPHERIC METHYL BROMIDE*

3.1. Introduction

CH_3Br, an important ozone-depleting substance (ODS), contributes about 34% of the total stratospheric bromine [*Montzka and Reimann*, 2011]. As the abundances and emissions of most ODSs decrease, the total tropospheric burden of organic chlorine and organic bromine are declining. Unlike other ODSs controlled by the Montreal Protocol, CH_3Br has both anthropogenic and natural sources. Since a significant portion of CH_3Br is emitted from natural sources [*Montzka and Reimann*, 2011; *Yvon-Lewis et al.*, 2009], the relative importance of natural CH_3Br in stratospheric ozone depletion will increase with the declining anthropogenic chlorine and bromine sources.

The ocean is the largest source and second largest sink for atmospheric CH_3Br [*World Meteorological Organization (WMO)*, 2003; *Yvon-Lewis et al.*, 2009]. The current best estimate for the pre-phaseout global emission of CH_3Br from the ocean is 42 Gg yr^{-1} [*Yvon-Lewis et al.*, 2009]. Phytoplankton are thought to be the primary source of CH_3Br in the surface ocean [*Saemundsdottir and Matrai*, 1998; *Scarratt and Moore*, 1996, 1998]. CH_3Br is also removed chemically and biologically in the ocean. The

---

chemical degradation of CH_3Br includes hydrolysis and chloride substitution, whichdepend on the *in-situ* temperature and salinity [*King and Saltzman*, 1997]. Biological degradation rate constants measured in the coastal and open ocean generally range from 0 to 0.26 d^{-1} [*King and Saltzman*, 1997; *Tokarczyk and Saltzman*, 2001; *Tokarczyk et al.*, 2001; *Tokarczyk et al.*, 2003]. It was widely observed that CH_3Br was undersaturated in the open ocean [*Groszko and Moore*, 1998; *King et al.*, 2002; *Lobert et al.*, 1996; *Yvon-Lewis et al.*, 2004], in contrast to the coastal ocean which is supersaturated with respect to CH_3Br [*Hu et al.*, 2010; *Lobert et al.*, 1995; *Sturrock et al.*, 2003]. The global net sea-to-air flux, including both the open ocean and the coastal ocean, was estimated at -20 Gg yr^{-1} to -10 Gg yr^{-1} before 1998 [*Groszko and Moore*, 1998; *King et al.*, 2002; *King et al.*, 2000; *Lobert et al.*, 1995; *Yvon-Lewis et al.*, 2009].

Because of the implementation of the Montreal Protocol and its amendments which called for the phaseout of fumigation - non-Quarantine and Pre-Shipment (non-QPS) uses of CH_3Br, the atmospheric mixing ratio of CH_3Br has been declining [*Montzka and Reimann*, 2011]. This should lead to an increase in the saturation state of CH_3Br in the surface ocean, assuming surface ocean annual production rates, and biological, chemical and eddy degradation rate constants remain the same as they were before the phaseout [*Butler*, 1994; *Yvon-Lewis et al.*, 2009]. Since chemical and eddy degradation rate constants are a function of salinity, sea surface temperature (SST), thermocline temperature and mixed layer depth, it is easy to assume that they have not changed significantly since 1994. Annual production rates and biological degradation rate constants are unlikely to have changed since 1994, but this is less certain.

In this study, we selected the cruise tracks similar to those covered during the Bromine Latitudinal Air-Sea Transect I and II (BLAST I and II) cruises (Figure 3.1) to determine the current global saturation state of CH_3Br in the surface ocean near the end of its fumigation-non-QPS phaseout. Another goal of this study was to assess the validity of the assumption in the prior modeling studies [*Butler*, 1994; *Yvon-Lewis et al.*, 2009] that annual production rates and biological degradation rate constants remain constant over time.

3. 2. Methods

The Halocarbon Air-Sea Transect - Pacific/Atlantic (HalocAST - P/A) cruises were conducted aboard *R/V* Thomas G. Thompson and the FS Polarstern, respectively. The HalocAST - P cruise, which had an almost identical cruise track to BLAST I (1/26 – 2/28, 1994), started from Punta Arenas, Chile, on 30 March, 2010 and ended in Seattle, Washington, US, on 27 April, 2010 (Figure 3.1). The HalocAST-A cruise, which covered a similar latitudinal range as BLAST II (10/18 – 11/21, 1994) but in the eastern Atlantic, departed from Bremerhaven, Germany, on 25 October, 2010 and arrived in Cape Town, South Africa, on 26 November, 2010 (Figure 3.1).

Continuous underway salinity, sea surface temperature (SST), wind speed, wind direction, air temperature and relative humidity data were collected for both cruises. Additional measurements include halocarbon air-sea measurements (including CH_3Br and other 19 halocarbon compounds), CH_3Br degradation rate constant measurements and plant pigment measurements.
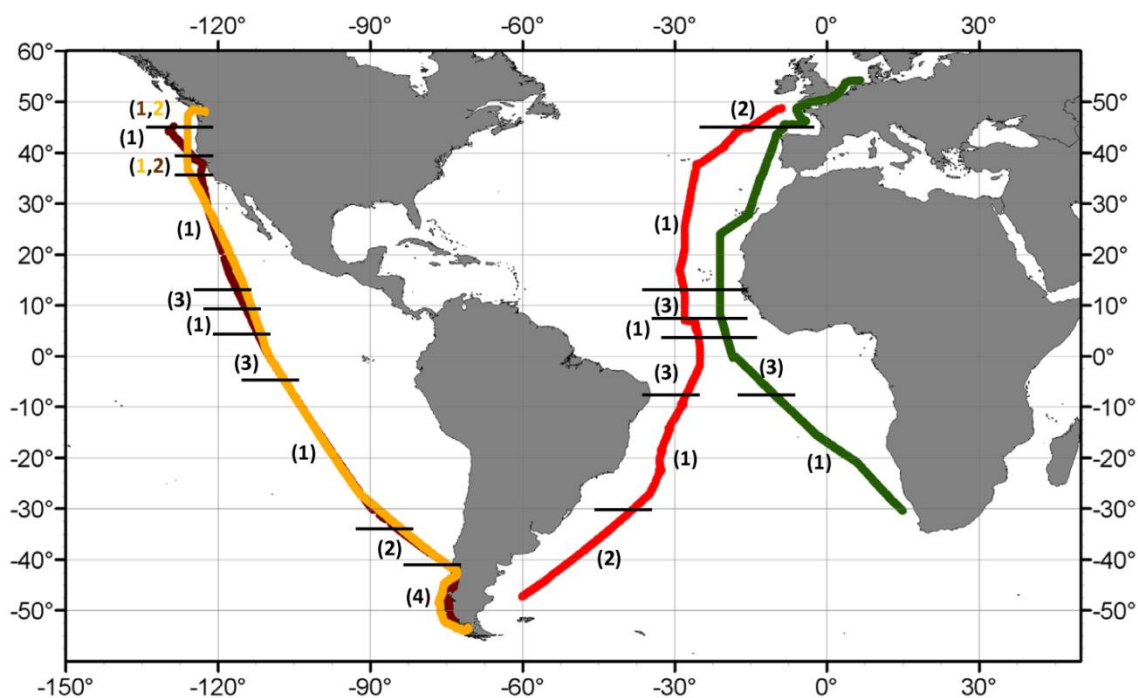
Figure 3.1. Cruise tracks of BLAST I (▬), BLAST II (▬), HalocAST-P (▬) and HalocAST-A (▬). Horizontal black lines along the cruise track indicate the edges of specified oceanic regions: (1) open ocean, (2) coastal and nearshore, (3) upwelling, and (4) inland passage. The division on the oceanic regions is from *Lobert et al.* [1995, 1996].

CH$_3$Br and a suite of other halocarbons were measured continuously in air and surface seawater using gas chromatograph with a mass spectrometer (GC-MS), equipped with a Weiss-type equilibrator. The details of the analytical system were described in *Hu et al.* [2010] (Appendices A and C). The only difference from the old analytical system [*Hu et al.*, 2010] is that the GC column was changed from a DB-VRX (I.D. 0.25 mm; Length 60 m; Film 1.4 μm) to a narrow bore DB-VRX (I.D. 0.18 mm; Length 40 m; Film 1.0 μm) column prior to the HalocAST - P/A cruises. The new column allowed for better separation and shorter chromatograms. The instrument was calibrated using two whole-air standards which were calibrated against a whole air standard from NOAA/ESRL Global Monitoring Division using the NOAA-03 scale (http://www.esrl.noaa.gov/gmd/ccl/scales.html). The reported concentrations in the air or surface seawater are expressed as dry air mole fractions (parts-per-trillion, ppt) and equilibrated dry gas mole fractions (ppt). The instrumental precision for CH$_3$Br was 4.7% (1σ) during HalocAST-P and 0.8% (1σ) during HalocAST-A. A better precision during HalocAST-A was because we changed a new filament in the mass spectrometer during this cruise.

Measurements of CH$_3$Br degradation rates were conducted in the eastern Atlantic during HalocAST-A. Samples were collected daily between 1200 and 1300 (local time) using the flow-through system on the ship. The inlet was located 4 m below the sea surface. The flow-through system was flushed with seawater continuously. Each sample was divided into 2 to 4 aliquots. One was filtered through 0.2 μm MediaKap Hollow Fiber Media Filter and used to determine the chemical degradation rate. Another one to

three aliquots were passed through 63 μm pore size mesh to remove the big particles and used to measure the total degradation rate. The biological degradation rate was determined by the difference between the total degradation rate and the chemical degradation rate. The degradation rate constants were measured by a stable isotope incubation technique which was described by *King and Saltzman* [1997], *Tokarczyk and Saltzman* [2001] and *Tokarczyk et al.* [2001]. The isotopic fractionation factor of $^{12}k/^{13}k=1.074$ from *King and Saltzman* [1997] was used to correct the measured ^{13}C rate constants to ^{12}C rate constants. The uncertainty of the measurement was < 0.01 d^{-1} and the precision between aliquots was $0.01 - 0.06$ (mean: 0.03) d^{-1}.

All plant pigment samples were filtered through GF/F filters (nominal pore size = 0.7 μm), stored in a -80 ^{o}C freezer on-board ship and brought back to the laboratory for analysis. Pigments were extracted according to the methods of *Wright et al.* [1991]. The extracted pigments were analyzed using a Waters HPLC (high-performance liquid chromatograph) with a 996 Photodiode array detector and a Shimadzu RF 535 Fluorescence detector (excitation set at 440 nm and emission set at 660 nm). The pigments were separated on a reverse phase Alltech Adsorbosphere C_{18} column (5 μm, 250 mm x 4.6 mm i.d.) using the gradient flow described by *Chen et al.* [2003]. A total of 18 dominant pigments, including total chlorophyll *a* (chlorophyll *a*+ divinylchlorophyll *a*), chlorophyll *b*, c_2 and c_3, total carotene (α + β), peridinin, 19-butanoyloxyfucoxanthin, fucoxanthin, 19-hexanoyloxyfucoxanthin, prasinoxanthin, pheophorbide *a*, violaxanthin, diadinoxanthin, alloxanthin, diatoxanthin, lutein,

pheophytin *a*, and zeaxanthin, was measured with a detection limit ≤ 1.0 nmol L^{-1} and an average precision of 4.0 % (1σ).

3.3. Results and discussion

3.3.1. Air and water concentrations and saturation anomalies

Atmospheric mixing ratios of CH$_3$Br ranged from 5.36 to 11.2 ppt (mean 7.49; sd. 0.85) for HalocAST-P (Figure 3.2a) and 6.28 to 9.04 ppt (mean 7.38; sd. 0.60) for HalocAST-A (Figure 3.3a). It is evident that the CH$_3$Br mixing ratios in the air have decreased more in the Northern Hemisphere (NH) than those in the Southern Hemisphere (SH) when compared to the pre-phaseout (BLAST I and II) values (Figures 3.2a and 3.3a; Table 3.1). The interhemispheric ratio of CH$_3$Br (NH/SH) was also lower than it was during the pre-phaseout BLAST cruises (Table 3.1). These are consistent with the atmospheric CH$_3$Br observations from NOAA/ESRL Global Monitoring Division (see ftp://ftp.cmdl.noaa.gov/hats/methylhalides/ch3br/) and the decreasing anthropogenic emission. A larger decline of CH$_3$Br mixing ratios in the NH than that in the SH is due to a larger reduction in the anthropogenic emissions in the NH compared to that in the SH (http://ozone.unep.org/Data_Reporting/Data_Access/).

Saturation anomaly ($\Delta\%$) is defined as the percent difference between the partial pressure of a trace gas in surface seawater (p_w) and air (p_a):

$$\Delta(\%) = \frac{p_w - p_a}{p_a} \times 100 \,. \tag{3.1}$$

where, partial pressures in the air or surface seawater were calculated by equations (3.2 − 3.3).
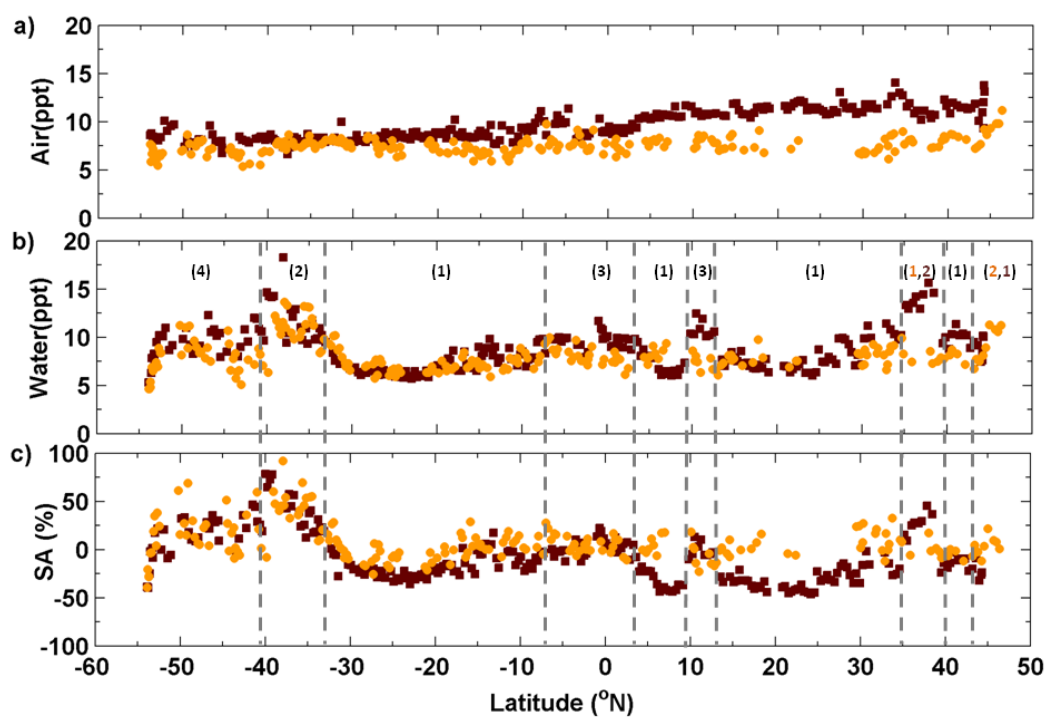
Figure 3.2. (a) CH$_3$Br atmospheric mixing ratios; (b) equilibrated dry gas mole fractions of CH$_3$Br in surface seawater and (c) saturation anomalies of CH$_3$Br in surface ocean for BLAST I (■) and HalocAST-P (●). The numbers between the dashed vertical lines indicate different oceanic regions with 1 = open ocean, 2 = coastal and coastal influential region, 3 = upwelling and 4 = inland passage.
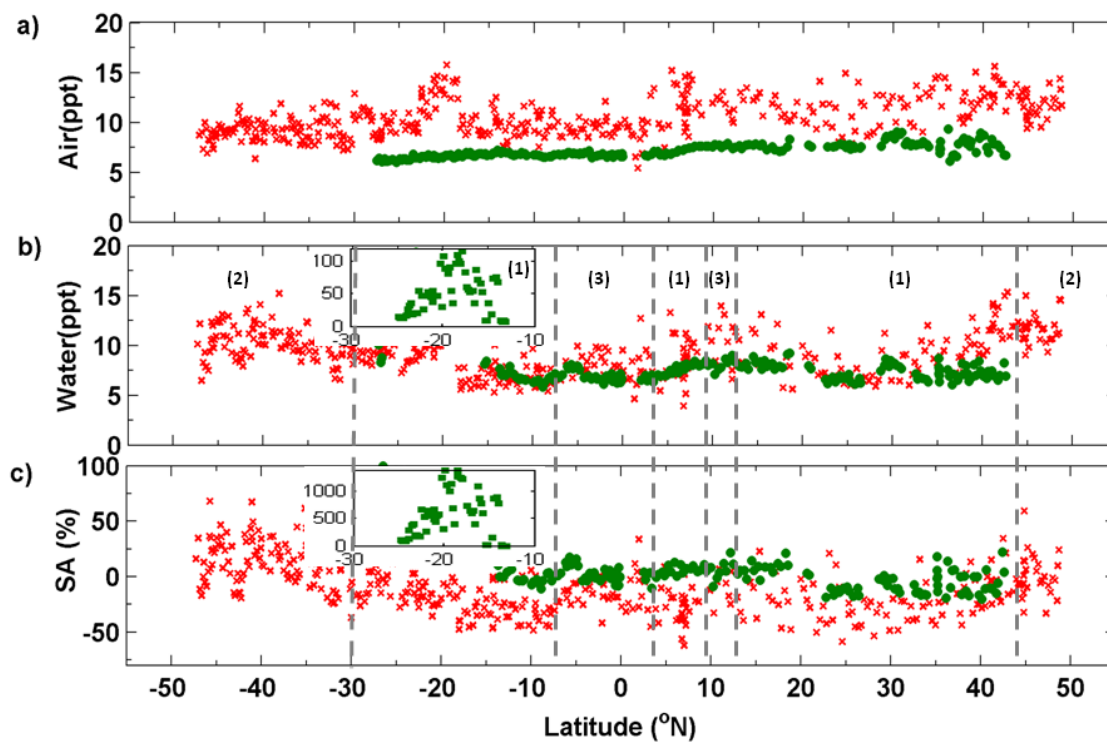
Figure 3.3. (a) CH₃Br atmospheric mixing ratios; (b) equilibrated dry gas mole fractions of CH₃Br in surface seawater and (c) saturation anomalies of CH₃Br in surface ocean for BLAST II (x) and HalocAST-A (■). The numbers between the dashed vertical lines indicate different oceanic regions with 1 = open ocean, 2 = coastal and coastal influential region and 3 = upwelling region.

Table 3.1. Hemispheric and global mean atmospheric mixing ratios of CH_3Br and the interhemispheric ratios (IHR) during BLAST I, BLAST II, HalocAST-P and HalocAST-A.

Cruises	Time Period	NH (ppt)	SH (ppt)	Global (ppt)	IHR (NH/SH)
BLAST I	Jan-Feb, 1994	11.1	8.55	9.62	1.29
HalocAST-P	Mar-Apr, 2010	7.85	7.31	7.52	1.07
BLAST II	Oct-Nov, 1994	11.5	9.79	10.5	1.18
HalocAST-A	Oct-Nov, 2010	8.02	7.00	7.50	1.15

$$p_a = \chi_a(p_t - \frac{RH}{100} p_{vp}) \qquad (3.2)$$

$$p_w = \chi_w(p_t - \frac{RH}{100} p_{vp}) \qquad (3.3)$$

where, χ_a stands for dry air mole fractions or atmospheric mixing ratios, χ_w stands for equilibrated dry gas mole fractions for surface seawater, p_t stands for surface atmospheric pressure, p_{vp} is water vapor pressure calculated by the formula given by *Weiss and Price* [1980], and *RH* stands for the relative humidity. To compare the CH_3Br surface seawater concentrations and the saturation anomalies from this study to previous studies, we used the same water mass designations of open-ocean, coastal and coastal-influential region, upwelling and inland passage as *Lobert et al.* [1995, 1996]. In most regions, the equilibrated dry gas mole fractions of CH_3Br in surface seawater observed during the current study were not significantly different than those observed during BLAST I and II (Figures 3.2b and 3.3b; Table 3.2). However, the data showed an increase over the last 16 years in the saturation anomalies in the open ocean for both cruises (Figures 3.2 and 3.3) and in upwelling region of HalocAST-A (Figure 3.3) but little change in the inland passage, overlapped coastal and coastal influential regions and upwelling regions of HalocAST-P (Figure 3.2). The reason that the mean saturation anomaly in the coastal and coastal influential regions during HalocAST-P was about 10% lower than that during BLAST I (Table 3.2) is because saturation anomalies of CH_3Br in the coastal areas above 35 °N during HalocAST-P are much lower than those during BLAST I because of different locations (Figure 3.1). The most noticeable increase for saturation anomalies was observed in the open ocean region with a 24.7%

Table 3.2. Mean equilibrated dry gas mole fractions of CH_3Br in surface seawater, mean saturation anomalies (Δ_{CH3Br}) and mean corrected saturation anomalies (Δ_{CH3Br} -Δ_{CFC-11}) in open ocean, coastal ocean and upwelling areas during BLAST I/II and HalocAST-P/A.

	BLAST I	HalocAST-P	BLAST II [a]	HalocAST-A[a]
Open Ocean				
Water (ppt)	7.73	7.70	8.64	7.66
Δ_{CH3Br} (%)	-21.8	2.9	-23.5	-2.3
Δ_{CH3Br} -Δ_{CFC-11} (%)	-24.6	0.7	-25.0	- 6.0
Coastal				
Water (ppt)	12.1	10.3	10.6	n.a.[b]
Δ_{CH3Br} (%)	40.3	29.5	11.2	n.a.[b]
Δ_{CH3Br} -Δ_{CFC-11} (%)	37.1	27.3	7.3	n.a.[b]
Upwelling				
Water (ppt)	9.80	7.66	8.67	7.61
Δ_{CH3Br} (%)	1.4	0.4	-12.0	3.7
Δ_{CH3Br} -Δ_{CFC-11} (%)	2.6	1.3	-12.6	-1.3

[a]Exclude the data between 13° - 30° S, where elevated CH_3Br was observed during HalocAST-A;
[b]Not applicable.

increase between BLAST I and HalocAST-P and a 21.2% increase between BLAST II and HalocAST-A (Table 3.2).

The change of the saturation anomalies is not only controlled by the change of atmospheric mixing ratios, it is also affected by other physical processes, i.e. surface cooling or warming, mixing of water masses and injection of air bubbles [*Butler et al.*, 1991]. The physical effect on saturation anomalies could be corrected by conservative tracers (i.e. cholorofluorocarbon-11, CFC-11) when the molecular diffusivity, the solubility and the response of the solubility to the temperature change are similar between the trace gas and the conservative tracer [*Butler et al.*, 1991]. The previous studies [*Hu et al.*, 2010; *Lobert et al.*, 1995, 1996; *Yvon-Lewis et al.*, 2004] use saturation anomalies of CFC-11 to correct saturation anomalies of CH_3Br. Although the atmospheric CFC-11 is declining, the declining rate, ~2 ppt/yr [*Montzka and Reimann*, 2011], is relatively slow compare to the time needed to reach equilibrium with surface ocean (*Warner and Weiss* [1985] reported that, at temperatures from 0 to 40 ^{o}C, seawater or freshwater needs less than 16 hours to reach equilibrium with headspace CFC-11, which had concentrations ten times the ambient), indicating that the surface ocean should be in near equilibrium with atmospheric CFC-11 in 2010. Therefore, it can still be used to correct the effect of physical processes on the saturation anomalies of CH_3Br in 2010. Corrected saturation anomalies show similar magnitude of increase in the open ocean and upwelling areas as the uncorrected saturation anomalies (Table 3.2). Although the diffusivity and the response of the solubility to the temperature change are similar between CH_3Br and CFC-11 [*De Bruyn and Saltzman*, 1997a, b; *Hayduk and Laudie*,

1974; *Warner and Weiss*, 1985], the CFC-11 correction on the saturation anomalies cannot completely compensate the effect of the physical processes on the CH_3Br saturation anomalies since the absolute solubility of CH_3Br is two orders higher than the solubility of CFC-11. Therefore, it is worth noting that the errors of corrected saturation anomalies during HalocAST could be larger than those during BLAST since the magnitude of saturation anomalies between CH_3Br and CFC-11 were close in the open ocean and upwelling areas in the HalocAST studies.

During HalocAST-A, a large increase in surface seawater CH_3Br was observed between 13° S and 30° S in the eastern Atlantic. The equilibrated dry gas mole fraction of CH_3Br in surface seawater reached 106 ppt with 1040% of supersaturation. Correlation of surface seawater CH_3Br with chlorophyll c_2, c_3, fucoxanthin, 19-hexanoyloxyfucoxanthin, 19-butanoyloxyfucoxantin, diadinoxanthin, peridinin, pheophorbide *a* and pheophytin *a* (r > 0.58; p = 0.00; n=25) at a 95% confidence level and no correlation with other pigments (r < 0.32; p > 0.12; n=25) (Figure 3.4) suggest that elevated CH_3Br was associated with two main algal groups, prymnesiophytes and dinoflagellates [*Jeffrey et al.*, 1997]. Laboratory culture studies [*Saemundsdottir and Matrai*, 1998; *Scarratt and Moore*, 1996, 1998] suggest that CH_3Br is produced in both coastal and open ocean areas and that the ubiquitous species, *Emiliania huxleyi* and *Phaeocystis sp.*, can produce CH_3Br at significant rates. The presence of the signature pigments of these two species, 19-hexanoyloxyfucoxanthin, chlorophyll c_3, fucoxanthin, 19-butanoyloxyfucoxantin, and their accessory pigments, chlorophyll c_2 and diadinoxanthin [*Antajan et al.*, 2004; *Garrido and Zapata*, 1998; *Llewellyn and Gibb*,
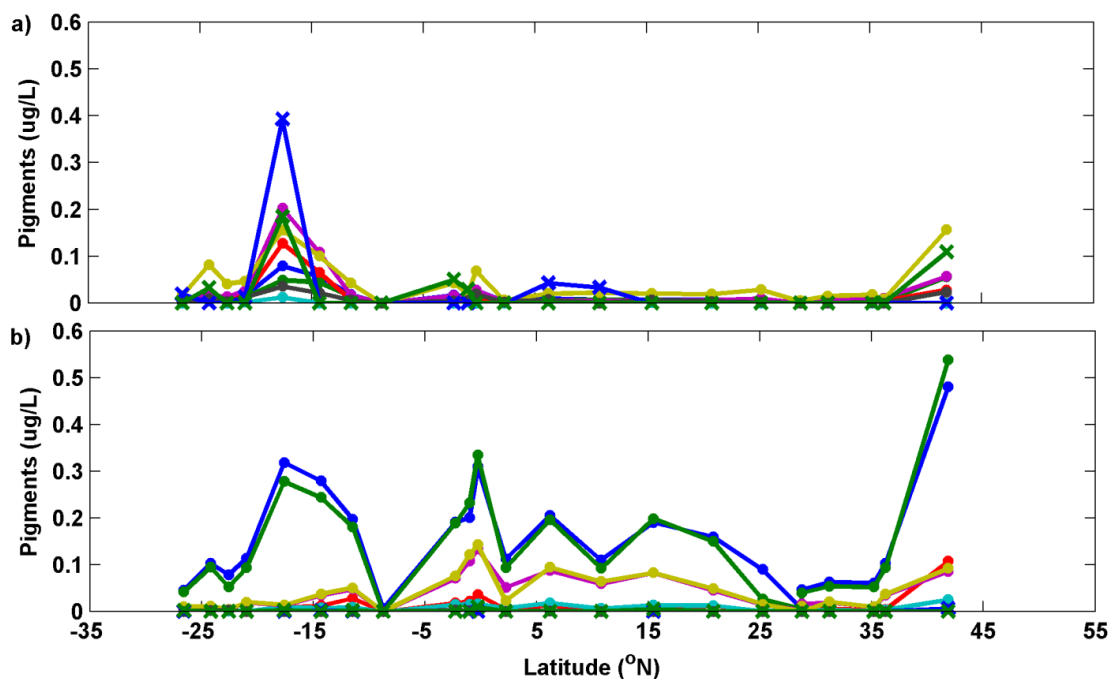
Figure 3.4. Latitudinal distributions of plant pigment concentrations in the surface of the eastern Atlantic; a) pigments which were correlated with surface seawater CH₃Br: chorophyll c_2 (————), chlorophyll c_3 (————), fucoxanthin (————), peridinin (————), 19-butanoyloxyfucoxanthin (————), 19-hexanoyloxyfucoxanthin (————), diadinoxanthin (————), pheophorbide a (————) and pheophytin a (————); b) pigments which were not correlated with surface seawater CH₃Br: total chlorophyll (————), chlorophyll a (————), chlorophyll b (————), total carotene (————), zeaxanthin (————), diatoxanthin (————), violaxanthin (————), alloxanthin (————) and lutein (————).

2000; *Schoemann et al.*, 2005], suggest these two species were likely contributors to the high concentrations of CH_3Br. However, we could not exclude the possibility of other prymnesiophytes and dinoflagellates species, which could also contribute to the elevated seawater CH_3Br. The most abundant pigment at this location, pheophorbide *a*, is a chlorophyll degradation product, which can be produced by macrocrustaceans grazing on *Phaeocystis c.f. puchetii* [*Vernet et al.*, 1996], conversion from ingested chlorophyll *a* by macrozooplankton and microzooplankton [*Goericke et al.*, 2000; *Welschmeyer and Lorenzen*, 1985], *Phaeocystis* autolysis, and senescent diatoms or *Phaeocystis* [*Head et al.*, 1994]. High correlation between pheophorbide *a* and surface seawater CH_3Br (r = 0.75; p = 0.00; n=25), along with the presence of the signature pigments of *Phaeocystis sp.*, suggests that elevated CH_3Br was at least partly associated with *Phaeocystis sp.*, some of which were grazed by zooplankton, or at the senescent stage or underwent autolysis.

3.3.2. Loss rate constants

CH_3Br loss rate constants were measured in the eastern Atlantic during HalocAST-A. Chemical loss rate constants, determined using filtered seawater samples, were normalized to a salinity of 35 and compared with the calculated values from the rate expression of *King and Saltzman* [1997]. Ninety percent of the measured chemical loss rate constants lay within $\pm$ 0.03 d^{-1} (or $\pm$ 20%) of the calculated rate constants.

Biological loss rate constants, determined by subtracting the chemical loss rate constants from the total loss rate constants, were in the range of 0 to 0.24 (mean 0.09; sd. 0.06) d^{-1}. They contributed 0 to 73% of the total loss rate. *Tokarczyk and Saltzman*

[2001] measured biological loss rate constants in some of the same areas as the current study during the Gas Exchange Experiment (GasEx 98) (Figure 3.5). Although these two studies were 12 years apart and they were conducted in different months, no significant discrepancy was observed in the measured biological degradation rate constants from the overlapped areas, suggesting that temporal variability of CH_3Br biological loss rate constants may be small. Geographically, CH_3Br biological loss rate constants in the eastern Atlantic are similar to those in the northern Pacific ($30^o - 60^o$ N) and the Southern Ocean, but higher than the biological loss rate constants observed in the Caribbean Sea, the eastern and central Pacific ($10^o - 30^o$ N) (Figure 3.5). There is not enough information at this time available to explain the spatial differences. Including results from all of the previous biological loss rate constant measurements (Figure 3.5) [*Tokarczyk and Saltzman*, 2001; *Tokarczyk et al.*, 2001, 2003] with the data from this study yields a global mean biological loss rate constant of 0.05 ± 0.01 d^{-1} (at a 95% confidence level) for the open ocean.

3.3.3 Extrapolated global net sea-to-air flux and global annual production rate of CH_3Br

The net sea-to-air flux, F (nmol m^{-2} d^{-1}), was determined from the following equation:

$$F = \frac{k_w}{H}\left(p_w - p_a\right) \tag{3.4}$$

where, H is Henry's Law constant of CH_3Br from *De Bruyn and Saltzman* [1997b] (m^3 atm mol^{-1}); k_w is gas transfer velocity (m d^{-1}); p_w *and* p_a are defined above
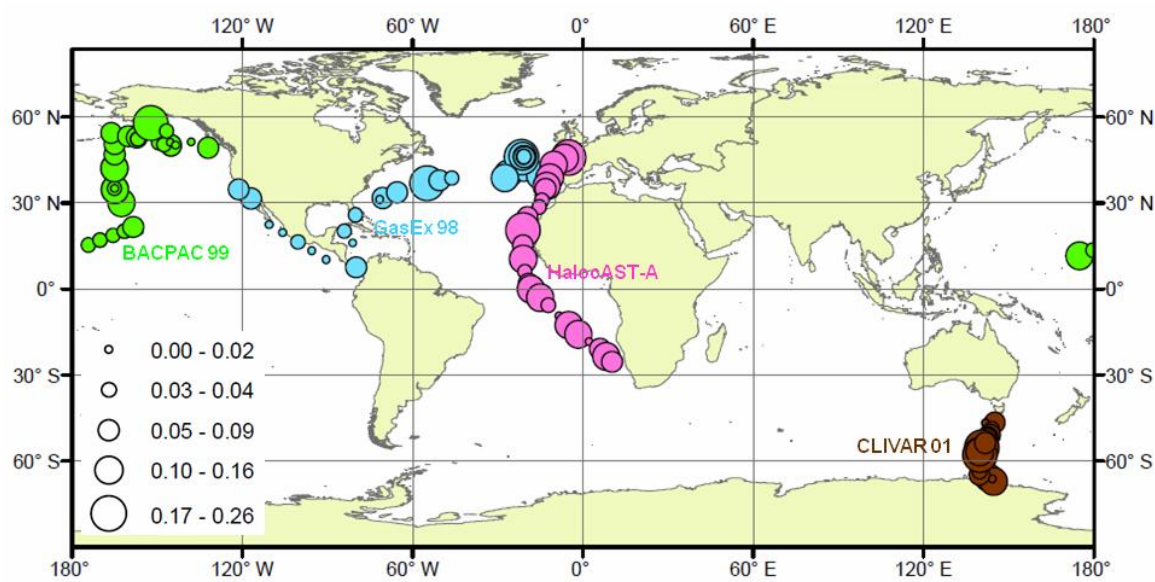
Figure 3.5. Biological degradation rate constants from this study (⊙), the Gas Exchange experiment (GasEx 98, ⊙) [*Tokarczyk and Saltzman*, 2001], the Bromine Air-sea Cruise Pacific (BACPAC 99, ⊙) [*Tokarczyk et al.*, 2001] and the Climate Variability SR3 (CLIVAR 01, ⊙) [*Tokarczyk et al.*, 2003].

(atm). To make a direct comparison with calculated fluxes from BLAST I and II, we used the parameterization of k_w from *Wanninkhof* [1992] (Equation 3.5).

$$k = 0.31u^2 \left(Sc/660 \right)^{-1/2}$$ (3.5)

where *u* stands for wind speed and *Sc* is the Schmidt number of CH_3Br.

According to the water mass designations from *Lobert et al.* [1995, 1996], we divided calculated fluxes into four regions: open ocean, coastal and coastal influential region, upwelling region and inland passage. Fluxes in open ocean, coastal and coastal influential region and upwelling region were used to estimate the global net sea-to-air flux from the surface ocean [*Lobert et al.*, 1995]. Estimated net sea-to-air fluxes for the open ocean, coastal and coastal influential region and upwelling areas in 2010 were 0.05 Gg yr^{-1}, 2.3 Gg yr^{-1} and 0.1 Gg yr^{-1} (Table 3.3), respectively. The global net sea-to-air flux was 2.5 Gg yr^{-1} in 2010, which was a 15 Gg yr^{-1} increase over that observed during the BLAST cruises in 1994 [*Lobert et al.*, 1995].

An assumed constant annual production rate of CH_3Br in surface ocean was used in time-dependent models to predict atmospheric CH_3Br concentration when removing anthropogenic emissions [*Butler*, 1994] or simulate atmospheric CH_3Br concentration during the atmospheric CH_3Br phase-down [*Yvon-Lewis et al.*, 2009]. However, whether this assumption is true is not clear. Data from BLAST and HalocAST studies provide observational evidences for this assumption. The CH_3Br production rate in the surface ocean, *P* (Gg yr^{-1}), was calculated with the equation given by *Yvon-Lewis et al.* [2002] and *Hu et al.* [2010]:

Table 3.3. The global CH_3Br saturation anomaly, the global net sea-to-air flux, and the global oceanic production rate of CH_3Br. The global ocean area, $361 \times 10^{12}\,m^2$, and the area weight are from *Kossina* [1921] and *Lobert et al.* [1995]. The calculated saturation anomaly, flux and production rates in open ocean excludes the data from $13^o - 20^o\,S$ during HalocAST-A.

	Area Weight	Wind Speed (m s^{-1})	Δ_{CH3Br} (%)	Flux (Gg yr^{-1})	Production (Gg yr^{-1})
Open Ocean	0.8	6.97	0.3	0.05	1.3×10^2
Coastal	0.1	7.72	29.5	2.3	9.4
Upwelling	0.1	6.28	2.4	0.1	23
Global			3.4	2.5	1.6×10^2

$$P = \left| \frac{k_w}{z} \frac{(\Delta - \Delta_{CFC-11})p_a}{100H} + \left(k_{chem} + k_{bio} + \frac{\sqrt{D_z k_z}}{z} \right) C_w \right| zA \qquad (3.6)$$

where, Δ and Δ_{CFC-11} are saturation anomalies of CH_3Br and CFC-11; k_{chem}, k_{bio} and

$\frac{\sqrt{D_z k_z}}{z}$ are chemical, biological and eddy degradation rate constants [e.g., *Butler*,

1994]; D_z is the thermocline diffusivity (1 ± 0.4 cm^2 s^{-1}[*Feely et al.*, 2002]); z is mixed

layer depth (m); k_z is chemical degradation rate constant in the thermocline; both k_z and

k_{chem} are functions of temperature and salinity [*King and Saltzman*, 1997]; C_w is CH_3Br

mass concentration in the surface seawater; A stands for the surface area of open ocean,

coastal ocean or upwelling regions; and all other variables are defined above. For

HalocAST-A, we used measured biological degradation rate constants in the calculation

of production rates whereas a global mean biological degradation rate constant (0.05 ($\pm$

0.06, 1 sd.) d^{-1}) was used to calculate the production rate during HalocAST-P. The

global oceanic production rate for CH_3Br was estimated at 1.6 (1.4 – 1.8) X 10^2 Gg yr^{-1}

in 2010. *Lobert et al.* [1995] did not include the biological loss when they estimated the

production rate in 1994. If considering the biological degradation (0.05 ($\pm$ 0.06, 1 sd.) d^{-}

^{1}), the annual production rate would be 1.6 (1.3 – 1.9) X 10^2 Gg yr^{-1}in 1994, suggesting

that the annual production rate of CH_3Br in surface ocean may have remained relatively

constant over the past 16 years.

3.3.4 Estimating global oceanic emission, global oceanic uptake rate and global net sea-to-air flux of CH_3Br using 1° x 1° gridded model

Extrapolated annual net sea-to-air flux of CH_3Br from HalocAST data, 2.5 Gg yr$^-$^{1}, suggests that the ocean became a net small source to atmospheric CH_3Br in 2010. Since the extrapolated flux could be biased by regional in-situ wind speeds or regional in-situ saturation anomalies from two cruises, a better approach is needed to evaluate how the spatial and temporal variability of wind speeds or surface seawater properties may affect the estimate of global fluxes. The global CH_3Br net sea-to-air flux before the phaseout was estimated with the global gridded climatological wind speeds and global gridded saturation anomalies derived from an empirical relationship observed between saturation anomaly and sea surface temperature ($\Delta\%$ - SST) [*King et al.*, 2002; *WMO*, 2003; *Yvon-Lewis and Butler*, 1997]. However, an increase in saturation anomalies of CH_3Br observed during this study results in an invalidation of this relationship (Figure 3.6). Simply moving the curve upward by the offset between the global mean open-ocean saturation anomaly in 2010 and that before the phaseout [*King et al.*, 2002], 15 %, can well represent the saturation anomalies from HalocAST-A, but not for those from HalocAST-P (Figure 3.6). It is not possible to build a new meaningful $\Delta\%$ - SST relationship until atmospheric CH_3Br reaches a new steady state.

Another approach to determine global net sea-to-air flux is to calculate the difference between global oceanic emission and global oceanic uptake rate [e.g., *Yvon-Lewis et al.*, 2009]. The oceanic emission (E, Gg yr^{-1}) can be determined by the production rate multiplying the fraction that is emitted to the atmosphere (Equation 3.7)
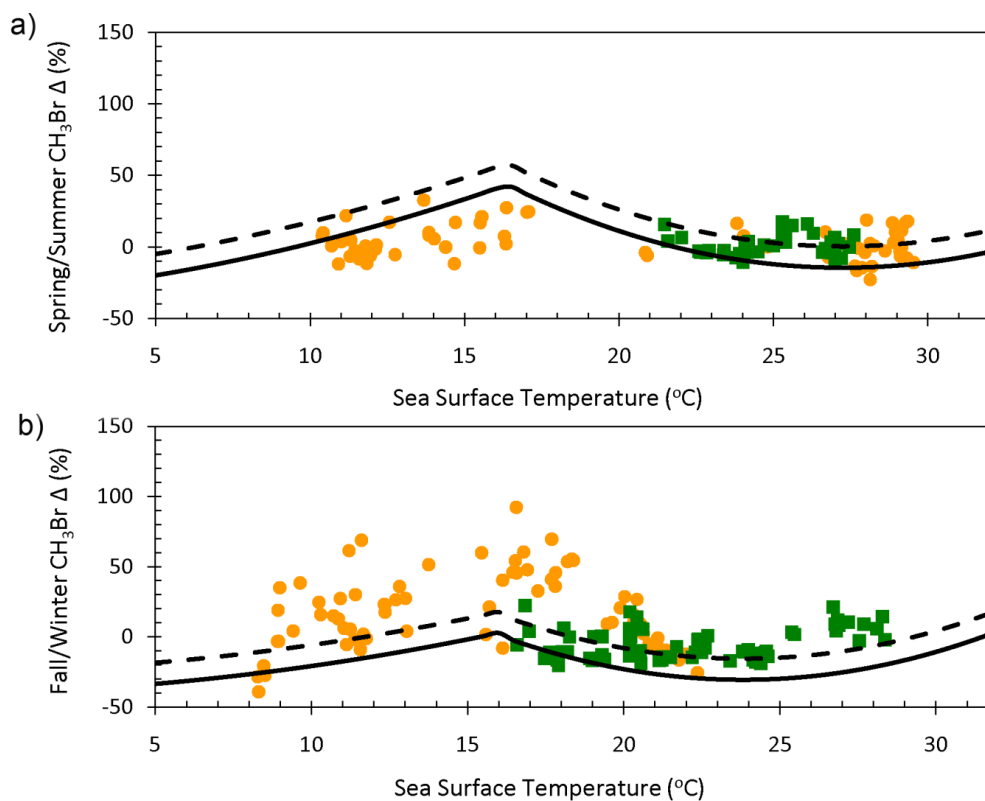
Figure 3.6. Observed CH$_3$Br saturation anomalies (Δ%) as a function of sea surface temperature (SST) in the spring/summer (a) and the fall/winter (b) during the HalocAST-P (⬤) and HalocAST-A (⬛). The solid black line represents the calculated saturation anomalies using the Δ(%) - SST relationship from *King et al.* [2002]. The black dash line stands for the derived Δ(%) from SA-SST relationship plus 15 %, which is the offset between the current global mean open-ocean saturation anomaly (Table 3) and the one before the phaseout (before 1998) [*King et al.*, 2002].

[*Lobert et al.*, 1996; *Yvon-Lewis and Butler*, 2002] whereas the oceanic uptake rate (U, Gg yr^{-1}) can be computed by the oceanic uptake rate constant times the atmospheric CH$_3$Br abundance (Equation 3.8) [*Yvon-Lewis and Butler*, 2002].

$$E = P \frac{\dfrac{k_w}{z}}{k_{chem} + k_{bio} + \dfrac{\sqrt{D_z k_z}}{z} + \dfrac{k_w}{z}} \tag{3.7}$$

$$U = k_{ocn} \chi_a n_{atm} = \chi_a p_{atm} \frac{k_w A}{H} \frac{k_{chem} + k_{bio} + \dfrac{\sqrt{D_z k_z}}{z}}{k_{chem} + k_{bio} + \dfrac{\sqrt{D_z k_z}}{z} + \dfrac{k_w}{z}} \tag{3.8}$$

where, k_{ocn} is the global oceanic uptake rate constant (yr^{-1}), χ_a is atmospheric CH$_3$Br mixing ratio; n_{atm} is the mass of the atmosphere (mol) and p_{atm} is the atmospheric pressure at the surface (1 atm). As mentioned above, chemical and eddy degradation rate constants are functions of temperature and salinity, which are not likely to have a significant change since 1994. The annual production rate and biological degradation rate constant of CH$_3$Br in surface ocean are likely to have remained constant over the past 16 years, as shown in our results (Sections 3.4.2 and 3.4.3). Therefore, the annual emission rate of CH$_3$Br is not likely to change significantly before and during the fumigation − non-QPS phaseout since it is a function of production rate, chemical, biological and eddy degradation rate constants (Equation 3.7). By substituting production rate (P) in equation (3.7) with equation (3.6), equation (3.7) can then be expressed as follows:

$$E = \frac{k_w A \chi_a P_{atm} \left[\dfrac{k_w}{z} \dfrac{\Delta}{100H} + \left(k_{chem} + k_{bio} + \dfrac{\sqrt{D_z k_z}}{z} \right)\left(\dfrac{100}{(100-\Delta)H} \right) \right]}{k_{chem} + k_{bio} + \dfrac{\sqrt{D_z k_z}}{z} + \dfrac{k_w}{z}}$$
(3.9)

Because saturation anomaly (Δ%) of CH_3Br in surface ocean was a function of sea surface temperature before the atmospheric CH_3Br phase-down, we can use this empirical relationship to calculate saturation anomalies of CH_3Br and its global oceanic emission during the pre-phaseout, and then apply it to 2010.

To account for spatial and monthly variation of surface ocean properties and surface wind speeds, equations (3.8) and (3.9) are applied to a 1° x 1° gridded dataset, DS279 (NOAA/GFDL Global Oceanographic Data Set Atlas, downloaded from http://dss.ucar.edu/datasets/ds279.0/), which contains monthly gridded sea surface temperature, salinity, wind speed, and mixed layer depth. The monthly global oceanic emission and monthly global oceanic uptake rate are then expressed by:

$$E_m = \sum_{i=-90}^{i=90} \sum_{j=-180}^{j=180} k_{w,i,j,m} A_{i,j,m} \chi_{a,1996\text{-}1998i,j,m} P_{atm} \left(\frac{\Delta_{i,j,m}(1 - R_{i,j,m})}{100 H_{i,j,m}} + \frac{100 R_{i,j,m}}{H_{i,j,m}(100 - \Delta_{i,j,m})} \right)$$
(3.10)

$$U_m = p_{atm} \sum_{i=-90}^{i=90} \sum_{j=-180}^{j=180} \frac{k_{w,i,j,m} A_{i,j,m} R_{i,j,m} x_{a,year,m,i,j}}{H_{i,j,m}}$$
(3.11)

where, $R = \dfrac{k_{chem} + k_{bio} + \dfrac{\sqrt{D_z k_z}}{z}}{k_{chem} + k_{bio} + \dfrac{\sqrt{D_z k_z}}{z} + \dfrac{k_w}{z}}$; i and j stand for the indices of latitude and

longitude of each grid cell; m stands for the index of month; $\chi_{a,1996\text{-}1998,m}$ and $\chi_{a,year,m}$ are monthly mean atmospheric mixing ratios of CH_3Br during $1996 - 1998$ (before the

CH$_3$Br phase-down) and monthly CH$_3$Br mixing ratio in the year of interest (e.g. 2010). We use the northern hemispheric or southern hemispheric mean mixing ratios for gridded cells in the NH or the SH. The monthly hemispheric CH$_3$Br mixing ratios are from NOAA/ESRL Global Monitoring Division, Boulder, CO (ftp://ftp.cmdl.noaa.gov/hats/methylhalides/ch3br/flasks/CH3BR_GCMS_flask.txt).

Equations (3.10 − 3.11) present an approach used in prior studies [*Yvon-Lewis and Butler*, 1997; *Yvon-Lewis et al.*, 2009] to calculate the global oceanic emission and global oceanic uptake rate before and during the atmospheric CH$_3$Br phase-down. However, they did not consider the difference between the coastal ocean and the open ocean. This may result in an underestimate on the global net sea-to-air flux since the coastal ocean is more supersaturated with CH$_3$Br [e.g., *Hu et al.*, 2010; *Sturrock et al.*, 2003] compared to the open ocean [e.g., *Lobert et al.*, 1995]. Therefore, we improved equations (3.10 − 3.11) by separating the open-oceanic and coastal-oceanic areas and used a different approach to calculate the coastal oceanic emission because the Δ% - SST relationship was only applicable in the open ocean. Here, we define the areas with water depths less than 200 m as coastal ocean. Coastal oceanic area in each gridded cell was calculated based on the bathymetric data from the 1' X 1' global relief database, ETOPO (http://www.ngdc.noaa.gov/mgg/gdas/gd_designagrid.html). Improved global oceanic emission and global oceanic uptake rate were calculated by equations (12 − 13).

$$E_m = \left(\sum_{i=-90}^{i=90} \sum_{j=-180}^{j=180} k_{w,i,j,m} A_{o,i,j,m} \chi_{a,1996\text{-}1998i,j,m} P_{atm} \left(\frac{\Delta_{i,j,m}(1-R_{i,j,m})}{100 H_{i,j,m}} + \frac{100 R_{i,j,m}}{H_{i,j,m}(100-\Delta_{i,j,m})} \right) \right)_{open\text{-}ocean}$$
$$+ \left(\sum_{i=-90}^{i=90} \sum_{j=-180}^{j=180} P_c R_{i,j,m} A_{c,i,j,m} z_{i,j,m} \right)_{coastal\text{-}ocean}$$

$$(3.12)$$

$$U_m = \left(P_{atm} \sum_{i=-90}^{i=90} \sum_{j=-180}^{j=180} \frac{k_{w,i,j,m} A_{o,i,j,m} R_{i,j,m} x_{a,2010 m,i,j}}{H_{i,j,m}} \right)_{open\text{-}ocean}$$
$$+ \left(P_{atm} \sum_{i=-90}^{i=90} \sum_{j=-180}^{j=180} \frac{k_{w,i,j,m} A_{c,i,j,m} R_{i,j,m} x_{a,2010 m,i,j}}{H_{i,j,m}} \right)_{coastal\text{-}coean}$$

$$(3.13)$$

where, A_o and A_c stand for the open-oceanic and coastal-oceanic areas in gridded cells; and P_c represents CH_3Br production rate in the coastal ocean (nmol m^{-3} yr^{-1}).

Five scenarios were run to evaluate the effect of our improvement (Equations 3.12 – 3.13) on the estimate of global oceanic emission, global oceanic uptake rate and global net sea-to-air fluxes. We also examined the sensitivities of the model on the production rates of CH_3Br in the coastal ocean because the production rate in coastal ocean may be highly variable from one location to another [*Hu et al.*, 2010; *Sturrock et al.*, 2003], depending on the biological productivity, phytoplankton groups, influence from terrestrial transport and human impact. In scenarios (1 – 2), we used the old gridded ocean model (Equations 3.10 – 3.11) [*Yvon-Lewis and Butler*, 1997; *Yvon-Lewis et al.*, 2009] and looked at the effect of an updated parameterization of gas transfer velocity on the estimated oceanic budget of CH_3Br. Results suggest that the use of an updated parameterization from *Sweeney et al.* [2007] would yield a lower global oceanic emission, a less negative oceanic uptake rate and a more positive net sea-to-air flux

(Table 3.4), compared to using an old parameterization from *Wanninkhof* [1992]. In contrast to the first two scenarios, we separated the coastal-oceanic areas from the open-oceanic areas in scenarios (3 − 5) (Equations 3.12 − 3.13). In scenario 3, we assigned a uniform production rate of 0.61 nmol m^{-3} d^{-1} (the mean production rate of CH_3Br from coastal areas of HalocAST and GOMECC [*Hu et al.*, 2010]) and a biological degradation rate constant of 0.09 d^{-1} (the mean biological degradation rate constant observed off the coast of Florida [*King and Saltzman*, 1997]) to all coastal-oceanic areas and used a global mean biological degradation rate constant of 0.05 d^{-1} in open-oceanic areas. This yields a global net sea-to-air flux of -7 Gg yr^{-1} during 1996 − 1998 and 2 Gg yr^{-1} for 2010, which are 3 Gg yr^{-1} higher than the estimated fluxes from scenarios (1 − 2) for both the pre-phaseout and the end of phaseout (Table 3.4), suggesting it is important to consider the difference between coastal ocean and open ocean. Although the spatial distribution of biological degradation rate constants and production rates may affect our estimate on the oceanic emission, oceanic uptake rates and net sea-to-air fluxes, it is difficult to find a spatial pattern or seasonal variation in the surface ocean for these two parameters (Figure 3.5 and *Hu et al.* [2010]), which can be applied to our model. Scenarios 4 and 5 test the sensitivity of our model on the production rate of CH_3Br in the coastal ocean. The mean production rate of CH_3Br in the coastal areas of GOMECC, 0.76 nmol m^{-3} d^{-1} [*Hu et al.*, 2010], is significantly higher than that from the coastal areas of HalocAST, 0.25 nmol m^{-3} d^{-1}. Since both studies were conducted in different regions and different seasons, it is difficult to argue either one is more representative than the other. Therefore, we ran the model (Equations 3.12 − 3.13) by using a coastal

Table 3.4. Estimated global oceanic emissions, global oceanic uptake rates and global net sea-to-air fluxes of CH$_3$Br before the atmospheric CH$_3$Br phase-down (1996 – 1998) and at the end of its phase-down (2010) with the 1° x 1° gridded model described in Section 3.4.4. Scenarios (1 – 2) use the old gridded ocean model (Equations 3.10 – 3.11) [*Yvon-Lewis and Butler*, 1997] with higher spatial resolution. Scenario (1) uses the parameterization of gas transfer velocity from *Wanninkhof* [1992] whereas scenario (2) uses an updated parameterization from *Sweeney et al.* [2007]. Scenarios (3 – 5) use the improved gridded ocean model (Equations 3.12 – 3.13) with different production rates of CH$_3$Br in the coastal ocean, which are 0.61 nmol m^{-3} d^{-1}, 0.76 nmol m^{-3} d^{-1} and 0.25 nmol m^{-3} d^{-1}, respectively.

Scenarios	1996 - 1998 or 2010	1996 - 1998		2010	
	Oceanic Emission (Gg yr^{-1})	Oceanic Uptake Rate (Gg yr^{-1})	Net Sea-to-Air Fluxes (Gg yr^{-1})	Oceanic Uptake Rate (Gg yr^{-1})	Net Sea-to-Air Fluxes (Gg yr^{-1})
1	40	-54	-14	-41	-1
2	31	-41	-10	-32	-1
3	34	-41	-7	-32	2
4	35	-41	-6	-32	3
5	32	-41	-9	-32	0

production rate of 0.76 nmol m^{-3} d^{-1} and 0.25 nmol m^{-3} d^{-1} in scenarios 4 and 5, resulting in a global net sea-to-air flux of 3 and 0 Gg yr^{-1}, respectively. Considering this as one of the uncertainties for the model, along with the uncertainties from the mean biological degradation rate constants (±0.01 d^{-1} in open ocean and ±0.02 d^{-1} in coastal ocean), gas transfer velocity (± 32 %, *Sweeney et al.*, 2007), the solubility (± 4 %, *De Bruyn and Saltzman*, 1997b), the mixed layer depth (± 30 % [*Yvon-Lewis and Butler*, 2002]), the global net sea-to-air flux of CH$_3$Br in 2010 was estimated at 2 (-0.5 – 3) Gg yr^{-1}.

3.3.5. An improved estimate of the oceanic lifetime of atmospheric CH$_3$Br

The current best estimate of the partial atmospheric lifetime of CH$_3$Br with respect to the oceanic loss, 1.8 − 1.9 (a full range: 1.1 - 3.9) years [*Yvon-Lewis and Butler*, 1997], was based on a 2° x 2° grid of physical properties in and over the global ocean. Biological loss rate constants used in their study were based on the measurements conducted on samples from the coast of Florida [*King and Saltzman*, 1997]. Here, we revised the partial atmospheric lifetime using the numerical model described in *Yvon-Lewis and Butler* [2002] with modifications to address the coastal and open ocean areas separately and with a better understanding of the biological loss rate constant.

The partial atmospheric lifetime (τ_{ocn}, years) was calculated by the reciprocal of the global oceanic uptake rate constant (k_{ocn}). It is expressed as follows:

$$
\tau_{ocn} = \frac{1}{\sum\limits_{i=-90}^{i=90} \sum\limits_{j=-180}^{j=180} k_{ocn,i,j}}
$$

$$
= \frac{n_{atm}}{p_{atm}} \frac{1}{\left(\sum\limits_{i=-90}^{i=90} \sum\limits_{j=-180}^{j=180} \frac{k_{w,i,j,m} A_{o,i,j,m} R_{i,j,m}}{H_{i,j,m}} \right)_{open-ocean} + \left(\sum\limits_{i=-90}^{i=90} \sum\limits_{j=-180}^{j=180} \frac{k_{w,i,j,m} A_{c,i,j,m} R_{i,j,m}}{H_{i,j,m}} \right)_{coastal-coean}}
$$

(3.14)

where, all the variables are defined above. The best estimate of the partial atmospheric lifetime of CH_3Br with respect to oceanic uptake is now estimated at 3.1 (2.3 − 5.0) years, which is about 1.3 years longer than the prior best estimate.

The total atmospheric lifetime, τ, was determined from the sum of the reciprocal of each loss process:

$$\frac{1}{\tau} = \frac{1}{\tau_{OH}} + \frac{1}{\tau_{soil}} + \frac{1}{\tau_{ocn}} + \frac{1}{\tau_{str}} \qquad (3.15)$$

where, τ_{OH}, τ_{soil}, τ_{ocn}, and τ_{str} are partial atmospheric lifetimes due to reaction with OH radicals (1.7 years with a range of 1.5 -1.9 years [*Montzka and Reimann*, 2011; *Yvon and Butler*, 1996]), loss to soils (3.3 − 3.4 years [*Montzka and Reimann*, 2011), uptake by the ocean (3.1 years with a range of 2.3 − 5.0 years), and loss to stratospheric photolysis (35 years [*WMO*, 1994, 2011]). The overall atmospheric lifetime of CH_3Br was estimated at 0.8 (0.7 − 0.9) years, which is comparable with the best prior estimate on the atmospheric lifetime [*Montzka and Reimann*, 2011; *Yvon-Lewis et al.*, 2009].

3.4. Summary and conclusions

Saturation anomalies of CH_3Br observed during this 2010 study in the eastern Pacific and the eastern Atlantic, near the end of the phase-out of fumigation-non-QPS uses of CH_3Br, were less negative than those observed 16 years prior in similar regions. The global mean saturation anomalies of CH_3Br in the open ocean, coastal ocean and upwelling region were positive with values of 0.3 %, 29.5 %, and 2.6 % in 2010.

Measured CH_3Br biological loss rate constants in the eastern Atlantic ranged from 0 to 0.24 d^{-1}, with little difference from results from the same regions examined in

previous studies. When considering all previous biological loss rate constant measurements and those from this study, the mean biological loss rate constant for the open ocean is 0.05 ($\pm$ 0.01) d^{-1}. Using the calculated chemical and eddy loss rate constants and the modified global mean biological loss rate constant, the estimated partial atmospheric lifetime of CH_3Br is 3.1 (2.3 – 5.0) years, yielding an overall atmospheric lifetime for CH_3Br of 0.8 (0.7 – 0.9) years.

The global net sea-to-air flux ranged from -0.5 Gg yr^{-1} to 3 Gg yr^{-1} in 2010 based on both simple global extrapolation and a $1^\circ \times 1^\circ$ grid model. Given the uncertainties, this suggests that CH_3Br in the surface ocean has reached, on average, a near-equilibrium with CH_3Br in the atmosphere, owing to the declining in atmospheric burden following anthropogenic emission reductions. If anthropogenic CH_3Br emissions continue to decline, the atmospheric CH_3Br mixing ratio will continue to decrease and the CH_3Br saturation anomaly in the surface ocean should become more positive. This would result in a positive net sea-to-air flux for CH_3Br.

Calculated annual production rates of CH_3Br in surface ocean are comparable between 1994 and 2010, suggesting that annual production rate of CH_3Br in surface ocean may have remained constant over the past 16 years. Since the oceanic production rates and biological, chemical and eddy loss rate constants are relatively constant, the oceanic emission rate and the oceanic uptake rate constant will remain the same. Therefore, for those compounds with oceanic sources and sinks and changing atmospheric abundances, it is better to link their atmospheric budgets to the oceanic production rates and the uptake rate constants rather than their net fluxes.

4. AN IMPROVED OCEANIC BUDGET OF METHYL CHLORIDE*

4.1 Introduction

Chlorine-containing gases catalytically destroy ozone in the stratosphere. CH_3Cl is the most abundant natural chlorine contributor to the stratospheric chlorine. Although the atmospheric mixing ratio of CH_3Cl has remained relatively constant over the past decades, its relative importance in stratospheric ozone depletion is increasing as anthropogenic chlorine decreases in the atmosphere. Nevertheless, sources and sinks of atmospheric CH_3Cl remain poorly quantified [*Montzka and Reimann et al.*, 2011].

The ocean, both a source and a sink for atmospheric CH_3Cl, plays a significant role in the global biogeochemical cycling of CH_3Cl. The net sea-to-air flux of CH_3Cl is a function of the gas transfer velocity, the solubility and the saturation anomaly. In turn, all of these are fundamentally a function of temperature, salinity and wind speed, each of which is anticipated to change in the future with changing climate. The parameterization for gas transfer velocity was recently revised by *Sweeney et al.* [2007], reducing the gap between parameterizations based on field measurements [*Liss and Merlivat*, 1986; *Nightingale et al.*, 2000] and those based on radiocarbon estimates [*Tans et al.*, 1990; *Wanninkhof*, 1992].

The solubility of CH$_3$Cl in seawater was measured by *Elliott and Rowland* [1993], *Moore et al.* [1995] and *Moore* [2000] and expressed as only a temperature-dependent function. Variation in salinity can change the solubility from one place to another [e.g., *De Bruyn and Saltzman*, 1997; *Weiss and Price*, 1980]. It is necessary to include the salinity dependence into the solubility function of CH$_3$Cl so that we can have a better estimate on its global net sea-to-air flux.

The saturation anomaly (Δ%) is defined here as the percent difference between the partial pressure in air and that in surface seawater. A relationship between the saturation anomaly of CH$_3$Cl and sea surface temperature (SST) has been used in the past to assess the global air-sea flux of CH$_3$Cl [*Khalil et al.*, 1999; *Yoshida et al.*, 2004]. However, there are two limitations to the old CH$_3$Cl Δ% - SST relationship. First, it does not include the seasonality of CH$_3$Cl in surface seawater. Second, it may not be applicable to coastal environments since there were few coastal measurements included at the time when the Δ% - SST relationship was developed. Results from field campaigns over the past two decades provide an extensive database from the oceans around the world [*Butler et al.*, 2007; *Hu et al.*, 2010; *Khalil et al.*, 1999; *King et al.*, 2002; *Lobert et al.*, 1996; *Moore et al.*, 1996; *Yvon-Lewis et al.*, 2004], allowing a better quantification of spatial distribution and temporal variability of CH$_3$Cl saturation anomalies in surface ocean.

Here, we present the results of CH$_3$Cl solubility measurements made over the range of temperatures and salinities applicable to the global surface ocean. We also develop a more robust relationship between CH$_3$Cl saturation anomaly and SST and

wind speed. We then use the new solubility function, the new $\Delta\%$ - (SST, wind speed) relationship and the revised gas exchange coefficient from *Sweeney et al.* [2007] to examine the global oceanic emission and oceanic uptake of CH_3Cl using a 1° x 1° grid model [e.g., *Butler*, 1994; *Hu et al.*, submitted; *Yvon-Lewis and Butler*, 2002]. Results of this study provide a substantial improvement on the current knowledge of CH_3Cl in the surface ocean.

4.2 Methods

4.2.1 Solubility experiment

To determine the solubility of CH_3Cl, a gas mixture of CH_3Cl and chlorofluorocarbons 11 and 12 (CFC-11 and CFC-12) was equilibrated with pure water and seawater at temperatures from 0 to 40 ^{o}C. The solubilities of CFC-11 and CFC-12 were well quantified by *Warner and Weiss* [1985] and were used as reference gases to determine the reliability of our experimental setup.

Our equilibrium apparatus was a modified version of the one used by *Warner and Weiss* [1985] (Figure 4.1). A 1-L cylindrical glass equilibration chamber (~ 0.6 L of water and ~ 0.4 L of headspace) was placed inside a jacket filled with 30% ethylene glycol solution that circulates in a temperature-controlled water bath. The temperature of the equilibrium chamber varied within < ±0.04 ^{o}C during the equilibration time (about 32 hours, which was determined at the most soluble condition studied in the lab, 0.5 ^{o}C in MilliQ water). The gas mixture with concentrations 6 - 14 times above ambient flowed through a humidifier into the headspace of the chamber at 25 ml min^{-1}. The gas
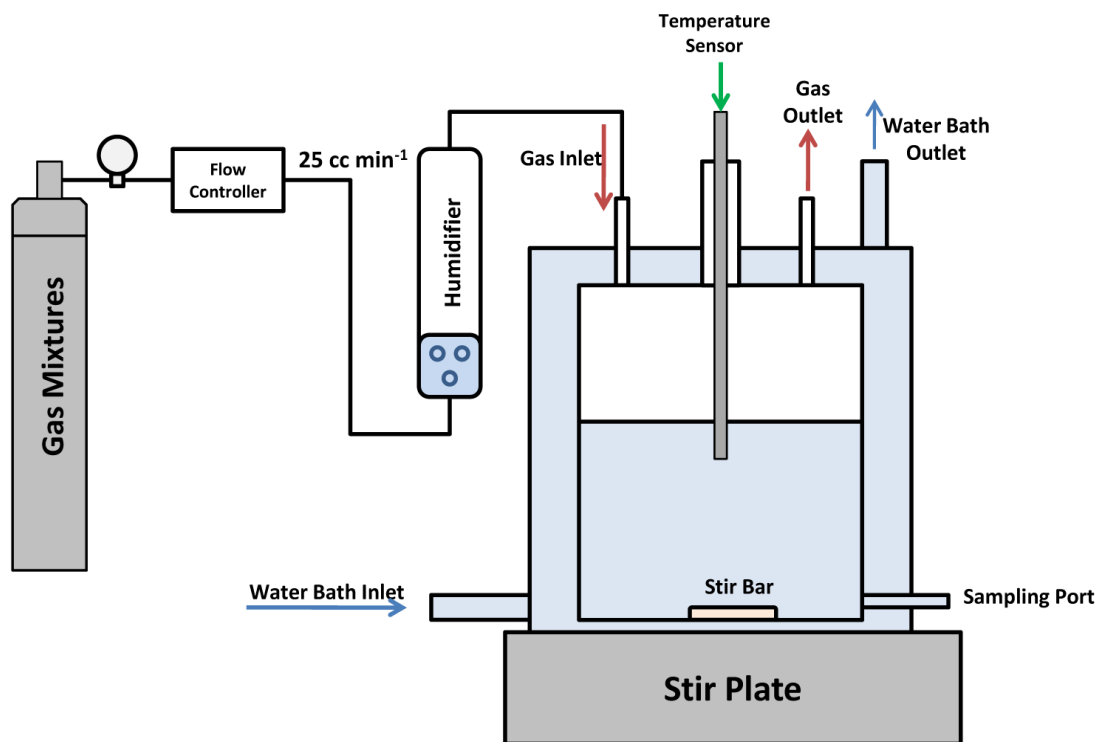
Figure 4.1. Schematic diagram of the equilibration apparatus. Gas mixtures of CH_3Cl, CFC-11 and CFC-12 flow through a humidifier to the equilibrator headspace at 25 ml min^{-1}. Gases in the headspace are constantly equilibrating with the well-mixed seawater or fresh water at a controlled temperature. The gas outlet that comes out of the equilibrator chamber is submerged into a beaker filled with water by 2 - 4 cm to avoid backflow of outside air. A digital temperature sensor is inserted into the water to constantly monitor and log the temperature of the water.

outlet from the chamber headspace was then submerged into a beaker filled with water by 2 - 4 cm to avoid backflow of outside air. The pure water used in the experiment was MilliQ water with a resistance of 18 Ω. The seawater (salinity = 31.84) used in the experiment was filtered through a 0.2 μm nylon membrane with glass microfiber prefilter. Filtered seawater with salinity of 16.08 was used to validate the derived solubility function. The aliquants of equilibrated water containing CH_3Cl, CFC-11 and CFC-12 were analyzed using purge-and-trap gas chromatography and mass spectrometry (GC-MS). Headspace concentrations were also quantified by GC-MS. Both the headspace concentrations and the water concentrations were calibrated by a whole air standard that was calibrated against a gravimetric standard from NOAA/ESRL Global Monitoring Division, in Boulder, Colorado.

When the total pressure is close to 1 atm and the dry mole air fraction of a trace gas, x, is much less than 1, as it is for these gases, the equilibrium concentration, C (mol L^{-1}), can then be expressed by:

$$C = Hx(p - p_{H_2O}) \tag{4.1}$$

where, H is the solubility coefficient (mol L^{-1} atm^{-1}); p is the total pressure (atm), and p_{H_2O} is the partial pressure of water vapor (atm), which can be calculated using equation (4.2) [*Weiss and Price*, 1980].

$$\ln p_{H_2O} = 24.4543 - 67.4509(100/T) - 4.8489\ln(T/100) - 0.000544S \tag{4.2}$$

where, T is temperature (Kelvin) and S is salinity. Therefore, if the equilibrium concentration (C), dry mole air fraction (x), temperature (T) and salinity (S) are known, the solubility coefficient (H) can then be calculated with equations (4.1 – 4.2).

The solubility coefficient can also be formulated as a function of temperature and salinity [e.g., *Weiss*, 1970], which is expressed as:

$$\ln H = a_1 + a_2(100/T) + a_3 \ln(T/100) + S[b_1 + b_2(T/100) + b_3(T/100)^2] \qquad (4.3)$$

where, a_i and b_i (i =1, 2, and 3) are constants, which can be obtained by fitting H with T and S.

4.2.2. Saturation anomaly measurements

CH$_3$Cl and a suite of other halocarbons were measured during the Halocarbon Air-Sea Transect cruises in the eastern Pacific and the eastern Atlantic (HalocAST-P/A) in 2010 (Figure 4.2). Concentrations of CH$_3$Cl in the air and sea surface were continuously measured with a GC-MS equipped with a Weiss-type equilibrator [*Butler et al.*, 1988; *Johnson*, 1999] (Appendix C). The details of the method are described in *Hu et al.* [submitted]. The precision for the measurement of CH$_3$Cl was 7.0 % during HalocAST-P and 0.3 % during HalocAST-A. The reason that signals during HalocAST-P were much noisier than those during HalocAST-A is because we changed a new filament during HalocAST-A.

4.3. Results and discussion

4.3.1. Solubilities

Measured solubilities of CFC-11 and CFC-12 (Table 4.1; Figure 4.3) agree with calculated solubilities using the functions from *Warner and Weiss* [1985] within a difference of 1.8 (± 3.1, 1σ) % and 0.8 (± 4.4, 1σ) %. The consistency between results
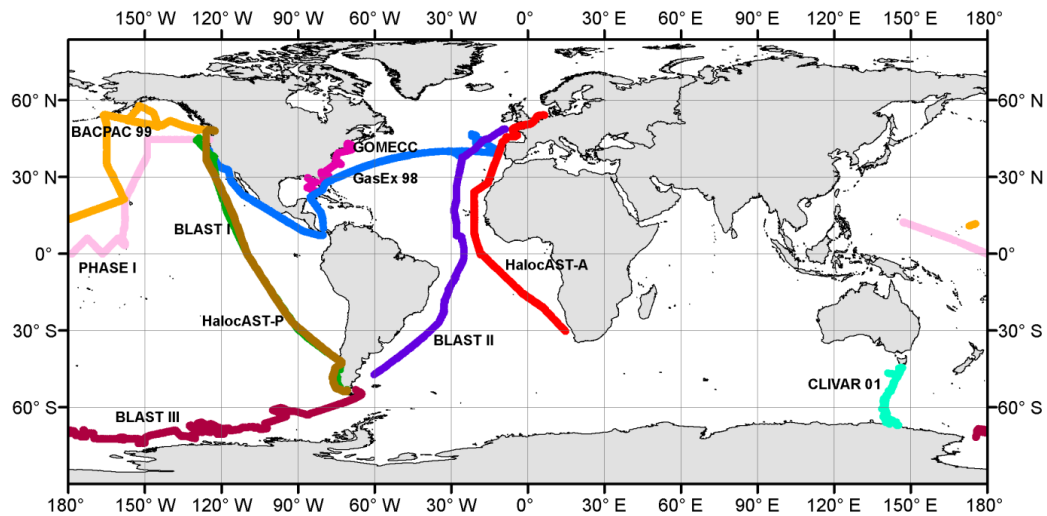
Figure 4.2. Cruise tracks of BLAST I (●, 1/28 - 2/17, 1994) [*Lobert et al.*, 1995], BLAST II (●, 10/18 - 11/21, 1994) [*Lobert et al.*, 1996], BLAST III (●, 2/22 - 4/7, 1996) [*Lobert et al.*, 1997], GasEx 98 (●, 5/7 - 7/27, 1998) [*King et al.*, 2000], BACPAC 99 (●, 9/14 - 10/23, 1999) [*King et al.*, 2002], CLIVAR 01(●,10/29 - 12/13, 2001) [*Yvon-Lewis et al.*, 2004], PHASE I 04 (●, 5/22 - 7/2, 2004) [*Butler et al.*, 2007], GOMECC (●, 7/10 – 8/4, 2007) [*Hu et al.*, 2010], HalocAST – P (●, 3/30/10 – 4/27/10) [*Hu et al.*, submitted] and HalocAST - A (●, 10/25 – 11/26，2010).
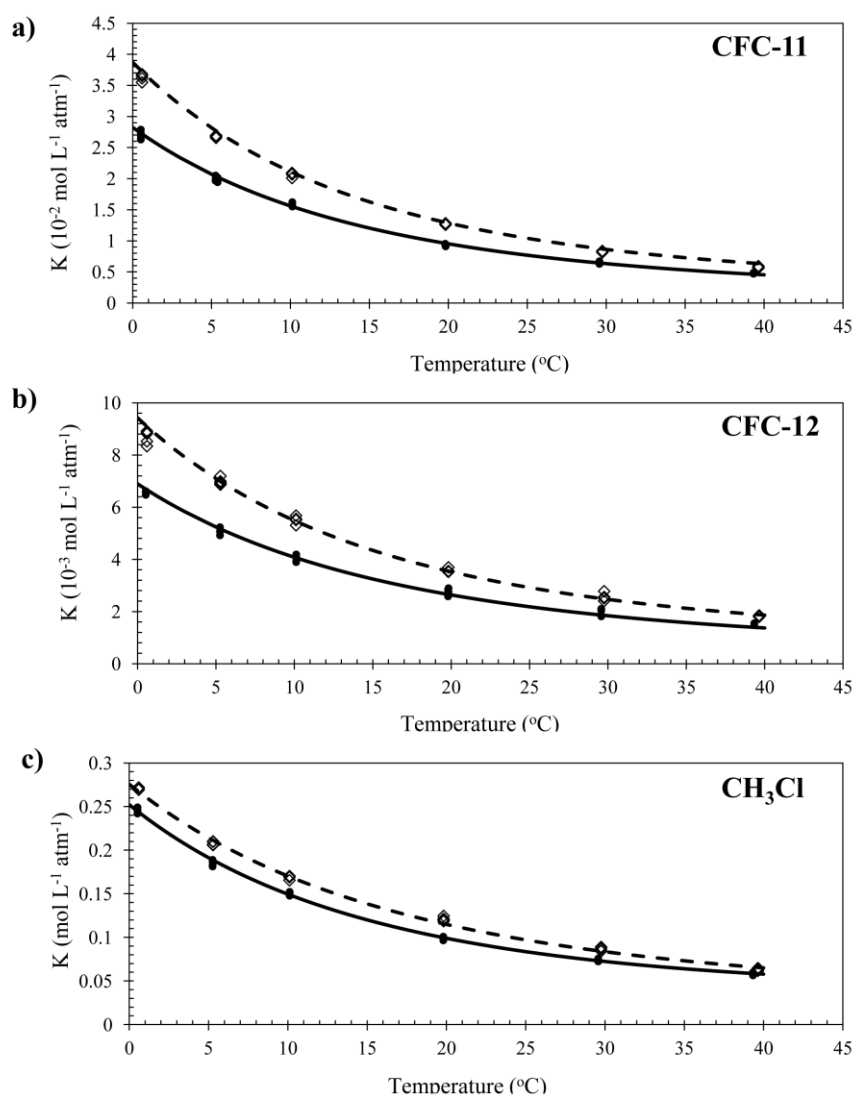
Figure 4.3. Solubility of CFC-11, CFC-12 and CH$_3$Cl in pure water and seawater (Salinity = 31.84) as a function of temperature. Open diamonds and solid circles stand for measured solubilities in pure water and seawater from this study. Dashed and solid lines in panels (a – b) represent calculated solubilities based on solubility functions from *Warner and Weiss* [1985] for pure water and seawater. Dashed and solid lines in panel (c) are the fit of equation (3) to the measured solubilities of CH$_3$Cl in pure water and seawater from this study.

Table 4.1. Solubilities of CH_3Cl, CFC-11 and CFC-12 in pure water and seawater at different temperatures. The standard deviation and the number of replicates are listed in parentheses.

Temperature	Solubilities		
	CH_3Cl (mol L^{-1} atm^{-1})	CFC-11 (10^{-2} mol L^{-1} atm^{-1})	CFC-12 (10^{-3} mol L^{-1} atm^{-1})
Pure Water			
0.594	0.2706 (±0.0014, 4)	3.630 (±0.051, 5)	8.688 (±0.247, 5)
5.283	0.2083 (±0.0020, 5)	2.682 (±0.016, 5)	6.976 (±0.136, 5)
10.1	0.1687 (±0.0022, 4)	2.061 (±0.035, 4)	5.510 (±0.154, 4)
19.82	0.1211 (±0.0025, 4)	1.272 (±0.012, 4)	3.572 (±0.082, 4)
29.8	0.0858 (±0.0020, 5)	0.8261 (±0.0109, 5)	2.495 (±0.065, 4)
39.64	0.0632 (±0.0014, 5)	0.5799 (±0.0133, 4)	1.821 (±0.027, 3)
Seawater (S=31.84)			
0.5198	0.2457 (±0.0030, 4)	2.706 (±0.062, 5)	5.609 (±0.062, 4)
5.255	0.1851 (±0.0035, 4)	2.016 (±0.042, 4)	5.074 (±0.157, 3)
10.12	0.1504 (±0.0018 5)	1.575 (±0.028 5)	4.049 (±0.127 5)
19.8	0.0991 (±0.0017, 5)	0.9438 (±0.0104, 5)	2.669 (±0.010, 5)
29.57	0.0741 (±0.0014, 5)	0.6439 (±0.0167, 5)	1.931 (±0.132, 5)
39.33	0.0577 (±0.0015, 5)	0.4777 (±0.0067, 5)	1.524 (±0.274, 4)
Seawater (S=16.08)			
14.94	0.1326 (±0.0018, 5)	1.369 (±0.024, 5)	3.861 (±0.109, 5)
27.61	0.0858 (±0.0007, 4)	0.7835 (±0.0207, 5)	2.362 (±0.112, 5)

from this study and the previous study provides assurance that our approach is not biasing results and that solubilities determined for this investigation are reliable. Solubilities of CH_3Cl at various temperatures in pure water and seawater are listed in Table 4.1. The precision (1σ) of our measurements (N = 3 – 5) was $\leq$ 2%. The constants in equation (4.3) were determined with measured solubilities and corresponding temperatures in pure water and seawater (Figure 4.3). The resulting fit to the T and S dependent solubility function is expressed as follows:

$$\ln H = -104.9 + 160.9(100/T) + 44.49\ln(T/100) \\ + S[0.3137 - 0.2150(T/100) + 0.03629(T/100)^2]$$

(4.4)

The standard error for the estimated solubility from equation (4.4) is ±0.0032 mol L^{-1} atm^{-1}, which is equivalent to an uncertainty of ±3 (±1, 1σ) %. Validation of equation (4.4) was conducted by comparing the measured solubilities to the estimated solubilities using equation (4.4) for salt water (S = 16.08) at 14.94 $\pm$ 0.03 $^{\circ}$C and 27.61 $\pm$ 0.03 $^{\circ}$C. The observed discrepancy between the measured and calculated solubilities was within the uncertainty of our experiment, ±3%, suggesting that the derived solubility expression can represent CH_3Cl solubility well.

Solubilities of CH_3Cl in seawater (S = 35) from 0 $^{\circ}$C to 40 $^{\circ}$C were calculated based on expressions from this study, *Elliott and Rowland* [1993], *Moore et al.* [1995] and *Moore* [2000] (Figure 4.4). Results using the solubility expressions from *Elliott and Rowland* [1993] and *Moore et al.* [1995] are 16 ($\pm$ 6, 1σ) % and 9 ($\pm$ 7, 1σ) % higher than those from the current study. Although the mean difference between results
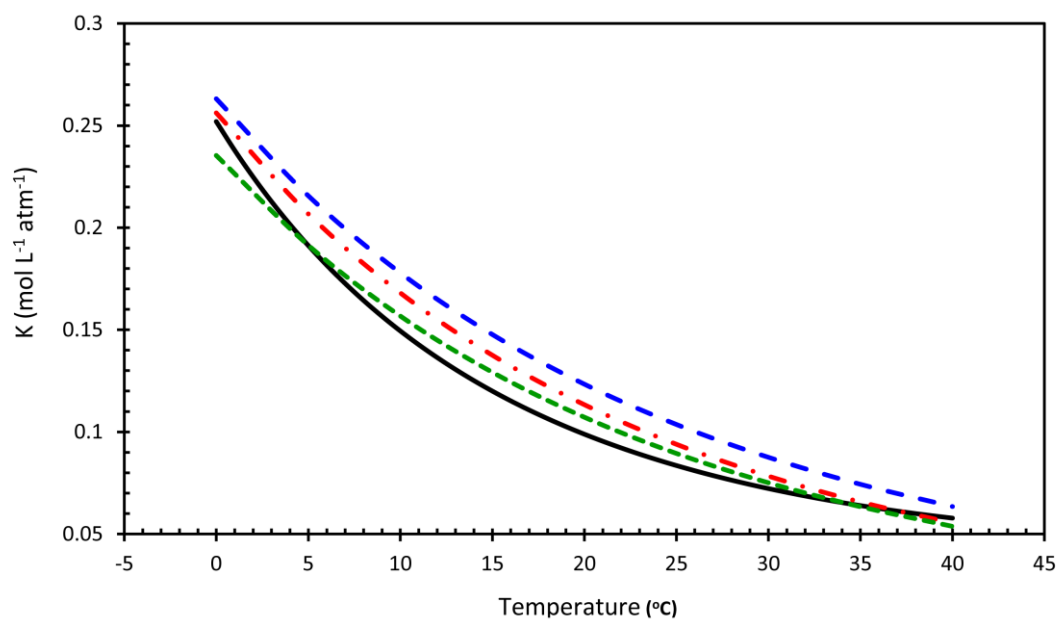
Figure 4.4. Calculated solubilities of CH₃Cl in seawater (Salinity = 35) with solubility functions from this study (Equation 4.4) (black line), *Elliott and Rowland* [1993] (blue dashed line), *Moore et al.* [1995] (red dotted dash line) and *Moore* [2000] (green dashed line).

calculated from *Moore* [2000] and the current study is small (3%), the discrepancy in the calculated solubilities from these two studies could become more pronounced at temperatures ≤ 0 ^{o}C or ≥ 40 ^{o}C or between 10 ^{o}C to 30 ^{o}C. In addition, a 10 – 18 % salt effect was observed between pure water and seawater (S = 31.84) over a temperature range of 0 – 40 ^{o}C in the present study (Figure 4.3c). Since the solubility function from *Moore* [2000] is only applicable in seawater, an observed 10 – 18 % salt-out effect suggests that using the solubility expression determined by *Moore* [2000] would result in a 10 – 18 % underestimation of CH$_3$Cl solubility in pure water. *Elliott and Rowland* [1993] reported a 6 % salt effect between pure water and seawater (S = 33.34). However, *Elliott and Rowland* [1993] only measured the solubilities at two different temperatures, which could result in a bias or larger errors than the present study. The higher salt effect reported in this study reinforces the importance of including the salinity dependence in the solubility function.

4.3.2. HalocAST data

Observed atmospheric mixing ratios of CH$_3$Cl from the HalocAST and the Bromine Latitudinal Air Sea Transect (BLAST) cruises [*Khalil et al.*, 1999; *Lobert et al.*, 1996] conducted 16 years prior (Figures 4.5 and 4.6) are comparable in most regions. Saturation anomalies of CH$_3$Cl are corrected using CFC-11 to remove the effect of physical processes, i.e., surface warming or cooling, air bubble injection, etc. [*Butler et al.*, 1991; *Yvon-Lewis et al.*, 2004]. The equilibrium partial pressures in the surface seawater and corrected saturation anomalies from HalocAST are similar to those from BLAST (Figures 4.5 and 4.6) except the regions between 0° – 15°N and 28° – 35°N in
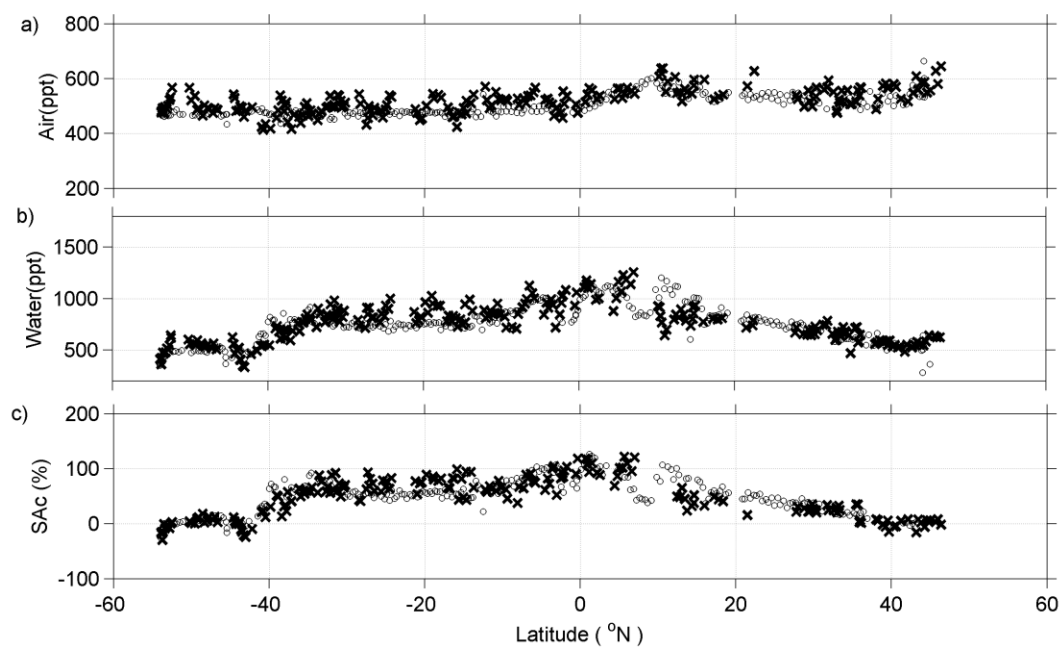
Figure 4.5. (a) Atmospheric CH$_3$Cl mixing ratios, (b) CH$_3$Cl moisture air mole fractions in the surface seawater and (c) corrected CH$_3$Cl saturation anomalies using saturation anomalies of CFC-11 during BLAST I (circles) and HalocAST-P (crosses), both coursing the eastern Pacific Ocean.
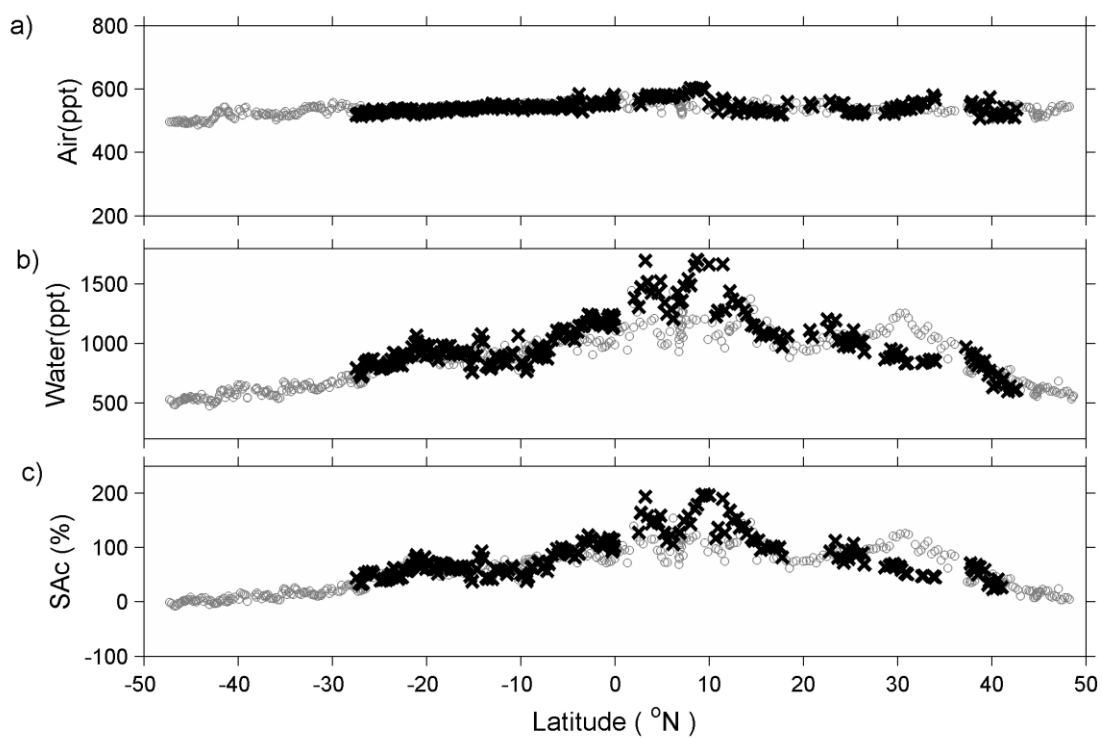
Figure 4.6. (a) Atmospheric CH$_3$Cl mixing ratios, (b) CH$_3$Cl moisture air mole fractions in the surface seawater and (c) corrected CH$_3$Cl saturation anomalies using saturation anomalies of CFC-11 during BLAST II (circles) and HalocAST-A (crosses), both coursing the Atlantic Ocean.

the Atlantic (Figure 4.6). Since HalocAST-A in the northern Atlantic was more influenced by the eastern Atlantic boundary currents while BLAST II cruise passed through the North Atlantic Gyre, the difference in concentrations observed between BLAST II and HalocAST-A at $0^o - 15^o$ N and $28^o - 35^o$ N in the Atlantic were likely because HalocAST ran closer to coastal waters and captured a different water mass than BLAST.

4.3.3. Saturation anomaly as a function of sea surface temperature and wind speed

Because CH$_3$Cl saturation anomalies in the surface ocean were relatively consistent over the past sixteen years (Figures 4.5 and 4.6), the HalocAST data, along with additional data from seven major long-transit cruises from NOAA/ESRL Global Monitoring Division during 1994 to 2004 (ftp://ftp.cmdl.noaa.gov/hats/ocean/) and one coastal study from *Hu et al.* [2010], are used to construct seasonal saturation anomaly functions for open-ocean areas and a separate saturation anomaly function for coastal-ocean areas. The additional cruises include the Bromine Latitudinal Air Sea Transect I, II and III (BLAST I, II and III) [*Khalil et al.*, 1999; *Lobert et al.*, 1997; *Lobert et al.*, 1996], the first Gas Exchange experiment (GasEx 98) [*King et al.*, 2000], the Bromine Air-sea Cruise Pacific (BACPAC 99) [*King et al.*, 2002], the Project Halocarbon Air Sea Exchange (PHASE-1) [*Dahl et al.*, 2005], the Climate Variability SR3 (CLIVAR 01) [*Yvon-Lewis et al.*, 2004], and the Gulf of Mexico and the East Coast Carbon (GOMECC) cruises [*Hu et al.*, 2010] (Figure 4.2).

Here, we define the regions with water depth > 200 m as open-ocean areas, and the regions with water depths ≤ 200 m as coastal-ocean areas. The whole dataset was

divided into three sub-datasets, open-ocean spring/summer, open-ocean fall/winter and coastal-ocean. Because data from coastal ocean were limited as to their coverage, we cannot examine the seasonality in the coastal region. All three datasets show strong correlation between Δ% and SST: r = 0.82 (N = 1874) for open-ocean spring/summer, r = 0.91 (N=1398) for open-ocean fall/winter and r = 0.83 (N= 349) for coastal ocean. Since it was suggested that a quadratic relationship exists between saturation anomalies and SST [*Khalil et al.*, 1999], all three datasets were fitted with quadratic equations using the least-squares method (Figure 4.7). The derived quadratic equations are expressed as follows.

Open Ocean

Spring/Summer: $\quad \Delta(\%) = 0.1257t^2 + 0.5183t - 14.2960 \quad$ (-2 $^{\circ}$C < t < 31 $^{\circ}$C) $\quad$ (4.5)

Fall/Winter: $\quad \Delta(\%) = 0.1442t^2 + 0.5642t - 25.5360 \quad$ (-2 $^{\circ}$C < t < 31 $^{\circ}$C) $\quad$ (4.6)

Coastal Ocean

Annual: $\quad \Delta(\%) = 0.0598t^2 + 4.3574t - 56.5752 \quad$ (7 $^{\circ}$C < t < 31 $^{\circ}$C) $\quad$ (4.7)

where t stands for SST ($^{\circ}$C). The standard errors for the saturation anomalies estimated by equations (5 − 7) are ±23.0%, ±18.5% and ±35.2%. The new Δ% - SST relationships substantially improve our ability to calculate CH_3Cl saturation anomalies in surface ocean compared to the old Δ% - SST relationship [*Khalil et al.*, 1999], especially in coastal areas and regions in the middle and high latitudes of the open ocean (Table 4.2).

Saturation anomalies of CH_3Cl in the surface ocean are mainly controlled by CH_3Cl partial pressures in the surface seawater versus those in the atmosphere (Figures 4.8a and 4.8c). Their latitudinal distributions are similar to that of SST (Figure 4.8d).

Table 4.2. Measured and calculated mean CH_3Cl saturation anomalies (%)[a] according to cruise data from BLAST I, II, III, GasEx 98, BACPAC 99, PHASE I 04, CLIVAR01, HalocAST-P/A, and GOMECC.

	Measured	Annual[b]	Seasonal[c]	Seasonal + Wind Speed[d]
Open Ocean - Spring/Summer	58.5 ± 43.3 (1874)	53.9 ± 42.1 (1874)	58.3 ± 36.8 (1874)	58.5 ± 37.0 (1874)
High Latitudes (60° - 90°)	-15.8 ± 12.3 (49)	-23.9 ± 0.1 (49)	-14.7 ± 0.1 (49)	-12.8 ± 7.0 (49)
Middle Latitudes (30° - 60°)	31.8 ± 28.2 (910)	22.3 ± 21.0 (910)	31.1 ± 18.6 (910)	31.7 ± 19.5 (910)
Low Latitudes (0° - 30°)	89.0 ± 33.3 (915)	89.5 ± 24.7 (915)	89.3 ± 21.1 (915)	88.9 ± 22.4 (915)
Open Ocean - Fall/Winter	21.6 ± 53.5 (1398)	19.8 ± 48.2 (1398)	21.1 ± 49.9 (1398)	21.6 ± 50.2 (1398)
High Latitudes (60° - 90°)	-25.8 ± 7.3 (512)	-23.7 ± 0.5 (512)	-25.5 ± 1.2 (512)	-25.6 ± 2.7 (512)
Middle Latitudes(30° - 60°)	15.7 ± 32.2 (483)	10.7 ± 25.7 (483)	13.9 ± 26.1 (483)	14.7 ± 26.4 (483)
Low Latitudes (0° - 30°)	89.0 ± 19.2 (403)	86.0 ± 18.9 (403)	89.1 ± 18.1 (403)	89.9 ± 18.1 (403)
Coastal Ocean	83.2 ± 60.5 (349)	73.0 ± 47.3 (349)	83.0 ± 49.0 (349)	83.1 ± 49.3 (349)

[a]Uncertainties are given as standard deviation, and the number of samples is given in parentheses. [b]Calculated saturation anomalies using the annual Δ% - SST relationship from *Khalil et al.* [1999]. [c]Calculated saturation anomalies using the seasonal Δ% - SST relationships (Equations 4.5 – 4.7). [d]Calculated saturation anomalies using the seasonal Δ% - (SST, wind speed) relationships (Equations 4.8 – 4.10).
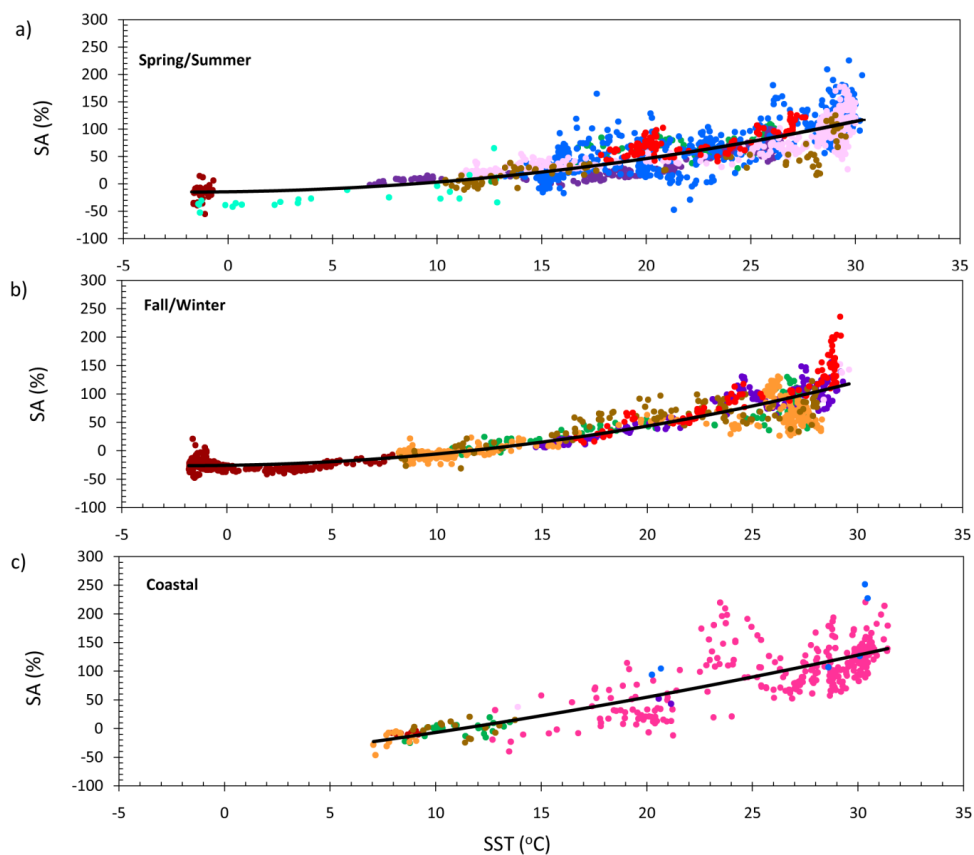
Figure 4.7. Saturation anomaly of CH₃Cl as a function of sea surface temperature in open ocean (a: spring/summer; b: fall/winter) and coastal ocean (c). Colored points stand for observed saturation anomalies of CH₃Cl from BLAST I (●), BLAST II (●), BLAST III (●), GasEx 98 (●), BACPAC 99 (●), PHASE I 04 (●), CLIVAR 01 (●), GOMECC (●), HalocAST–P (●) and HalocAST-A (●). Black lines are quadratic regressions between saturation anomaly of CH₃Cl and SST.
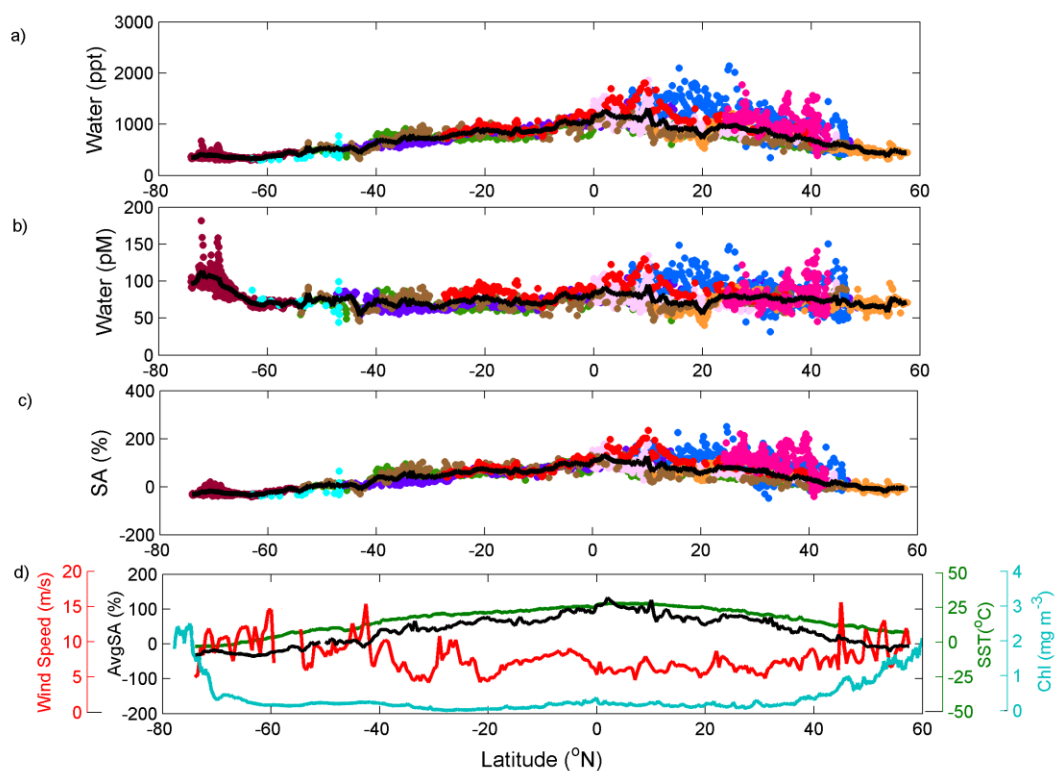
Figure 4.8. Latitudinal distributions of CH₃Cl moisture air mole fractions (a), CH₃Cl mass concentrations (b), CH₃Cl saturation anomalies (c) in surface ocean. Colored points in panels (a – c) stand for data from BLAST I (●), BLAST II (●), BLAST III (●), GasEx 98 (●), BACPAC 99 (●), PHASE I 04 ( ), CLIVAR 01 (●), GOMECC (●), HalocAST – P (●) and HalocAST-A (●). Black lines represent longitudinal average CH₃Cl partial pressures (a), longitudinal average CH₃Cl mass concentrations (b) and longitudinal average CH₃Cl saturation anomalies (c) at different latitudes of surface ocean. (d) Latitudinal distributions of longitudinal average saturation anomalies of CH₃Cl (━) in surface ocean, longitudinal average sea surface temperature (━), longitudinal average wind speed (━), and longitudinal average chlorophyll-a concentrations (━).

Converting partial pressures of CH_3Cl in the surface seawater to mass concentrations can remove the dominant trend of CH_3Cl partial pressures in surface seawater (Figures 4.8a and 4.8b), suggesting that the strong relationship between CH_3Cl saturation anomalies or CH_3Cl partial pressures in surface seawater and SST is likely due to the dependence of CH_3Cl solubility on the temperature. We also examined the correlation between saturation anomaly and wind speed. Results suggest that saturation anomalies of CH_3Cl in surface ocean are inversely correlated with wind speed at a 99% confidence level (r = -0.43, p=0.00). The correlation between saturation anomalies of CH_3Cl and sea surface temperature or wind speed explains high super-saturation of CH_3Cl in warm waters. In warm waters, the released gas cannot escape the surface water fast enough to keep the concentrations from building up owing to both physical warming and relatively low wind speed (Figure 4.8d), resulting in CH_3Cl being highly super-saturated in the tropical ocean (Figure 4.8c). Therefore, with the sea surface temperature as the primary controlling factor for saturation anomalies of CH_3Cl and wind speed as a secondary influence, we rebuilt the saturation anomaly equations as a function of both sea surface temperature and wind speed using the least-squares method:

Open Ocean

Spring/Summer: $\Delta(\%) = 0.1344t^2 + 0.0340t - 1.3687u + 1.5436$ (-2 $^{\circ}$C $< t <$ 31 $^{\circ}$C) (4.8)

Fall/Winter: $\Delta(\%) = 0.1369t^2 + 0.6927t - 0.6198u - 19.2661$ (-2 $^{\circ}$C $< t <$ 31 $^{\circ}$C) (4.9)

Coastal Ocean

Annual: $\Delta(\%) = 0.036t^2 + 6.8104t + 1.3955u - 86.9970$ (7 $^{\circ}$C $< t <$ 31 $^{\circ}$C) (4.10)

where u is the wind speed (m s^{-1}). The standard errors using equations (4.8 – 4.10) were calculated at ±22.6%, ±18.4% and ±35.0%, which are slightly lower than those using equations (4.5 – 4.7). Compare to calculated saturation anomalies from equations (4.5 – 4.7), results computed from the Δ% - (SST, wind speed) relationships (Equations 4.8 – 4.10) can explain more observed variability for CH$_3$Cl saturation anomalies in high latitudinal regions (Table 4.2), and they are more representative for the mean CH$_3$Cl saturation anomalies in various zonal regions (Table 4.2).

Variability of latitudinal mean mass concentrations of CH$_3$Cl in the global surface ocean is relatively small between 60°S to 60°N when compared to latitudinal mole fractions of CH$_3$Cl in the surface ocean. This might be due to a combination of relatively long lifetime of CH$_3$Cl in surface ocean and a ubiquitous production mechanism among various types of marine algae, i.e. methyl transferase [*Itoh et al.*, 1997; *Wuosmaa and Hager*, 1990]. Elevated CH$_3$Cl concentrations between 60° – 80° S coincide with increased chlorophyll-a, whereas no significant increase in CH$_3$Cl mass concentrations was observed above 40°N, where chlorophyll-a concentrations are significantly higher (Figures 4.8b and 4.8d). The contradiction in high latitudinal waters between the northern and southern hemispheres might associate with different phytoplankton assemblages in these two regions [*Alvain et al.*, 2005; *Alvain et al.*, 2008]. In the Southern Ocean, there are large blooms of diatoms and *phaeocystis*-like during the spring and summer [*Alvain et al.*, 2008], whereas in the high latitudes of the North Atlantic or the North Pacific, nanoeucaryotes dominate the populations of phytoplankton all year around, except small areas of diatom blooms during the summer

[*Alvain et al.*, 2008]. The group of *phaeocystis*-like organisms was identified as the one with high production rate of CH_3Cl [*Scarratt and Moore*, 1996; 1998]. This could explain the high mass concentrations of CH_3Cl observed in the Southern Ocean.

4.3.4. Estimating the global net sea-to-air flux of CH_3Cl

Regional net sea-to-air flux, F (nmol m^{-1} d^{-1}), can be calculated by the gas transfer velocity (k_w, m d^{-1}), CH_3Cl solubility (H, mol L^{-1} atm^{-1}), saturation anomaly (Δ, %) and CH_3Cl partial pressure in the air (p_a, patm atm^{-1}). The formula is expressed as follows [*Yvon-Lewis et al.*, 2004]:

$$F = k_w H \frac{\Delta}{100} p_a .$$

(4.11)

If we divide the global ocean into 1° x 1° grids, the global net sea-to-air flux, F_g (Gg yr^{-1}), can then be estimated by the sum of the net sea-to-air fluxes from gridded cells:

$$F_g = n_{atm} M t_m P_{atm} \sum_{m=1}^{m=12} \left(\sum_{i=-90}^{i=90} \sum_{j=-180}^{j=180} k_{w,i,j,m} H_{i,j,m} \frac{\Delta_{i,j,m} P_{a,i,j,m}}{100} A_{i,j,m} \right)$$

(4.12)

where, n_{atm} is the mass of the atmosphere (mol); M is the molecular weight of CH_3Cl (g mol^{-1}); t_m stands for one month period; P_{atm} is the atmospheric pressure at the surface ocean (1 atm); $A_{i,j,m}$ is the oceanic area in each grid cell; m is the month index; i and j are the latitude and longitude indices; and the other variables are defined above. Here, we use the parameterization from *Sweeney et al.* [2007] to calculate k_w.

$$k_w = \frac{14.6}{u_{avg}^2} u^2 (Sc/660)^{-0.5}$$

(4.13)

where, u_{avg} is the global average climatological wind speed; u is the average climatological wind speed in each grid cell; and Sc is the Schmidt number of CH_3Cl

calculated from the kinematic viscosity [*Millero*, 1974] and the diffusivity [*Hayduk and Laudie*, 1974]. We obtained monthly 1° x 1° gridded wind speed, SST and sea surface salinity from the DS279 database (http://dss.ucar.edu/datasets/ds279.0/). In addition, we calculated the fractions of land area, open-ocean area and coastal-ocean area in each grid based on bathymetric data from the 1' X 1' global relief database, ETOPO (http://www.ngdc.noaa.gov/mgg/gdas/gd_designagrid.html). For grids with only open-ocean or coastal-ocean area, Δ% was calculated based on either seasonal open-ocean Δ% - (SST, wind speed) relation or coastal Δ% - (SST, wind speed) relation. For grids containing both coastal-ocean and open-ocean areas, Δ% is the area-weighted mean saturation anomaly. Monthly hemispheric CH$_3$Cl partial pressures are the monthly average from 1995 to 2010 (Flask data from NOAA/ESRL GMD: ftp://ftp.cmdl.noaa.gov/hats/methylhalides/ch3cl/flasks/).

To determine the effect of the new solubility function and the new seasonal Δ% - (SST, wind speed) relationships on the estimate of the global net sea-to-air flux of CH$_3$Cl, we computed the global net sea-to-air flux in four different scenarios using the same gas transfer velocity parameterization [*Wanninkhof*, 1992] as the prior studies [*Khalil et al.*, 1999; *Moore*, 2000; *Moore et al.*, 1996; *Yoshida et al.*, 2004] and compared our results with the prior estimates. The base scenario uses the old solubility function from *Moore* [2000] and the old Δ% - SST relationship [*Khalil et al.*, 1999], which yields a best global annual net sea-to-air flux of 460 Gg yr^{-1}. The second scenario examines the impact of the new solubility parameterization on the global net flux. By replacing the old solubility function [*Moore*, 2000] with equation (4.4), it yields a best

global net flux of 420 Gg yr^{-1}, which is about 10% lower than the estimate using the solubility expression from *Moore* [2000]. This is because *Moore* [2000] tends to overestimate CH$_3$Cl solubility in waters with SST from 6 – 35$^{\mathrm{o}}$C and underestimate the solubility in waters with SST ≥ 35$^{\mathrm{o}}$C or SST ≤ 6$^{\mathrm{o}}$C (Figure 4.4) relative to this study, thus yielding higher effluxes in warm waters with SST between 12$^{\mathrm{o}}$C (12$^{\mathrm{o}}$C is the critical temperature to control the direction of the net flux [*Moore et al.*, 1996]) and 35$^{\mathrm{o}}$C and lower influxes in waters with SST ≤ 6$^{\mathrm{o}}$C. In scenario three, we ran the model using the old solubility function but replacing the old Δ% - SST relationship [*Khalil et al.*, 1999] with equations (4.8 – 4.10). The model produces a best global net flux of 550 Gg yr^{-1}, suggesting the old Δ% - SST relationship tends to underestimate the global net sea-to-air flux by 16%. When using the new parameterizations of the solubility and the saturation anomalies (scenario four), part of the differences resulted from both parameterizations are canceled out, yielding a best annual global net sea-to-air flux of 500 Gg yr^{-1}, which is about 40 Gg yr^{-1} higher than the result from the base scenario. The range of the prior estimates on the global CH$_3$Cl net flux is from 300 to 650 Gg yr^{-1} [*Khalil et al.*, 1999; *Moore*, 2000; *Moore et al.*, 1996; *Yoshida et al.*, 2004]. Our estimate using the parameterization of the gas transfer velocity from *Wanninkhof* [1992], 500 Gg yr^{-1}, is in the middle of this range.

Parameterization of the gas transfer velocity from *Sweeney et al.* [2007] is an improvement on that from *Wanninkhof* [1992] because *Sweeney et al.* [2007] considered the spatial variation in solubility as a function of temperature and salinity and partial pressures of ^{14}CO$_2$ in the atmosphere and the surface ocean, along with the effect of an
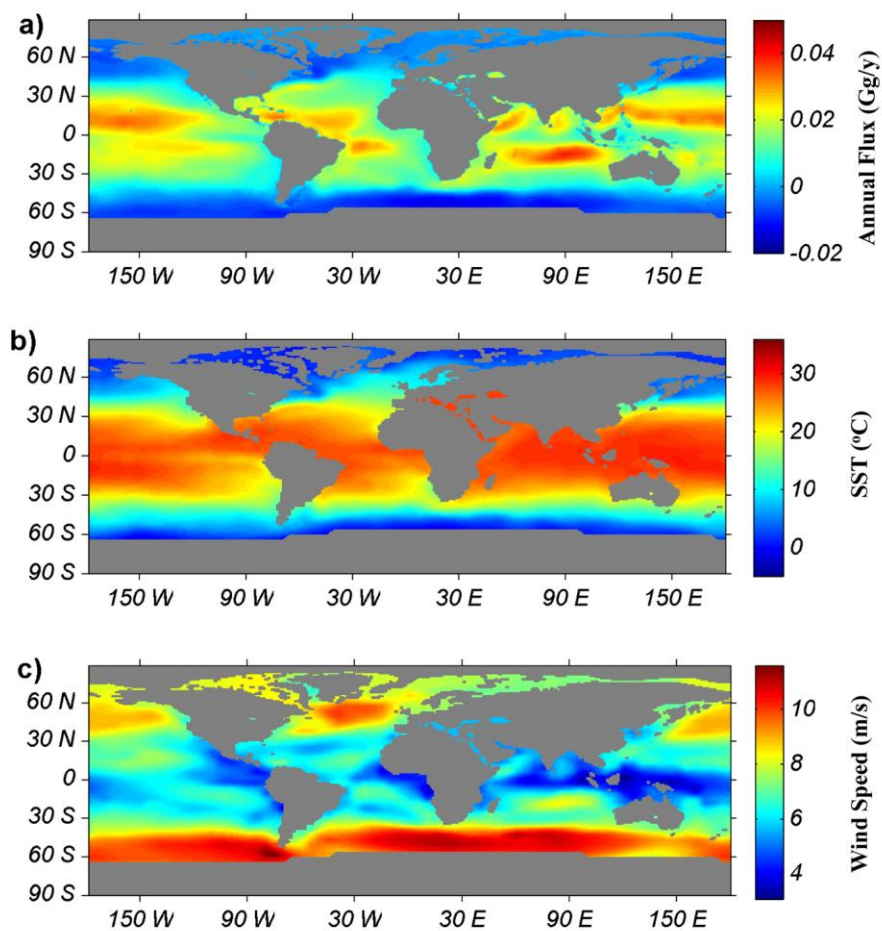
Figure 4.9. (a) Annual mean net sea-to-air fluxes of CH$_3$Cl, (b) annual mean sea surface temperature and (c) annual mean wind speed in 1$^\text{o}$ x 1$^\text{o}$ grids.

improved ocean inventory of bomb-produced dissolved inorganic ^{14}C. Therefore, we updated our estimate using the new parameterization from *Sweeney et al.* [2007], yielding a best global net flux of 335 Gg yr^{-1}. The global distribution of annual net sea-to-air fluxes show similar spatial trends but different magnitudes than those from *Khalil et al.* [1999] (Figure 4.9a). Regions with elevated annual net sea-to-air fluxes include the tropical western Atlantic, the eastern and central Pacific, and the central and northwestern Indian Ocean, which coincide with areas with elevated annual sea surface temperature (Figure 4.9b) and increased wind speed (Figure 4.9c).

Although atmospheric CH$_3$Cl has an apparent seasonality [*Khalil and Rasmussen*, 1999], only small seasonality is shown in the average net fluxes in the regions studied here (Figure 4.10). Overall, the polar region (latitude $\geq 60^{o}$) is a net sink for atmospheric CH$_3$Cl all year around (Figure 4.10); temperate seawater ($30^{o} \leq$ latitude $< 60^{o}$) is a net source during the spring, summer and fall but a net sink in some months during the winter (Figure 4.10); the tropical region (latitude $< 30^{o}$) is always a net source to atmospheric CH$_3$Cl (Figure 4.10).

The uncertainty of the calculated global net sea-to-air fluxes mainly arises from the errors on the gas transfer velocity (k_w), the saturation anomaly (Δ) and the solubility (*H*). The possible error given by the gas transfer velocity is $\pm$ 32% [*Sweeney et al.*, 2007]. The standard error for the solubility is $\pm$ 3% (see Section 3.1). Because saturation anomaly in each gridded cell is the mean saturation anomaly in that gridded area, we estimated the standard errors of the mean saturation anomalies calculated from equations (8 - 10), which are 1.3%, 1.0% and 3.7% at a 95% confidence level for the open-ocean
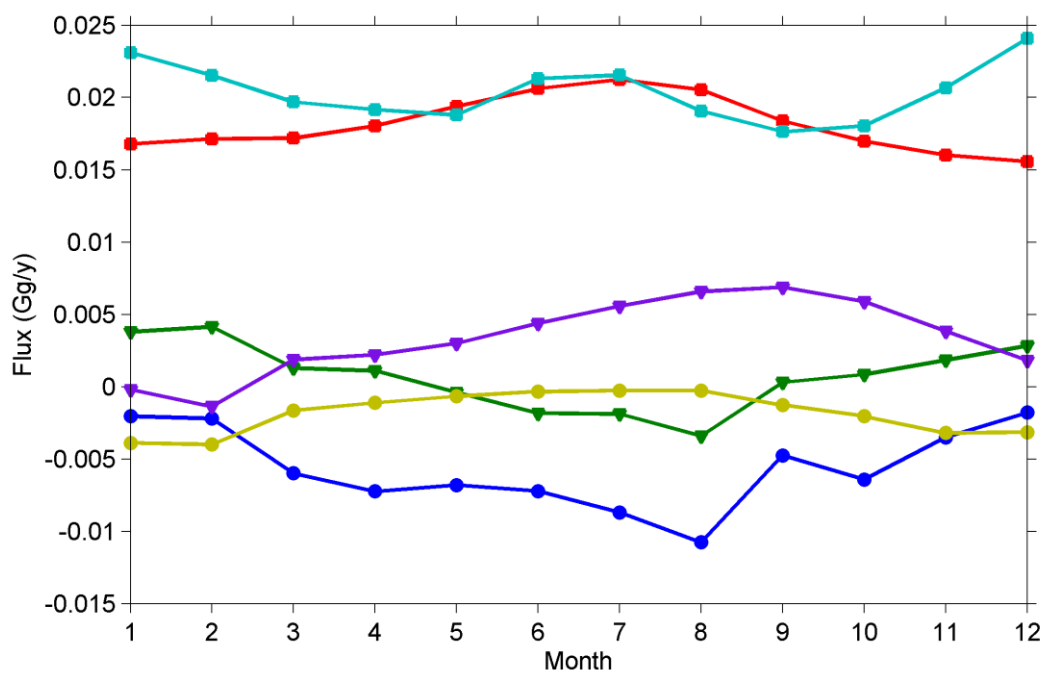
Figure 4.10. Monthly mean net sea-to-air fluxes of CH₃Cl in the NH tropical ($\blacksquare$), SH tropical ($\blacksquare$), NH temperate ($\blacktriangledown$), SH temperate ($\blacktriangledown$), NH polar ($\bullet$) and SH polar ($\bullet$) regions.

spring/summer, the open-ocean fall/winter, and the coastal ocean. Therefore, the possible range of our estimated global net sea-to-air flux of CH_3Cl is revised at 210 - 480 Gg yr^{-1}.

4.3.5. Estimating the global oceanic emission and oceanic uptake rate

A net sea-to-air flux cannot fully represent the role of the ocean (both a source and a sink to atmospheric CH_3Cl) in the atmospheric CH_3Cl budget. Therefore, it is important to break down the net flux into unidirectional oceanic emission and unidirectional oceanic uptake [*Butler and Rodriguez*, 1996; *Lobert et al.*, 1996; *Yvon-Lewis and Butler*, 2002]. In the studies from *Butler and Rodriguez* [1996] and *Lobert et al.* [1996], they define the portion that is produced in the ocean and emitted to the atmosphere as the oceanic emission and the portion that enters from the atmosphere to the ocean and gets destroyed in the ocean as the oceanic uptake. This definition has been used for the CH_3Br oceanic budget [*Butler*, 1994; *Hu et al.*, 2010; *Lobert et al.*, 1995; *Lobert et al.*, 1996; *Montzka and Reimann et al.*, 2011; *Montzka et al.*, 2003; *Yvon-Lewis and Butler*, 1997; *Yvon-Lewis and Butler*, 2002; *Yvon and Butler*, 1996]. The strengths of this approach are: (1) it implicitly contains the information about the partial atmospheric lifetime, which could be estimated by the total mass in the atmosphere divided by the oceanic uptake rate; and (2) the annual oceanic emission remains relatively constant over time unless there are significant changes in oceanic production rate, biological degradation rate constant, wind speed, temperature and salinity [*Hu et al.*, submitted]. Estimated oceanic emissions can be used in the time-dependent models for CH_3Cl source and sink studies.

Previously, the net flux from the ocean to the atmosphere in warm waters is used as a source term whereas the net flux from the atmosphere to the ocean in cold waters is used as a sink term in the atmospheric budget of CH$_3$Cl [*Clerbaux and Cunnold et al.*, 2007; *Montzka and Fraser et al*, 2003]. The net fluxes incorporate both oceanic emission and uptake. In this study, we estimated the unidirectional oceanic emission and uptake based on the definitions above. The oceanic uptake rate constant, k_{ocn} (yr^{-1}), can be estimated using equation (4.14) [*Yvon-Lewis and Butler*, 2002]:

$$k_{ocn} = \frac{p_{atm}}{n_{atm}} \left[I_g \frac{2}{1+I_g} \sum_{i=-90}^{i=90} \sum_{j=-180}^{j=180} k_{w,i,j} A_{i,j} H_{i,j}(R_{i,j}) + \frac{2}{1+I_g} \sum_{i=-90}^{i=0} \sum_{j=-180}^{i=180} k_{w,i,j} A_{i,j} H_{i,j}(R_{i,j}) \right] (4.14)$$

where, $R = \dfrac{k_{chem} + k_{bio} + k_{eddy}}{k_{chem} + k_{bio} + k_{eddy} + \dfrac{k_w}{z}}$; k_{chem}, k_{bio} and k_{eddy} are the chemical, biological and eddy loss rate constant (d^{-1}); I_g is the inter-hemispheric ratio of CH$_3$Cl; the other variables are defined above. Hydrolysis is the dominant pathway for the chemical degradation. The chemical loss rate constant (k_{chem}) or the hydrolysis rate constant is from *Elliott and Rowland* [1995]. Calculated global annual mean chemical loss rate constant is about 0.0015 d^{-1}. The eddy degradation loss rate constant, k_{eddy}, is the loss due to downward mixing into the thermocline, which can be calculated by diffusion coefficient, chemical loss rate constant and mixed layer depth [e.g., *Yvon-Lewis and Butler*, 2002]. The calculated global annual mean eddy degradation rate constant is 0.0015 d^{-1}. The biological loss rate constant (k_{bio}) measurements were limited to measurements only in the Southern Ocean and the coast off Nova Scotia [*Tokarczyk et al.*, 2003a, 2003b]. The observed mean biological degradation rate constant was 0.07 ($\pm$

0.01) d^{-1} in the surface seawater of the Southern Ocean, which was higher than what was required, 0.02 d^{-1}, to maintain a steady state in the mixed layer [*Tokarczyk et al.*, 2003a]. *Tokarczyk et al.* [2003a] suggest that 0.02 d^{-1} averaged out the whole mixed layer and 0.07 d^{-1} only represented for the biological loss rate constant for the surface layer. The annual mean biological degradation rate constant off Nova Scotia was observed at 0.07 (± 0.08, 1σ) d^{-1} [*Tokarczyk et al.*, 2003b]. No calculation was provided to evaluate whether using a biological degradation rate constant of 0.07 d^{-1} can maintain a steady state for CH$_3$Cl in the coast off Nova Scotia in the study of *Tokarczyk et al.* [2003b]. Since the biological loss rate constant measurements of CH$_3$Cl were conducted in a limited temporal and spatial scale, we made the following assumptions for the estimate of the global oceanic uptake rate constant: (1) the annual mean biological loss rate constant, 0.07 d^{-1}, measured in the coast off Nova Scotia is representative for the annual mean biological loss rate constant in other coastal regions in the world; and (2) the biological loss rate constant, 0.02 d^{-1}, in the Southern Ocean is representative for the biological loss rate constant in the other open-ocean areas. Based on these assumptions, the global oceanic uptake rate constant was estimated at 0.088 yr^{-1} and the partial atmospheric lifetime with respect to the oceanic loss is 11 years. Including uncertainties on the biological loss rate constant measurements [*Tokarczyk et al.*, 2003a; *Tokarczyk et al.*, 2003b] and those from gas transfer velocity, solubility and chemical degradation rate constants, the possible range for the global oceanic uptake rate constant and the partial atmospheric lifetime are 0.067 – 0.10 yr^{-1} and 9.6 - 15 years. *Yvon-Lewis and Butler* [2002] estimated the partial atmospheric lifetime with respect to the oceanic loss without

considering the biological loss rate constant. This yielded a partial atmospheric lifetime of 70 (50 -104) years. It is evident that with and without the biological loss rate constant, the partial atmospheric lifetime is significantly different. Further research is needed to quantify the spatial and temporal variations of the biological loss rate constant of CH_3Cl in the surface ocean in order to better estimate its partial atmospheric lifetime. Using the new estimated partial atmospheric lifetime with respect to the oceanic loss would change the overall atmospheric lifetime of CH_3Cl from 1.0 year [*Montzka and Reimann, et al.*, 2011] to 0.9 year.

The annual global oceanic uptake rate was estimated by multiplying the global oceanic uptake rate constant by the global atmospheric abundance of CH_3Cl, yielding an uptake rate of -370 (-440 to -280) Gg yr^{-1}. The oceanic emission, 700 (490 – 920) Gg yr^{-1}, was calculated as the difference between the net sea-to-air flux and the uptake rate.

4.4. Summary and conclusions

We re-examined the empirical Δ% - SST relationship using more extensive datasets. The strong observed relationship between saturation anomalies and SST is likely due to the dependence of the CH_3Cl solubility on the temperature. In addition, we found a dependence of the saturation anomaly of CH_3Cl in surface ocean on wind speed although the correlation was weaker than that between Δ% and SST. Derived seasonal Δ% - (SST, wind speed) relationships substantially improved our ability to calculate the distribution of saturation anomalies of CH_3Cl in the surface ocean.

To determine how the new solubility function and the new Δ% - (SST, wind speed) parameterizations affect the global net sea-to-air flux of CH_3Cl, we estimated the

fluxes under four different scenarios by replacing the old parameterizations with the new ones. Results suggest that part of the differences resulting from the new solubility function and the new $\Delta\%$ - (SST, wind speed) relations are canceled out when calculating the global net sea-to-air flux. Using the improved solubility function, the new seasonal $\Delta\%$ - (SST, wind speed) relationships and an updated gas transfer velocity [*Sweeney et al.*, 2007], the global net sea-to-air flux of CH_3Cl is estimated at 335 (210 to 480) Gg yr^{-1}.

The gross emission and uptake rates of CH_3Cl in the surface ocean were estimated at 700 (490 to 920) Gg yr^{-1} and -370 (-440 to -280) Gg yr^{-1}. The corresponding best estimate of the partial atmospheric lifetime with respect to irreversible oceanic uptake is 11 (9.6 - 15) years. Since the biological uptake rates of CH_3Cl in the surface ocean are only based on data from two regional studies, they might not be representative of the global biological degradation rate constants. Until more biological loss rate constant measurements are made, the estimates given above are the best estimates according to our current knowledge. With the revised partial atmospheric lifetime of CH_3Cl regarding the oceanic loss, the overall atmospheric lifetime of CH_3Cl becomes 0.9 year.

5. USING "TOP-DOWN" APPROACH TO EXAMINE ATMOSPHERIC BUDGETS OF METHYL CHLORIDE AND METHYL BROMIDE*

5.1. Introduction

CH_3Cl and CH_3Br are the most abundant natural sources of stratospheric chlorine and bromine, and contributed about 17% of the total chlorine and 30% of the total bromine to the stratosphere in 2008 [*Fahey and Hegglin*, 2011]. About one quarter of total stratospheric ozone loss is attributed to the release of chlorine and bromine from CH_3Cl and CH_3Br [*Butler*, 2000]. In response to the Montreal Protocol and its amendments, most long-lived halogenated compounds that originate from anthropogenic sources are declining in the atmosphere. The relative importance of natural halogenated compounds is increasing. Quantifying the natural emissions of CH_3Cl and CH_3Br has become one focus of current active research [e.g. *Blei et al.*, 2010; *Gebhardt et al.*, 2008; *Manley et al.*, 2007; *Mead et al.*, 2008; *Mead et al.*, 2008; *Moore et al.*, 2005; *Rhew et al.*, 2007; *Saito and Yokouchi*, 2006; 2008; *Saito et al.*, 2008; *Yokouchi et al.*, 2007]. However, large uncertainties remain in individual sources and sinks.

Atmospheric CH_3Cl and CH_3Br have common natural sources and sinks. The common identified natural sources include the ocean [e.g. *Hu et al.*, 2010; *Moore et al.*, 1996], biomass burning [e.g. *Lobert et al.*, 1999; *Yvon-Lewis et al.*, 2009], fungi [*Lee-*

---

*This section is to be submitted to the journal of Atmospheric Physics and Chemistry.

Taylor and Holland, 2000; *Mead et al.*, 2008; *Watling and Harper*, 1998], salt marshes [e.g.*Rhew et al.*, 2000], wetlands [*Dimmer et al.*, 2001; *Varner et al.*, 1999a], rice paddies [*Lee-Taylor and Redeker*, 2005], mangroves [*Manley et al.*, 2007] and tropical rainforests [*Blei et al.*, 2010; *Gebhardt et al.*, 2008]. The common identified sinks include reaction with hydroxyl radicals [*Clerbaux and Cunnold et al.*, 2007; *Montzka and Reimann et al.*, 2011], uptake by soils [*Keene et al.*, 1999; *Keppler et al.*, 2005; *Shorter et al.*, 1995], aquatic degradation in the ocean [e.g. *Tokarczyk et al.*, 2003a; *Yvon-Lewis and Butler*, 2002] and photolysis in the stratosphere [*Clerbaux and Cunnold et al.*, 2007; *Montzka and Reimann et al.*, 2011]. The best estimate of the total known sinks exceeds the best estimate of the total known sources by ~35 Gg yr^{-1} for CH$_3$Br in its pre-industrial, pre-phaseout and phaseout budgets [*Montzka and Reimann et al.*, 2011; *Saltzman et al.*, 2004; *Yvon-Lewis et al.*, 2009]. For CH$_3$Cl, the gap between the best estimate of its total annual emission and that of its annual uptake rate was closed by utilizing emissions from tropical plants and tropical leaf litter [*Clerbaux and Cunnold et al.*, 2007; *Xiao et al.*, 2007; *Yoshida et al.*, 2004]. However, the question of an imbalance in the atmospheric budget of CH$_3$Cl was raised again in recent years due to a suggested higher soil uptake rate, > 1000 Gg yr^{-1}, by *Keppler et al.* [2005].

About 42 (± 15) Gg yr^{-1} of CH$_3$Br (about 30% of the total known emission) [*Montzka and Reimann et al.*, 2011] was released from fumigated soils during pre-planting applications before 1998. The use of CH$_3$Br for soil fumigation started to be phased out at the beginning of 1998, and the atmospheric mixing ratio of CH$_3$Br has been declining since then. Given that atmospheric CH$_3$Cl is not being phased-out and it

shares many natural sources and sinks with CH_3Br, observed variability of atmospheric CH_3Cl may provide insights into the variability of natural emissions of CH_3Br.

In this study, we used the observed atmospheric CH_3Cl and CH_3Br, along with the strength and the temporal variability of their well-characterized sources and sinks, to examine the poorly-quantified emissions. The objective of this study is to improve the current understanding on the "missing sources" of methyl halides and predict the atmospheric CH_3Br burden at its new steady state.

5.2. Model description

The model we used divides the atmosphere into two boxes by the equator, the Northern Hemisphere (NH) and the Southern Hemisphere (SH). The change in the hemispheric abundance of CH_3Cl or CH_3Br can be expressed as follows [*Montzka et al.*, 2000; *Montzka et al.*, 2011]:

$$\frac{dN}{Ndt} = \frac{E_n}{N} - k_n - k_{ex}(\frac{N}{S}-1) \tag{5.1}$$

$$\frac{dS}{Sdt} = \frac{E_s}{S} - k_s + k_{ex}(\frac{N}{S}-1) \tag{5.2}$$

where, N and S stand for the hemispheric abundances of trace gases in the NH and SH; E_n and E_s are the hemispheric emissions in the time period of dt; k_n and k_s are the total loss rate constants in the NH and SH, which include the oceanic loss rate constant, the soil uptake rate constant, the pseudo-first order reaction rate constant for the reaction with hydroxyl radicals and the loss rate constant for stratospheric photolysis; and k_{ex} is the interhemispheric exchange rate constant, which is 1.1 ± 0.3 years [*Montzka et al.*, 2000].

Dividing the total emission into the known emission (E_k) and the unknown emission (including both poorly quantified sources and unidentified sources; E_u), the unknown emissions in both hemispheres can be calculated by the following equations:

$$E_{n,u} = \left[\frac{\ln(\chi_{t,n} / \chi_{o,n})}{t} + k_n + k_{ex}(\frac{\chi_{o,n}}{\chi_{o,s}} - 1) \right] \chi_{o,n} M_{atm} - E_{n,k} \qquad (5.3)$$

$$E_{s,u} = \left[\frac{\ln(\chi_{t,s} / \chi_{o,s})}{t} + k_s - k_{ex}(\frac{\chi_n}{\chi_s} - 1) \right] \chi_{o,s} M_{atm} - E_{s,k} \qquad (5.4)$$

where, $E_{n,u}$ and $E_{n,k}$ are the total unknown and known emissions in the Northern Hemisphere (NH); $E_{s,u}$ and $E_{s,k}$ are the total unknown and known emissions in the Southern Hemisphere (SH); $\chi_{o,n}$ and $\chi_{t,n}$ are the mixing ratios at time zero and time t in the NH; $\chi_{o,s}$ and $\chi_{t,s}$ are the mixing ratios at time zero and time t in the SH; M_{hem} is the total hemispheric air mass. The hemispheric mixing ratios for CH_3Cl and CH_3Br during 1995 – 2011 are from the flask network at NOAA/ESRL Global Monitoring Division (GMD) (ftp://ftp.cmdl.noaa.gov/hats/).

5.3. Sources

5.3.1. Anthropogenic sources

Anthropogenic emissions of CH_3Cl, including coal combustion, waste incineration, and other industrial activities, account for 4% in the total known emissions [*McCulloch et al.*, 1999] (Table 5.1). In contrast to CH_3Cl, anthropogenic emissions of CH_3Br are more important in its atmospheric budget. The primary anthropogenic emission of CH_3Br before the pre-phaseout was from soil fumigation, which accounts for 27% of its total known emissions (Table 5.1). In accordance with the Montreal

Table 5.1. Sources and sinks for atmospheric CH_3Cl and CH_3Br in Gg yr^{-1}. The best values are shown with their possible ranges in parentheses.

	CH_3Cl (Gg yr^{-1})	CH_3Br (Gg yr^{-1}) 1995 - 1998	CH_3Br (Gg yr^{-1}) 2009
SOURCES			
Anthropogenic Source	275 (85 - 464)	57 (39 - 80)	21 (17 - 25)
Leaded Gasoline	n.q.	3 (0.6 - 6)[16-19]	<3
Coal Combustion; Waste Incineration; Industrial Activity	162 (29 - 295)[1]	n.q.	n.q.
Fumigation - QPS [a]	n.q.	8.1 (7.5 - 8.7)	9.5 (8.8 - 10)
Fumigation – non-QPS [b]	n.q.	39.9 (28.2 - 55.9)	2.4 (1.7 - 3.4)
Biomass Burning - Indoor Biofuel Use [c]	113 (56 - 169)	6 (3 - 9)	6 (3 - 9)
Biomass Burning - Open Field Burning [d]	355 (142 - 569)	23 (9 - 37)	12 (5 - 19)
Ocean	700 (490 - 920)[2]	32 (22 - 44)[20]	32 (22 - 44)[20]
Terrestrial source	2780 (2354 – 3275)	36 (24 – 51)	36 (24 – 51)
Tropical and Subtropical Plants; Tropical Leaf Litters	2492 (2197 - 2900) [3-5]	*19 (0 - 20)[25,26]	*19 (0 - 20) [25,26]
Mangroves	12 (11 - 12)[6]	1.3 (1.2 - 1.3)[6]	1.3 (1.2 - 1.3)[6]
Rapeseed	n.q.	4.9 (3.8 - 5.8)[21]	5.1 (4.0 - 6.1)[21]
Fungus	145 (128 - 162)[7-8]	2.2 (1 - 5.7)[7,22]	2.2 (1 - 5.7)[7,22]
*Salt Marshes	85 (1.1 - 170)[10,11]	7 (0.6 -14)[23]	7 (0.6 -14)[23]
*Wetland	27 (5.5 - 48)[12,13]	0.6 (-0.1 - 1.3)[22]	0.6 (-0.1 - 1.3)[22]
*Rice Paddies	3.7 (2.7 - 4.9)[14]	0.7 (0.1- 1.7)[22]	0.7 (0.1- 1.7)[22]
*Shrublands	15 (9 - 21)[15]	0.7 (0.5 - 0.9)[15]	0.7 (0.5 - 0.9)[15]
Subtotal (Sources)	4110 (3071 – 5228)	148 (77 - 212)	102 (51 - 139)
SINKS			
Reaction with OH [f]	3302 (2543 - 4062)	86 (66 - 106)	66 (51 - 81)

Table 5.1. Continued.

Soil [f]	970 (180 - 1600)	49 (42 – 56)	37 (32 – 43)
Ocean	370 (280 - 440)[2]	41 (29 - 50)[20]	32 (23 - 39)[20]
Loss to Stratosphere	200 (100 - 300)[9]	4[24]	3[24]
Subtotal (Sinks)	4842 (3103 - 6402)	178 (142 – 214)	137 (110 – 165)

Notes: all asterisked items are showing net fluxes; n.q. stands for not quantified.

a. Data for fumigation - QPS consumptions of CH_3Br were downloaded from UNEP (http://ozone.unep.org/Data_Reporting/Data_Access) and the emission ratio is 84 % (78 % - 90 %) from *UNEP* [2007].

b. Data for fumigation - non-QPS consumptions of CH_3Br were downloaded from UNEP (http://ozone.unep.org/Data_Reporting/Data_Access) and the emission ratio is 65 % (46 % – 91 %) from *UNEP* [2007].

c. Emissions of indoor biofuel use was estimated based on the total dry matter burned for indoor biofuel use in 1995 [*Yevich and Logan*, 2003] and emission factors from [*Andreae and Merlet*, 2001].

d. Calculations of biomass burning emissions from open field fire are described in section 5.4.

f. Calculations on the loss to the reaction with hydroxyl radicals and soil uptake rates are described in section 5.5.

[1]*McCulloch et al.* [1999], [2]*Hu et al.* [in prep], [3]*Xiao et al.* [2007], [4]*Yoshida et al.* [2004], [5]*Lee-Taylor et al.* [2001], [6]*Manley et al.* [2007], [7]*Lee-Taylor et al.* [2001], [8]*Watling and Harper* [1998], [9]*Clerbaux and Cunnold et al.* [2007], [10]*Rhew et al.* [2000], [11]*Cox et al.* [2004], [12]*Varner et al.* [1999a], [13]*Dimmer et al.* [2001], [14]*Lee-Taylor and Redeker* [2005], [15]*Rhew et al.* [2001], [16]*Thomas et al.* [1997], [17]*Chen et al.* [1999], [18]*Baker et al.* [1998], [19]*Bertram and Kolowich* [2000], [20]*Hu et al.* [submitted], [21]*Mead et al.* [2008], [22] *Lee-Taylor and Holland* [2000], [23]*Montzka and Reimann et al.* [2011], [24]*Penkett et al.* [1994], [25]*Blei et al.* [2010], [26]*Gebhardt et al.* [2008].

Protocol, CH_3Br consumption for use in soil fumigation decreased by 50 Gg yr^{-1} in the NH and 5 Gg yr^{-1} in the SH, and the corresponding emission dropped by 32 (23 – 46) Gg yr^{-1} and 3 (2 – 5) Gg yr^{-1} in the NH and SH (Figure 5.1). Uncertainty in the emission from soil fumigation mainly results from uncertainty in the emission rate which is dependent on soil moisture, organic content, acidity and injection depth of the treated area [*Yagi et al.*, 1995]. The estimated average emission rate given by *United Nations Environment Programme (UNEP)* [2007] ranges from 46% to 91%. In this study, we used their best estimate, 65%, in the initial scenario. CH_3Br consumption for fumigation – Quarantine and Pre-Shipment (QPS) uses was about 7.6 – 12.4 Gg yr^{-1} during 1995 – 2009 (http://ozone.unep.org/Data_Reporting/Data_Access/). The emission rate for QPS uses is 84% (78% – 90%) [*UNEP*, 2007]. Calculated emission rates from fumigation during 1995 – 2009 are shown in Figure 5.1.

Leaded gasoline is another anthropogenic source for atmospheric CH_3Br. It contributes 0.6 – 6 Gg yr^{-1} of CH_3Br to the atmosphere [*Baker et al.*, 1998; *Bertram and Kolowich*, 2000; *Chen et al.*, 1999; *Thomas et al.*, 1997]. According to the previous studies, the average of the best estimates on the CH_3Br emission from leaded gasoline is 3 Gg yr^{-1} (Table 5.1), of which 80% is from the NH and 20% is from the SH [*Thomas et al.*, 1997].

5.3.2. Biomass burning

Biomass burning emission is one of the largest sources for atmospheric CH_3Cl and CH_3Br. It includes emissions from open field fires and indoor biofuel combustion. Emissions of CH_3Cl and CH_3Br in open field fires were calculated using the version 3 of
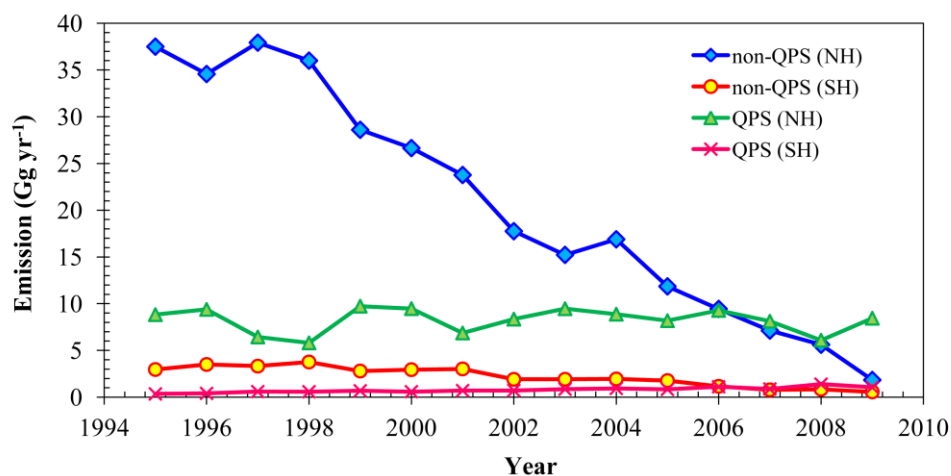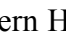
Figure 5.1. Emissions of CH$_3$Br from fumigation - Quarantine and Pre-Shipment (QPS) and fumigation - non-QPS uses. ( ) and ( ) stand for fumigation – non-QPS emissions from the Northern Hemisphere (NH) and Southern Hemisphere (SH). ( ) and ( ) represent fumigation – QPS emissions in the NH and SH. Annual consumption rates are from the United Nations Environment Programme (http://ozone.unep.org/Data_Reporting/Data_Access/) and the emission ratio of CH$_3$Br is 65% [*UNEP*, 2007]

the Global Fire Emissions Database (GFED3) (http://www.falw.vu/~gwerf/GFED/). The GFED3 is based on satellite-derived estimates of burned area, fire activity and plant productivity during the period of 1997 – 2009 on a 0.5^{o} spatial resolution with a monthly time step [*van der Werf et al.*, 2010]. We estimated the biomass burning emissions using two approaches: (1) using CO emissions times emission ratios of CH_3Cl or CH_3Br relative to CO; and (2) multiplying burned dry matter with emission factors of CH_3Cl or CH_3Br. Uncertainties in calculated biomass burning emission rates originate from the estimates of the burned area, combustion completeness, burning depth and emission factors [*Andreae and Merlet*, 2001; *van der Werf et al.*, 2010]. The uncertainty using approach (1) (about $\pm$ 90 %) is larger than that using approach (2) (about $\pm$ 60 %) since it incorporates extra uncertainty on the emission factor of CO. The calculated annual mean biomass burning emission rates for CH_3Cl and CH_3Br were 353 ($\pm$ 318) Gg yr^{-1} and 16 ($\pm$ 14) Gg yr^{-1} using approach (1), and they were estimated at 355 ($\pm$ 213) Gg yr^{-1} and 17 ($\pm$ 10) Gg yr^{-1} using approach (2) (Figure 5.2). Although the discrepancy is small between the annual mean biomass burning emission rates determined from these two approaches, significant differences exist over the course of the time series of interest (i.e. a 420 Gg yr^{-1} difference for CH_3Cl and an 11 Gg yr^{-1} difference for CH_3Br during August to September of 1997 in the SH). Using approach (1) will result in strong negative emission in the derived unknown sources in the SH during the spring of 1997. In the model, approach (2) will be used for our calculation of biomass burning emissions.

CH_3Cl and CH_3Br emission rates from indoor biofuel use were estimated at 113 Gg yr^{-1} (CH_3Cl) and 6.1 Gg yr^{-1} (CH_3Br) (Table 5.1) based on the total burned dry
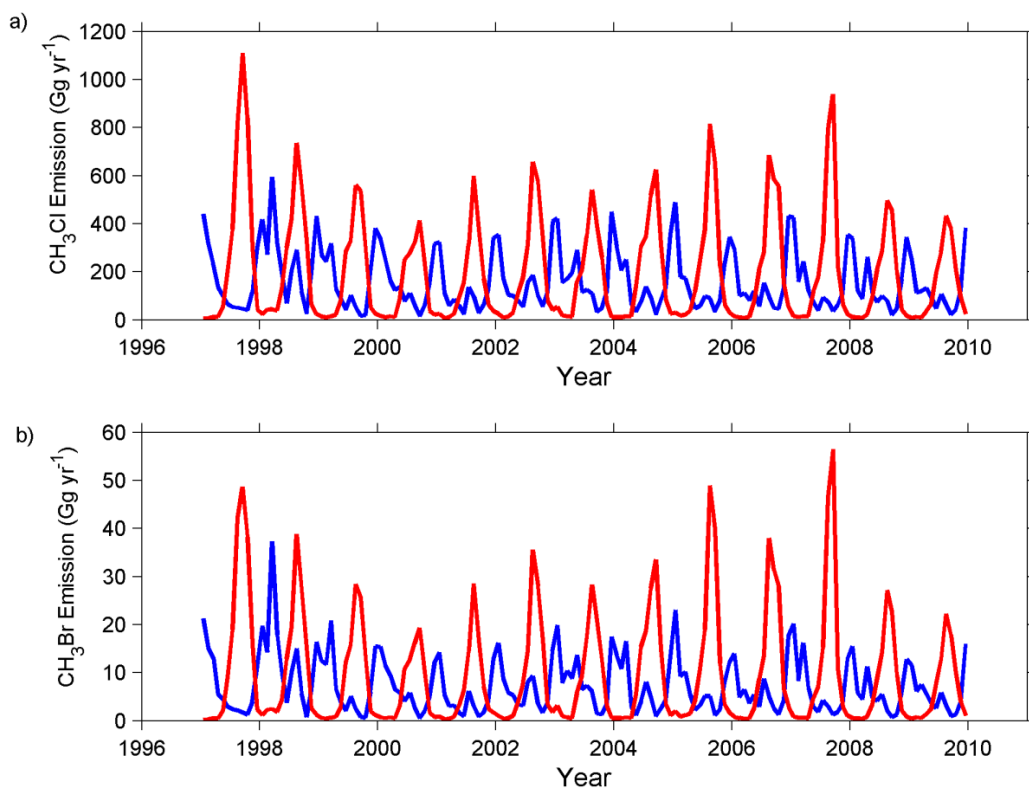
Figure 5.2. Open field biomass burning emission rates for (a) CH₃Cl and (b) CH₃Br in the NH (▬) and in the SH (▬). Burned dry matters are from Global Fire Emissions Database (GFED3) (http://www.falw.vu/~gwerf/GFED/) and emission factors are from *Andreae and Merlet* [2001].

matter during indoor biofuel use in 1995 [*Yevich and Logan*, 2003] and their emission factors from *Andreae and Merlet* [2001]. The uncertainties of the indoor biofuel emission rates for CH_3Cl and CH_3Br are ± 50% [*Andreae and Merlet*, 2001; *Yevich and Logan*, 2003].

The total annual biomass burning emissions of CH_3Cl and CH_3Br from open field burning and in-door biofuel use are 468 (± 270) Gg yr^{-1} and 23 (± 13) Gg yr^{-1}. The biomass burning emission rate for CH_3Br is in good agreement with previous estimates [*Montzka and Reimann et al.*, 2011], whereas the best biomass burning emission rate for CH_3Cl from this study is 143 − 182 Gg yr^{-1} lower than the prior best estimates [*Andreae and Merlet*, 2001; *Yoshida et al.*, 2004]. Although discrepancy of 143 − 182 Gg yr^{-1} is within the uncertainty of our estimate, it is worth noting that the global dry matter emission used in *Andreae and Merlet* [2001] is 40% higher than the total dry matter emissions from open-field fire and indoor biofuel combustion in this study.

5.3.3. Oceanic emissions

The ocean was considered as the largest source for atmospheric CH_3Cl and CH_3Br until the middle 1990s [*Lobert et al.*, 1995; *Moore et al.*, 1996]. As more air-sea flux measurements of CH_3Cl and CH_3Br were made around the world, empirical relationships between the saturation anomalies of CH_3Cl and CH_3Br and sea surface temperature and wind speed were developed [*Hu et al.*, in prep; *Khalil et al.*, 1999; *King et al.*, 2002], which allows better quantification on their global net sea-to-air fluxes. The unidirectional oceanic emission is defined as the portion which is produced in the ocean and emitted to the atmosphere [*Butler and Rodriguez*, 1996]. It was estimated at 700
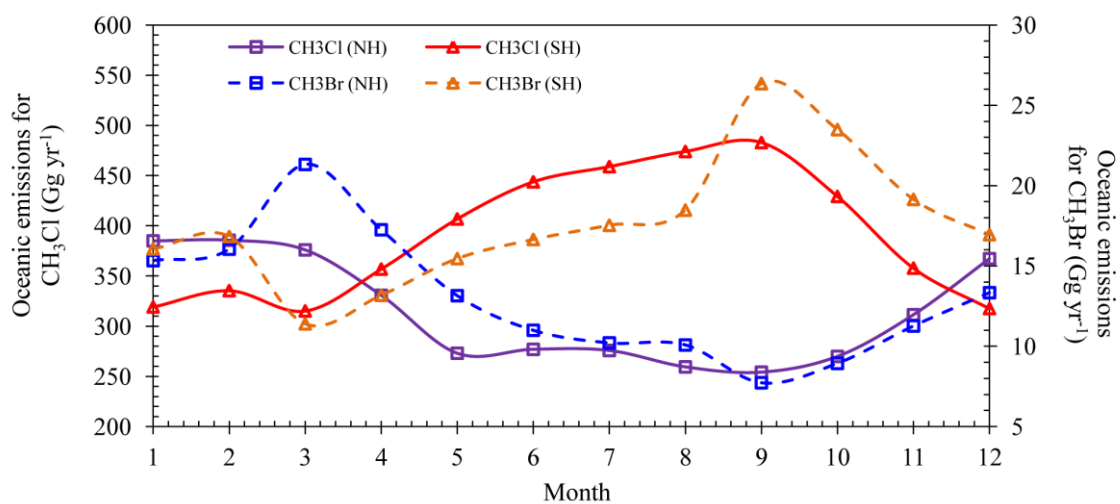
Figure 5.3. Monthly oceanic emissions of CH₃Cl and CH₃Br in both hemispheres. (—□—) and (—△—) represent monthly oceanic emissions of CH$_3$Cl in the NH and SH, whereas (‑□‑) and (‑△‑) stand for monthly oceanic emissions of CH$_3$Br in the NH and SH.

$(490 - 920)$ Gg yr^{-1} for CH$_3$Cl [*Hu et al.*, in prep] and 31 $(24 - 39)$ Gg yr^{-1} for CH$_3$Br [*Hu et al.*, submitted]. The seasonality of hemispheric oceanic emission rates for CH$_3$Cl and CH$_3$Br is shown in Figure 5.3.

5.3.4. Terrestrial emissions

Terrestrial emissions of CH$_3$Cl and CH$_3$Br are poorly quantified. The identified terrestrial sources include tropical plants, tropical leaf litter, wetlands, coastal salt marshes, fungus, shrublands, mangroves, rice paddies and rapeseed, in which tropical terrestrial ecosystems are the largest source for atmospheric CH$_3$Cl and CH$_3$Br (Table 5.1). Estimated terrestrial emissions from prior studies are listed in Table 5.1. Due to the substantial uncertainties and the unknown hemispheric distributions of terrestrial emissions, the terrestrial emissions along with the imbalance between the known sources and sinks are considered as the "unknown emissions" in the model.

5.4. Sinks

Hydroxyl radicals (OH) are the primary oxidant in the atmosphere. Reaction with OH is the largest sink for atmospheric CH$_3$Cl and CH$_3$Br. Since OH has a variety of formation and loss pathways, spatial variability of OH could be large and local OH measurements cannot represent the global or hemispheric OH concentrations. Thus, observations for OH-oxidized trace gases, especially methyl chloroform (CH$_3$CCl$_3$), were commonly used to characterize the global or hemispheric OH concentrations [*Montzka et al.*, 2011 and reference therein; *Prinn et al.*, 2005 and reference therein; *Spivakovsky et al.*, 2000]. In this study, we use monthly three-dimensional OH distributions from *Spivakovsky et al.* [2000] and reaction rate constants from *Sander et*

al. [2006] to calculate the pseudo-first reaction rate constant with OH for CH_3Cl and CH_3Br. Then hemispheric pseudo-first reaction rate constants were calculated based on air-mass weighted averages in both hemispheres. Since there was small inter-annual variability (2.3 ± 1.5 %) for the global atmospheric OH from 1998 to 2007 [*Montzka et al.*, 2011], we assume no inter-annual variation for the hemispheric OH in the model during 1995 – 2011. For the reason that the atmospheric abundances and the temporal variation of CH_3Cl and CH_3Br are sensitive to the change of the atmospheric OH, we tested the rationality of our assumption by simulating hemispheric CH_3CCl_3 concentrations using our calculated hemispheric OH concentrations without inter-annual variation. Simulated CH_3CCl_3 mixing ratios agree with the observations (Figure 5.4).

Soil uptake is another major sink for atmospheric CH_3Cl and CH_3Br. Soil uptake rate constants for CH_3Br were calculated based on the observed uptake rates from six different biomes (tropical forest and savanna; temperature forest, woodland and shrubland; temperature grassland; boreal forest; cultivated land; and tundra) [*Rhew and Abel*, 2007; *Shorter et al.*, 1995; *Varner et al.*, 1999b] multiplying the corresponding biome areas from *Matthews* [1983], then divided by their atmospheric abundances (Table 5.2). For CH_3Cl, the strength of the microbial soil sink is less certain. The global extrapolation based on observations in a Brazilian forest and Arctic grasslands and tundra yielded an estimate of 180 Gg yr^{-1} [*Khalil and Rasmussen*, 2000; *Montzka and Fraser et al*, 2003]. Evidences from stable carbon isotope ratios [*Keppler et al.*, 2005] and cultures on the isolated CH_3Cl-degrading microorganisms [*McAnulla et al.*, 2001]
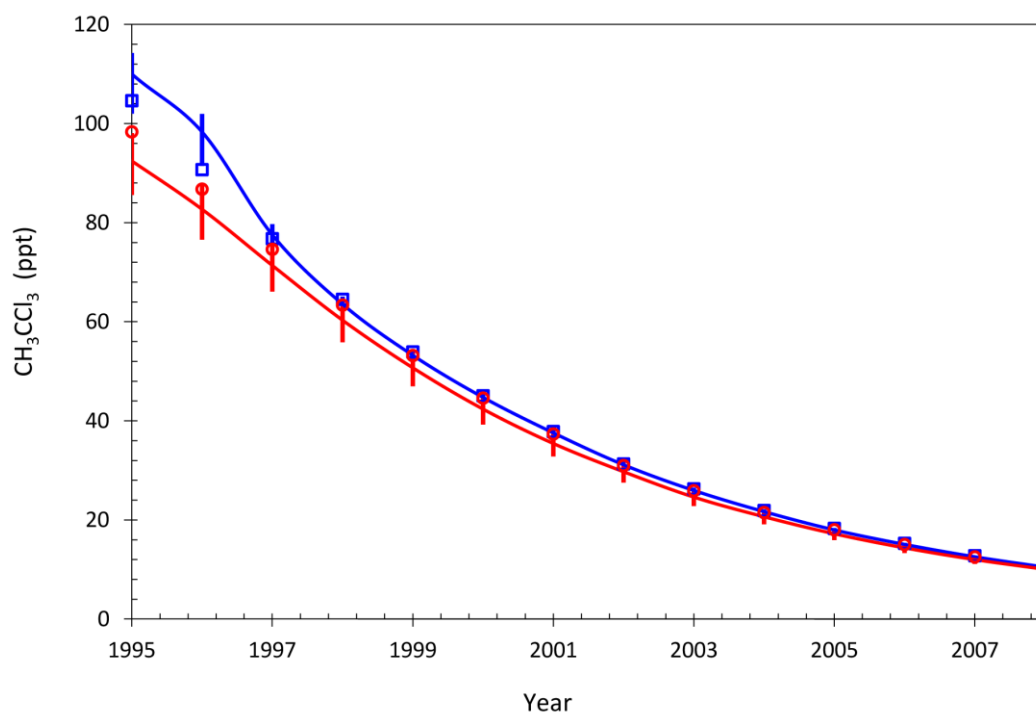
Figure 5.4. Simulated CH_3CCl_3 mixing ratios in the NH (——) and SH (——) using equations (3-4). Annual emissions of CH_3CCl_3 are from *Prinn et al.* [2005]. Hemispheric distributions are from *Midgley and McCulloch* [1995]. Pseudo-first reaction rates of $CH_3CCl_3$with OH were calculated with OH concentrations from *Spivakovsky et al.* [2000] and reaction rate constants from *Sander et al.* [2006]. Oceanic uptake rate constant and stratospheric photolysis loss rate constant of CH_3CCl_3 are from *Yvon-Lewis and Butler* [2002] and *Montzka and Reimann et al.* [2011], respectively. Blue rectangles and red circles are observed mixing ratios in the NH and SH from the Advanced Global Atmospheric Gases Experiment (AGAGE) (http://agage.eas.gatech.edu/data_archive/agage/).

Table 5.2. Hemispheric soil uptake rate constants for CH_3Br and CH_3Cl (yr^{-1}).

[a] Biome	$k_{soil}[CH_3Cl]$ / $k_{soil}[CH_3Br]$	NH Uptake Rate Constant (yr^{-1})		SH Uptake Rate Constant (yr^{-1})	
		CH_3Br[g]	CH_3Cl[h]	CH_3Br[g]	CH_3Cl[h]
Tropical forest and savanna	0.7[b]	0.065 (± 0.002)	0.045 (± 0.001)	0.062 (± 0.001)	0.042 (± 0.001)
Temperate forest, woodland and shrubland	0.6[c]	0.32 (± 0.18)	0.19 (± 0.11)	0.11 (± 0.06)	0.069 (± 0.04)
Temperate grassland	0.8[d]	0.037 (± 0.006)	0.029 (± 0.005)	0.025 (± 0.004)	0.020 (± 0.003)
Boreal forest	0.8[e]	0.017 (± 0.004)	0.014 (± 0.003)	0.0007 (± 0.00002)	0.0006 (± 0.002)
Cultivated land	0.7[b]	0.088 (± 0.008)	0.061 (± 0.006)	0.012 (± 0.001)	0.008 (± 0.001)
Tundra	1.3[f]	0.0045 (± 0.0009)	0.0058 (± 0.0012)	-	-
Total	-	0.53 (± 0.20)	0.34 (± 0.13)	0.20 (± 0.07)	0.14 (± 0.05)

[a] Areas of various biomes are from *Matthews* [1983].
[b] The average ratio of uptake rate constants between CH_3Cl and CH_3Br among those from temperate forest, woodland, and shrubland, temperature grassland, and boreal forest.
[c] Calculated ratio of uptake rate constants between CH_3Cl and CH_3Br based on measurements from *Rhew et al.* [2010].
[d] Calculated ratio of uptake rate constants between CH_3Cl and CH_3Br based on measurements from *Rhew and Abel* [2007] and *Rhew* [2011].
[e] Calculated ratio of uptake rate constants between CH_3Cl and CH_3Br based on measurements from *Rhew et al.* [2003].
[f] Calculated ratio of uptake rate constants between CH_3Cl and CH_3Br based on measurements from *Rhew et al.* [2007].
[g] Calculated based on reported uptake rates from *Shorter et al.* [1995], *Rhew et al.* [2007] and Rhew and Abel (2007), divided by the atmospheric abundance, then multiplied with the biome area in each hemisphere. Uncertainties were from the measured uptake rates by the previous studies.
[h] Calculated based on uptake rate constants of CH_3Br multiplying the ratio of uptake rate constants between CH_3Cl and CH_3Br.

suggest a much higher soil uptake rate for CH_3Cl that may be > 1000 Gg yr^{-1}. In this study, we calculated the ratios of soil uptake rate constants between CH_3Cl and CH_3Br based on the measured uptake rates in temperate grasslands, oak-savanna woodland, boreal forests and Alaskan tundra [*Rhew*, 2011; *Rhew and Abel*, 2007; *Rhew et al.*, 2003; *Rhew et al.*, 2007; *Rhew et al.*, 2010] and scaled the soil uptake rate constants of CH_3Br to those of CH_3Cl using the calculated ratios (Table 5.2).

Unidirectional oceanic uptake rate constants for CH_3Cl and CH_3Br are determined using 1° X 1° grid model [*Hu et al.*, submitted; *Yvon-Lewis and Butler*, 2002]. The strength of the annual oceanic uptake rate was estimated at 360 (250 – 470) Gg yr^{-1} for CH_3Cl, 41 (29 – 50) Gg yr^{-1} (years from 1995 – 1998) for CH_3Br (Table 5.1). Monthly variability for all the loss rate constants is plotted in Figure 5.5. Any uncertainty on the seasonality or inter-annual variability of various losses and known emissions will be incorporated into the calculated total "unknown emissions" ($E_{n,u}$ and $E_{s,u}$) (see Eqs. 5.3 – 5.4).

5.5. Results and Discussion

5.5.1. Derived "unknown emissions" of CH_3Cl and CH_3Br

The imbalance between the best estimates on the sources and those on the sinks is 732 Gg yr^{-1} for CH_3Cl and 35 Gg yr^{-1} for CH_3Br (average of the imbalances between the pre-phaseout and the phaseout budgets) (Table 5.1). Although the strength of the imbalance for atmospheric CH_3Br budget is comparable to that from *Montzka and Reimann et al.* [2011], there are some readjustments on biomass burning emission, oceanic emission and uptake, soil uptake and loss due to reaction with OH (Table 5.1).
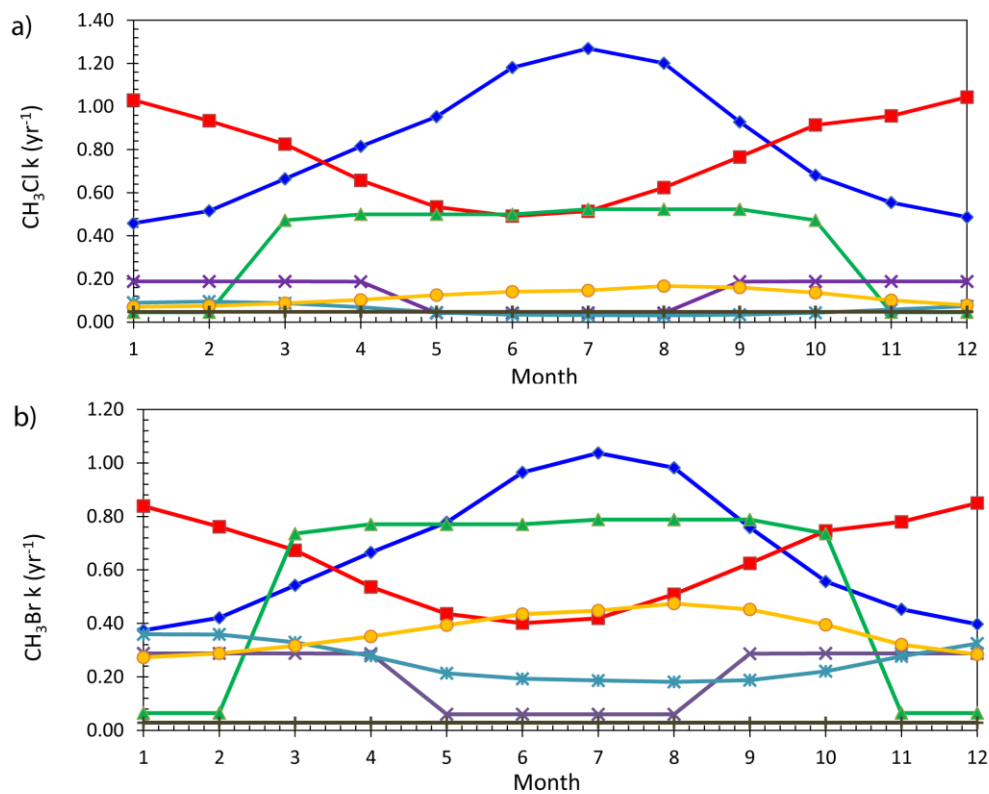
Figure 5.5. Monthly uptake rate constants for various losses (yr^{-1}). The pseudo-first loss rate constants for reaction with OH in the NH ( ) and SH ( ), uptake by the soil in the NH ( ) and SH ( ), uptake by the ocean in the NH ( ) and SH ( ), and loss to the stratosphere in both hemispheres ( ).

In our two-box model, we assume the imbalances in the atmospheric CH_3Cl and CH_3Br budgets, along with their total terrestrial emissions, as the "unknown emissions". Derived "unknown emissions" of CH_3Cl and CH_3Br during 1995 to 2011 using the "top-down" two-box model are 3515 (1476 - 5340) Gg yr^{-1} and 72 (38 – 105) Gg yr^{-1} (Table 5.3 and Figure 5.6). Negative "unknown emissions" of CH_3Br were produced during July to September in the SH in some years (Figure 5.6), which could be due to an underestimate of the loss rate constants, or overestimate of the known emissions or a combination of both. Derived "unknown emissions" of CH_3Cl and CH_3Br display the same seasonality and the same inter-annual variability in both hemispheres (Figure 5.6) and their correlation coefficients are as high as to 0.79 in the NH and 0.87 in the SH, suggesting they may share the same origin.

The "missing sources" of atmospheric CH_3Cl were suggested to be from tropical plants and tropical leaf litter [*Hamilton et al.*, 2003; *Yokouchi et al.*, 2002]. According to results from the previous three-dimensional model studies [*Lee-Taylor et al.*, 2001; *Xiao et al.*, 2007; *Yoshida et al.*, 2004], the total CH_3Cl emission from tropical terrestrial ecosystems was estimated to range from 2197 to 2900 Gg yr^{-1} (mean: 2492 Gg yr^{-1}). Their results were based on the soil uptake rate of CH_3Cl from *Khalil and Rasmussen* [2000], 256 Gg yr^{-1}, which is at the lower limit of the possible range (Table 5.1). Increasing their soil uptake rate to the best value we applied to the model will increase their derived tropical terrestrial emission by 714 Gg yr^{-1}, thereby yielding a total terrestrial emission of 3493 (3044 – 4031) Gg yr^{-1} when combined with other terrestrial emissions. This is comparable to our derived total "unknown emission" of CH_3Cl, 3515

Table 5.3. Derived emissions using equations 5.3 – 5.4 (Unit: Gg yr^{-1}). Emissions of CH_3Cl are the annual mean during 1995 - 2011. Emissions of CH_3Br were the annual emissions in 2009.

	CH$_3$Cl			CH$_3$Br		
	NH	SH	Global	NH	SH	Global
Total Emissions	2656 (1723 - 3467)	2178 (1630 - 2665)	4834 (3353 - 6132)	87 (79 - 95)	50 (47 - 53)	137 (126 - 148)
Total Known	713 (378 - 1058)	606 (413 - 819)	1319 (791 - 1877)	37 (25 - 50)	28 (18 - 38)	65 (43 - 88)
Total Unknown	1943 (665 - 3088)	1572 (811 - 2252)	3515 (1476 - 5340)	50 (29 - 70)	22 (9 - 35)	72 (38 - 105)
Total Natural	2409 (1306 - 3392)	2150 (1585 - 2654)	4559 (2891 - 6046)	69 (54 - 82)	47 (42 - 51)	106 (96 - 133)
Total Anthropogenic	246 (75 - 417)	28 (10 - 45)	274 (85 - 462)	18 (13 - 24)	3 (2 - 4)	21 (15 - 28)
Total Uptake	2624 (1691 - 3435)	2220 (1672 - 2706)	4844 (3363 - 6141)	80 (72 - 88)	58 (55 - 61)	138 (127 - 149)
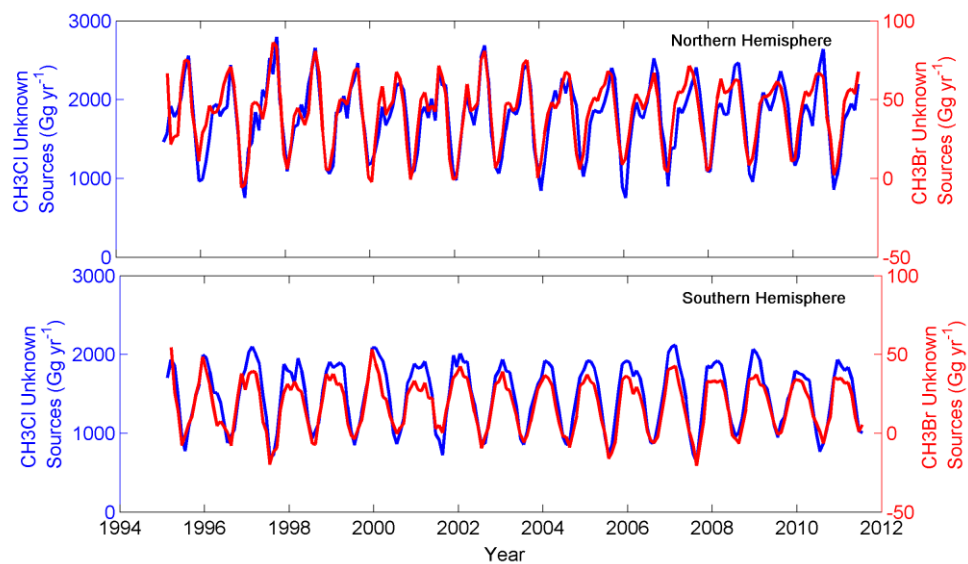
Figure 5.6. Derived hemispheric "unknown emissions" (Gg yr^{-1}) for CH$_3$Br and CH$_3$Cl using equations (5.3 – 5.4) and the best estimates on their known sources and sinks (Table 5.1).

Gg yr^{-1} (Table 5.3), suggesting the "missing source" of atmospheric CH$_3$Cl may be attributable to underestimation on tropical terrestrial emissions. However, we cannot exclude the possibility that part of the "missing source" could result from our overestimation on the sinks. Since the "unknown emissions" of CH$_3$Cl and CH$_3$Br may share the same origin, it is likely that a significant portion of the "missing source" of CH$_3$Br is located in the tropical terrestrial ecosystems. The best estimate for tropical terrestrial emission of CH$_3$Br in this study (Table 5.1) is from *Blei et al.* [2010] and *Gebhardt et al.* [2008]. Both of these studies report the net flux of CH$_3$Br from tropical rainforest rather than the gross emission. Since the tropical soil is also a sink for CH$_3$Br (Table 5.2) [*Shorter et al.*, 1995], the gross emission of CH$_3$Br should be higher than the net flux, 20 Gg yr^{-1} (Table 5.1). This is consistent with results from *Warwick et al.* [2006], which presents additional evidence that the "missing source" of CH$_3$Br, or at least part of it, should be from tropical terrestrial ecosystems.

Tropical rainforests are the dominant source in the total terrestrial emissions of CH$_3$Cl. Destruction of the tropical forests (i.e. deforestation and biomass burning) may cause a reduction on CH$_3$Cl emission from the tropical terrestrial ecosystems, and therefore a decline in its total terrestrial emissions. Based on a report from the *Food and Agriculture Organization of the United Nations (FAO)* [2010], the carbon stock in tropical living forests has decreased by 0.3 % yr^{-1} and 0.8 % yr^{-1} in the tropical NH and tropical SH over the past two decades. However, no apparent declining trend is displayed in the derived "unknown emission" of CH$_3$Cl that is predominated by tropical terrestrial sources. This could arise from several reasons. For example, emission rates of

CH$_3$Cl from tropical terrestrial ecosystems are not only related with carbon stock, they are also associated with plant species and plant growth stage. It is also possible that the amount of dominant CH$_3$Cl-emitting plants has not significantly decreased since 1995 or the average emission rate from tropical living forests has increased slightly because of their growing since 1995. Another possibility is slightly increasing emissions from other terrestrial sources which counteract the declining emission from tropical forests.

Since "unknown emissions" of CH$_3$Br and those of CH$_3$Cl are likely to share the same origin, it indicates that the "total unknown emission" of CH$_3$Br should have the same trend as that of CH$_3$Cl. This helps us to constrain the soil fumigation (fumigation - non-QPS) emissions of CH$_3$Br because if the emission ratio was estimated too high, it would result in an overestimate on the fumigation - non-QPS emissions, which could lead to an increasing trend in the derived "total unknown emissions" (Eqs. 5.3 – 5.4); and vice visa. Therefore, we tested various emission ratios for fumigation - non-QPS uses of CH$_3$Br. Results suggest that, considering the uncertainties of the known sources and sinks (Table 5.1), the emission ratio is likely to be in a range of 65 % to 80 %. The best estimate is 70%, which is higher than the best estimate given by the *United Nations Environment Programme (UNEP)* [2007] and *Yvon-Lewis et al.* [2009], 65 %.

5.5.2. Verification on derived emissions

To verify the derived emissions for CH$_3$Cl and CH$_3$Br and the CH$_3$Br emission ratio of fumigation - non-QPS uses, we ran the coupled 1° x 1° ocean-atmosphere model [*Butler*, 1994; *Montzka et al.*, 2003; *Saltzman et al.*, 2004; *Yvon-Lewis et al.*, 2009] using the derived parameters, along with known emission and uptake rates. Simulated

hemispheric mixing ratios are in good agreement with the observed flask data from NOAA/ESRL GMD (Figure 5.7), suggesting that the derived emissions and the emission ratio of CH_3Br are reliable.

5.5.3. Predicting the new steady-state of atmospheric CH_3Br

As the anthropogenic emission of CH_3Br decreases, the atmospheric CH_3Br has been declining and it will continue to decline until it reaches its new steady state. It is important to examine when the atmospheric CH_3Br reaches its new steady state, what the new steady-state concentration is and how much the tropospheric bromine would drop by removing the remaining anthropogenic uses of CH_3Br. Using the derived "unknown emissions", along with the known emission and uptake rates, we can project the atmospheric mixing ratio using equations (5.3 – 5.4). We ran the two-box model from 1995 to 2020 for three different scenarios. Scenario one assumes only fumigation - non-QPS uses of CH_3Br are phased out. Scenarios two and three assume that fumigation - QPS uses of CH_3Br and all the remaining anthropogenic emissions are eliminated after the phase-out of non-QPS uses, respectively. We also assume that the implementation of the elimination process is one year. For years from 1995 to 2011, we used the derived"unknown emissions", including their strength, seasonality and inter-annual variability, and ran the model forward with known sources and sinks. Calculated seasonality of the total "unknown emissions" during 1995 – 2011, along with the seasonality of known emission and uptake rates, were used in the model for years from 2012 – 2020. Inter-annual variability of the total unknown emissions for CH_3Cl and CH_3Br during 1995 – 2011 only accounts for less than 5% of their total natural
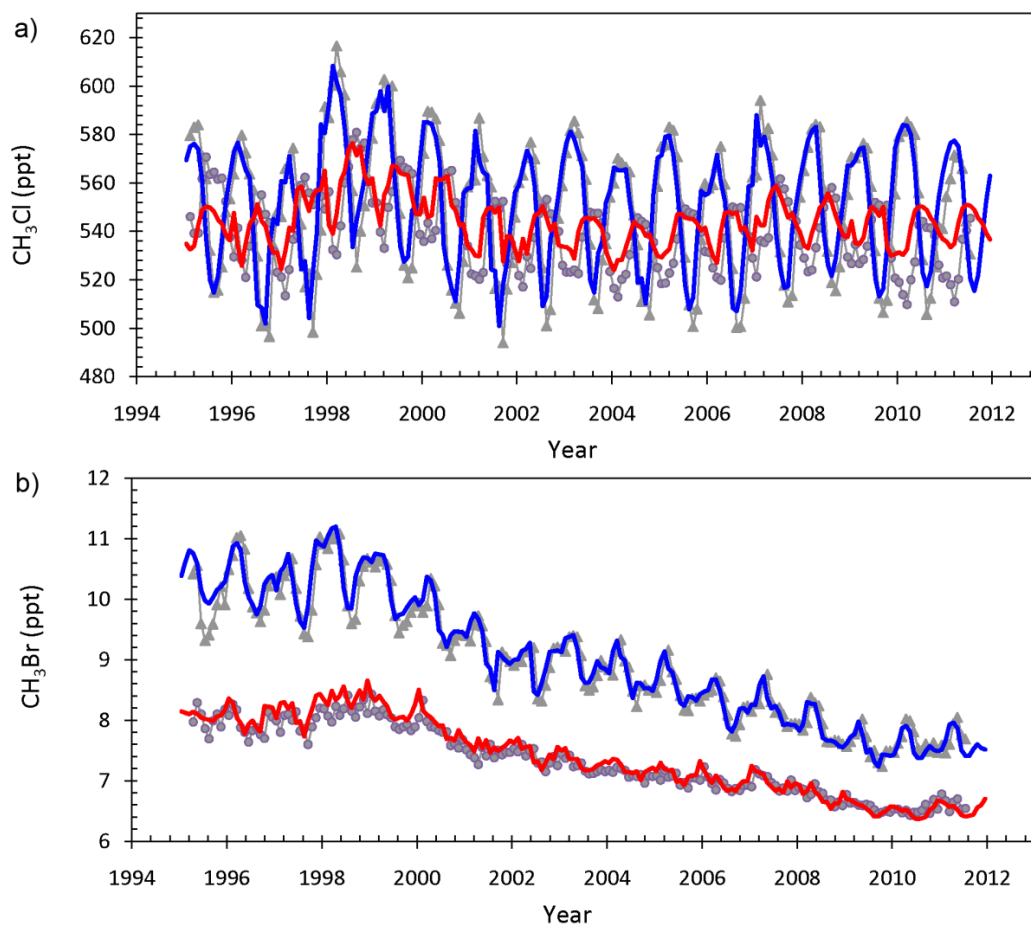
Figure 5.7. Simulated mixing ratios of CH₃Cl (a) and CH₃Br (b) in the NH (━) and SH
(━) using the coupled 1° x 1° coupled ocean-atmosphere model from *Yvon-Lewis et al.*
[2009] along with the calculated total "unknown emissions" and the emission ratio of
fumigation – non-QPS uses, and other known emission and uptake rates. The observed
mixing ratios in the NH (─▲─) and SH (─●─) during 1995 to 2011 are from
NOAA/ESRL GMD (ftp://ftp.cmdl.noaa.gov/hats/methylhalides/).

emissions. Therefore, we assume that there is no inter-annual variability for the natural emissions of CH_3Br and CH_3Cl for years from 2012 – 2020.

In the first scenario, atmospheric CH_3Br will reach its new steady state in 2013 with hemispheric mixing ratios of 7.4 ppt (parts per trillion) in the NH and 6.5 ppt in the SH (Figure 5.8a). The total tropospheric bromine was measured at 15.7 ± 0.2 ppt in 2008 [*Montzka and Reimann et al.*, 2011]. Assuming the tropospheric bromine drops 0.1 ppt yr^{-1} (average declining rate during 1998 – 2008), the tropospheric bromine would be 15.2 ppt in 2013. The atmospheric CH_3Br will contribute to 50 % of the total tropospheric bromine. If the fumigation - QPS uses of CH_3Br are eliminated in 2013 (scenario two), the atmospheric mixing ratio would be further reduced by ~0.5 ppt (NH=6.7 ppt; SH=6.1 ppt) (Figure 5.8b), which only accounts for 3 % of the total tropospheric bromine. If all the anthropogenic emissions are eliminated (scenario 3) (Figure 5.8c), the steady-state CH_3Br concentrations will drop to 6.3 (5.6 – 6.7) ppt in the NH and 5.8 (5.4 – 6.1) ppt in the SH, which is comparable to the mean CH_3Br mixing ratio in the pre-industrial era from the Antarctic ice core measurements, 5.8 ± 0.3 ppt [*Saltzman et al.*, 2004]. Different from CH_3Cl, the SH mixing ratio of CH_3Br is lower than that in the NH at its steady-state. This is likely due to an uneven distribution of natural emission and uptake rates for CH_3Br in both hemispheres (Figure 5.5; Table 5.3). It is also possible that the uneven distribution of CH_3Br at its steady state from the scenario three may result from uncertainties on the known emission and uptake rates.

The ocean acts as both a source and a sink in the atmospheric budgets of CH_3Br and CH_3Cl. It plays an important role in their global biogeochemical cycling. The ocean
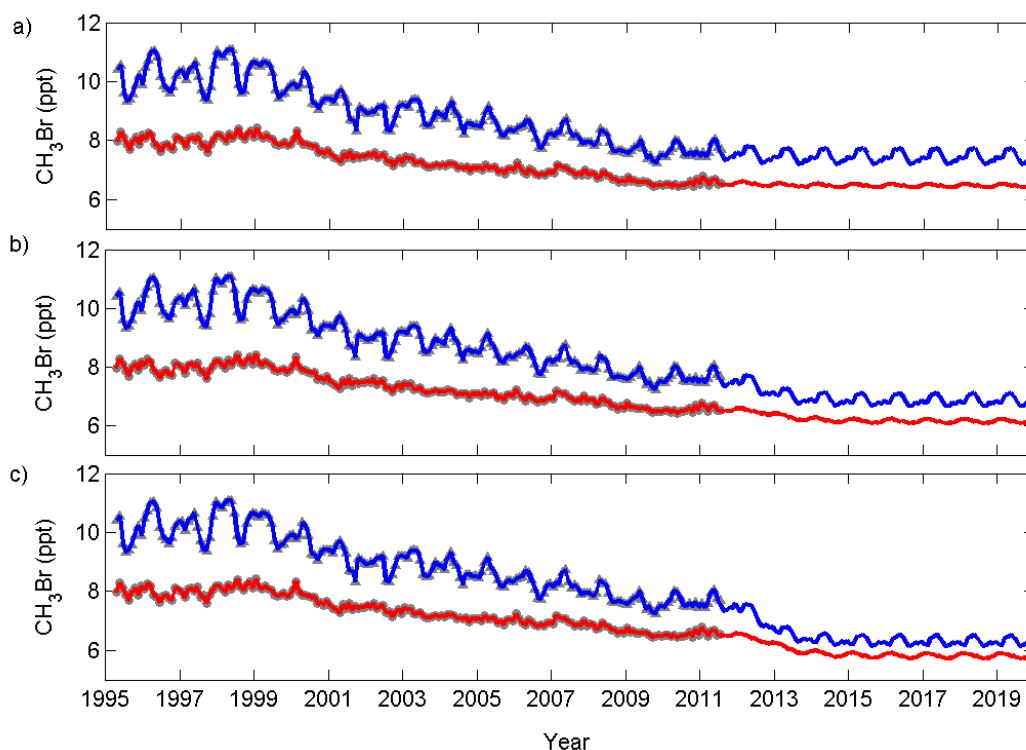
Figure 5.8. Predicted atmospheric CH$_3$Br mixing ratios in the NH (——) and SH (——). (a) Scenario one assuming that only fumigation - non-QPS emissions were phased out. (b) Scenario two assuming that the fumigation - QPS emissions of CH$_3$Br were removed following the end of the fumigation- non-QPS phase-out. (c) Scenario three assuming that all the remaining anthropogenic emissions of CH$_3$Br were eliminated at the end of fumigation non-QPS phase-out. For scenarios one to three, the elimination process was assumed to be one year. The observed mixing ratios in the NH (—▲—) and SH (—●—) during 1995 to 2011 are from NOAA/ESRL GMD (ftp://ftp.cmdl.noaa.gov/hats/methylhalides/).

was estimated to be near equilibrium with atmospheric CH$_3$Br at the end of its fumigation - non-QPS phase-out [*Hu et al.*, submitted]. If the anthropogenic emission continues to decline, the saturation state of CH$_3$Br in the surface ocean is expected to become more positive. Here, we calculated the net sea-to-air flux of CH$_3$Br for three scenarios described above. The global net sea-to-air flux of CH$_3$Br for scenarios one to three was estimated at 2, 4 and 6 Gg yr^{-1}, respectively, suggesting that the ocean will become a net small source if the remaining anthropogenic emissions are eliminated. This result is consistent with the estimated net flux in the pre-industrial budget of CH$_3$Br [*Saltzman et al.*, 2004].

5.5.4. Atmospheric lifetimes of CH$_3$Cl and CH$_3$Br

The total atmospheric lifetime, τ, is determined from the sum of the reciprocal of various loss process:

$$\frac{1}{\tau} = \frac{1}{\tau_{OH}} + \frac{1}{\tau_{soil}} + \frac{1}{\tau_{ocn}} + \frac{1}{\tau_{str}} \tag{5.5}$$

where, τ_{OH}, τ_{soil}, τ_{ocn}, and τ_{str} are partial atmospheric lifetimes due to reaction with OH radicals, loss to soils, uptake by the ocean, and loss to stratospheric photolysis. The partial atmospheric lifetimes with respect to the reaction with OH were estimated at 1.3 (1.1 − 1.5) years and 1.5 (1.3 − 1.8) years for CH$_3$Cl and CH$_3$Br, which are 0.2 years and 0.4 years shorter than the estimates given by *Montzka and Reimann et al.* [2011]. This difference is mainly due to the discrepancy in the use of OH concentrations. Partial atmospheric lifetimes regarding loss to soils were calculated at 4.2 (3.0 − 6.7) years for CH$_3$Cl and 2.7 (2.0 − 4.3) years for CH$_3$Br. Since field measurements on CH$_3$Cl uptake

rate constants by soils are limited, uncertainties on the corresponding partial atmospheric lifetime could be much larger than the range given above. Partial atmospheric lifetimes with respect to the oceanic uptake and stratospheric photolysis are all from prior estimates for CH_3Br and CH_3Cl [*Hu et al.*, submitted; *Montzka and Reimann et al.*, 2011]. The overall atmospheric lifetimes for CH_3Cl and CH_3Br were estimated at 0.9 (0.7 − 1.1) years and 0.7 (0.6 − 1.0) years. The best estimates are 0.1 year shorter than those from *Montzka and Reimann et al.* [2011], which mainly results from shorter partial atmospheric lifetimes regarding to reaction with OH and loss to the soils.

5.6. Summary and conclusions

Significant imbalances in atmospheric CH_3Br and CH_3Cl budgets remain despite substantial efforts made to quantify their sources and sinks over the past two decades. Although it was suggested that the "missing sources" of these two gases are likely to be located in the tropical terrestrial ecosystems [*Hamilton et al.*, 2003; *Warwick et al.*, 2006; *Yokouchi et al.*, 2002], there was no study that examined the linkage of the "missing sources" between these two trace gases. In this study, we investigated the total terrestrial emissions of CH_3Br and CH_3Cl along with the imbalances in their atmospheric budgets using a "top-down" approach. Results indicate that the total terrestrial emissions of CH_3Br and CH_3Cl along with the imbalances in their atmospheric budgets are highly correlated, suggesting that significant portions of these emissions, including emissions from their "missing sources", are likely to share the same origin. Combining these results with those from previous studies suggests that it is possible that part of the "missing sources" is from the underestimation on the gross emission from the tropical

terrestrial ecosystems. However, since uncertainties in the derived "unknown emissions" are associated with those of known emissions and known uptake rates (Eqs. 3 - 4), we cannot exclude the possibility that the imbalances in their budgets may be partially due to the overestimation on the strengths of various sinks. In order to target the location of the "missing sources" and test our hypotheses, gross emission and consumption rate measurements in the tropical terrestrial ecosystems are needed.

Atmospheric CH_3Br mixing ratios after the phase-out of agricultural fumigation are estimated at 7.4 ppt in the NH and 6.5 ppt in the SH at its new steady state. Compared to the peak global mixing ratios during 1996 – 1998, 10.4 ppt in the NH and 8.1 ppt in the SH, they decreased by 3.0 ppt in the NH and 1.6 ppt in the SH, which corresponds to a reduction of 36 – 45 Gg yr^{-1} and 3 – 4 Gg yr^{-1} in the NH and SH emissions. Additional reduction of the fumigation emissions (i.e. eliminating the fumigation-QPS emissions) will not result in a significant further decline in the atmospheric CH_3Br mixing ratios. If all of the remaining anthropogenic emissions were removed, the atmospheric CH_3Br may drop to the pre-industrial level and the ocean will become a small source to the atmospheric CH_3Br.

6. METHANE FLUXES TO THE ATMOSPHERE FROM DEEPWATER HYDROCARBON SEEPS IN THE NORTHERN GULF OF MEXICO*

6.1. Introduction

Methane (CH_4), one of the most important greenhouse gases, has a warming potential 23 times that of carbon dioxide over a 100 year time horizon [*Ramaswamy et al.*, 2001]. It is also actively involved in tropospheric ozone production and stratospheric ozone destruction. The total amount of methane reserved in the form of gas hydrate is about 2×10^6 Tg in a global inventory [*Boswell and Collett*, 2011]. It is comparable to about 400 times the total mass of the global atmospheric methane, 4850 ($\pm$242) Tg [*IPCC*, 2001]. Although the gas hydrate is an enormous methane reservoir, the contribution of the gas hydrate from the seafloor to the atmospheric methane budget is poorly characterized. It is estimated that marine seeps emit $18 - 48$ Tg yr^{-1} of methane from the continental shelves to the overlying water column [*Hornafius et al.*, 1999]. However, the global emission from gas hydrates to the atmosphere is less than 5 Tg yr^{-1} [*Reeburgh*, 2007].

Methane released from the seafloor or produced in microenvironments in the water column [e.g. *Cynar and Yayanos*, 1991; *de Angelis and Lee*, 1994] can reach the

atmosphere through turbulent diffusion or rising bubbles. In shallow water, rising bubbles are the predominant pathway for delivering methane from seeps to the atmosphere, while the net sea-to-air fluxes via diffusion are also considerable [*Mau et al.*, 2007; *Schmale et al.*, 2005]. In deep water systems, turbulent diffusion is a commonly cited pathway to deliver methane to the atmosphere, whereas it is still debatable whether or not bubbles are capable of surviving from the seafloor to the surface and, if so, how much methane would be displaced by other gases (i.e. oxygen, nitrogen etc.) as they are stripped out of the water as the bubble moves to the surface [*McGinnis et al.*, 2006; *Rehder et al.*, 2002, 2009]. Methane transport via rising bubbles from the deepwater seeps to the atmosphere depends on a variety of geological and physical parameters, including intensity and composition of the seepages, bubble initial size, release depth, bubble path, and dissolution rate [*Leifer and MacDonald*, 2003]. Most previous studies reported that the diffusive net sea-to-air fluxes of methane from deepwater seep systems (water depth > 200 m) are insignificant [e.g. *Kessler et al.*, 2006; *Reeburgh et al.*, 1991; *Schmale et al.*, 2005; *Yvon-Lewis et al.*, 2011]. However, one recent study suggests that the diffusive net sea-to-air flux of methane from the deepwater hydrocarbon seeps to the atmosphere could be considerable [*Solomon et al.*, 2009].

To better understand and quantify the diffusive net sea-to-air fluxes of methane from deepwater hydrocarbon seeps, we investigated three deepwater seeps featuring near-seafloor gas hydrate in the northern Gulf of Mexico. High spatial and temporal

resolution measurements were made to determine the net sea-to-air fluxes of methane over these hydrocarbon seeps.

6.2. Method

6.2.1. Location and measurements

The HYFLUX cruise took place in the northern Gulf of Mexico during July of 2009 (4 July – 19 July, 2009) aboard the *R/V Brooks McCall*. Intensive surface surveys were conducted above three active seeps, MC118 (Rudyville, 28.8522^{o} N, 88.4928^{o} W, 900 meters below sea level, mbsl), GC600 (Oil Mountain, 27.3652^{o} N, 90.5642^{o} W, 1250 mbsl), and GC185 (Bush Hill, 27.7823^{o} N, 91.5080^{o} W, 550 mbsl) (Figure 6.1), which were characterized by seafloor gas hydrate deposits that were partly exposed to seawater. Active oil and gas venting was confirmed by a remotely operated vehicle (ROV) at fixed locations within all three sampling sites. Air and surface seawater samples were analyzed continuously (except for brief maintenance intervals) during occupation of the sites and transits. The air-sea sampling plan had two modes: 1) a coarse regular grid, where samples were spaced at a kilometer scale, and 2) a fine sampling scale that occurred as the ship loitered above the ROV, where samples were spaced $\leq$ 10 m. The ship speed was kept below 4 knots over most of the seep areas (Figure 6.2e).

To measure the diffusive net sea-to-air fluxes of methane and infer its origin, atmospheric and surface seawater dissolved C_1 - C_3 hydrocarbons were measured continuously with an automated sampling system coupled to a Weiss-type equilibrator
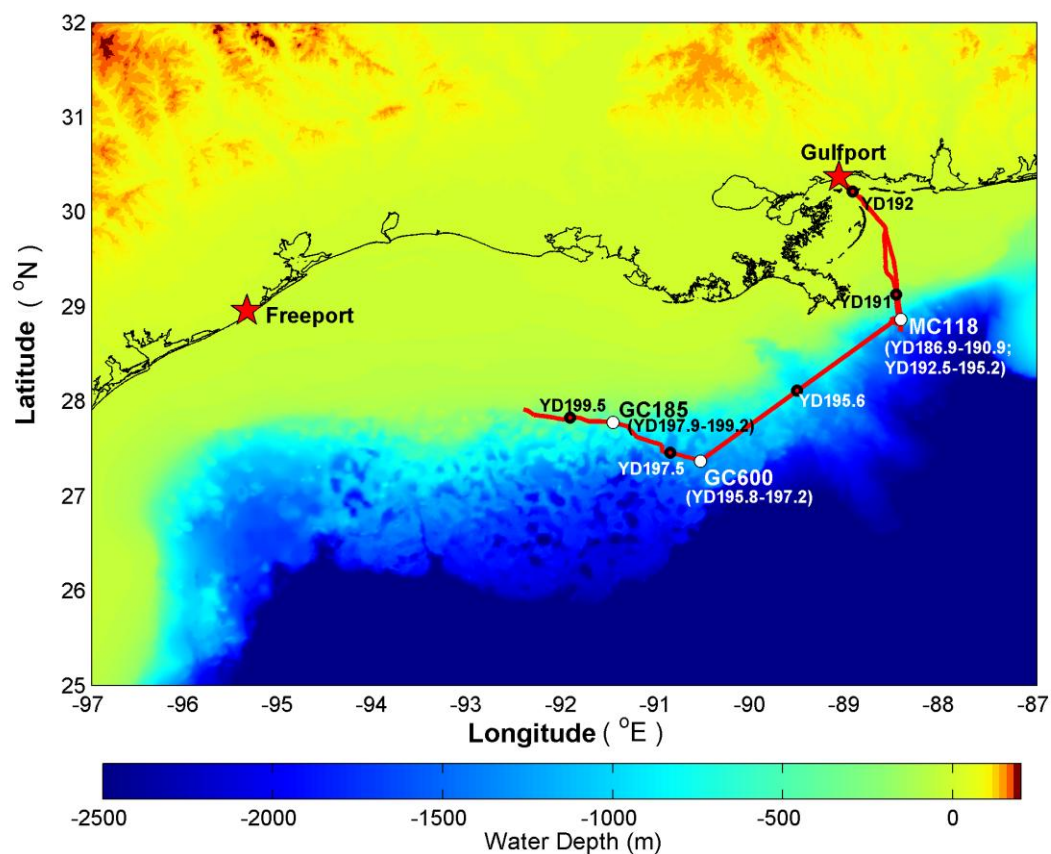
Figure 6.1. Cruise track (red line) of HYFLUX cruise in July of 2009. Colored surface of the map indicates the water depths and land surface elevations. The bathymetric data are from the NOAA National Geophysical Data Center (http://www.ngdc.noaa.gov/mgg/bathymetry/relief.html). White circles denote the locations of the three seep sites; black circles mark the year days (YD) along the cruise track; red stars stand for the ports where the ship departed or arrived.
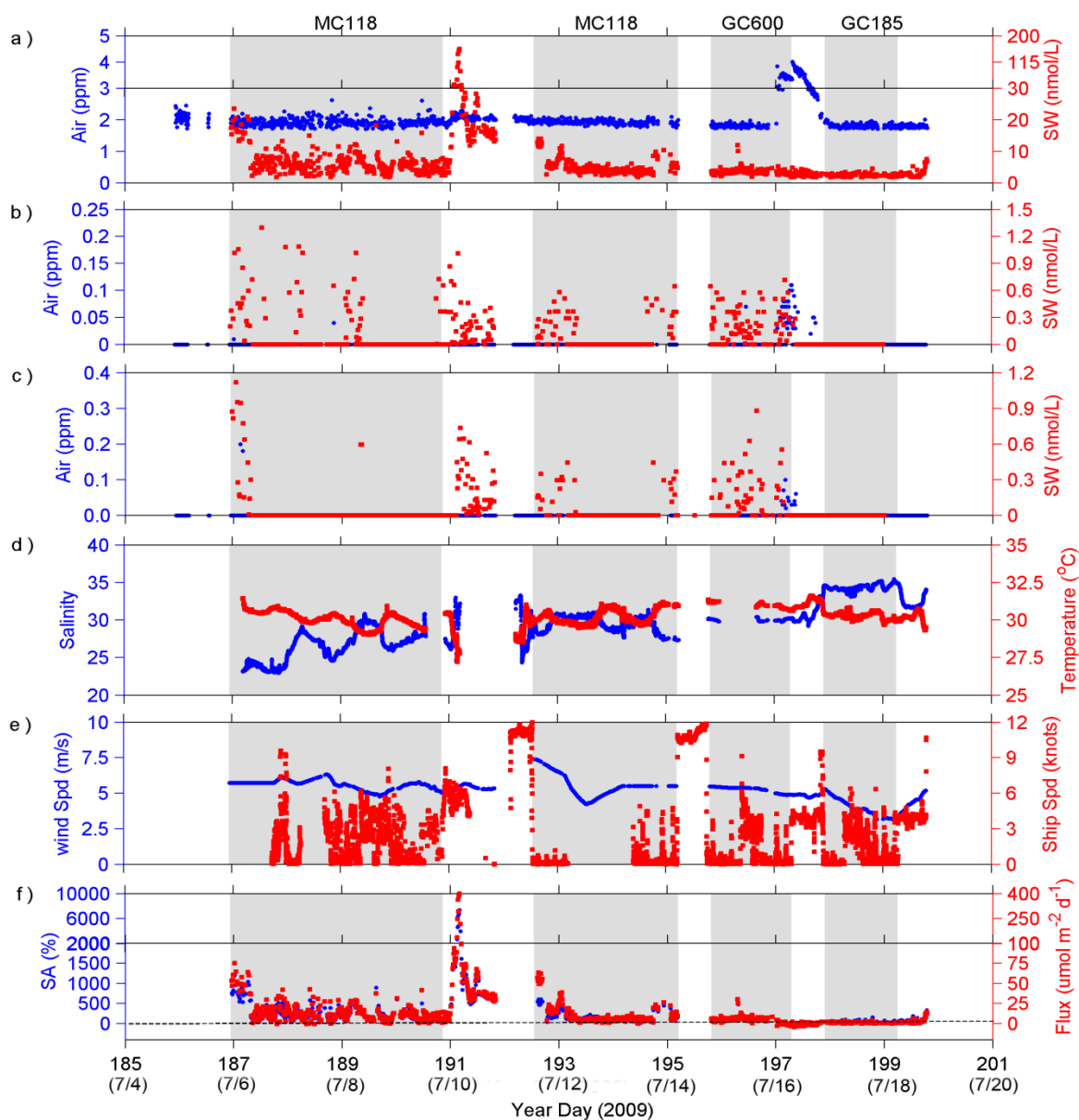
Figure 6.2. (a) Atmospheric mixing ratios (blue) and surface seawater concentrations (red) of methane; the scales for surface seawater methane in ranges of $0 - 30$ nmol L^{-1} and $30 - 200$ nmol L^{-1} are different. (b - c) Atmospheric mixing ratios (blue) and surface seawater concentrations (red) of ethane (b) and propane (c). (d) Sea surface salinity (blue) and temperature (red); (e) 24 hour averaged wind speeds at 10 m above sea level prior to sampling (blue) and ship speeds along the cruise track (red). (f) Saturation

Figure 6.2. Continued

anomalies (blue) and net sea-to-air fluxes (red) of methane; different scales for saturation anomalies in ranges of -40 – 2000 % and 2000 – 10000 % and fluxes in ranges of -20 – 100 μmol m^{-2} d^{-1} and 100 - 400 μmol m^{-2} d^{-1}; dash line marks zero saturation anomaly and zero flux. Concentrations of zeros for panels a – c indicate concentrations below the instrument detection limit. Grey shadows mark the time periods over three seep sites. X-axis is the year day of 2009 and the corresponding month/day is labeled in the brackets.

_____

and a Gas Chromatograph / Flame Ionization Detector (GC/FID, Agilent 6850) system (Appendix B). This technique only quantifies the diffusive net sea-to-air flux of dissolved methane and not the direct bubble injection of methane to the atmosphere; however, direct bubble injection to the atmosphere could be manifested in the data as enhanced atmospheric concentrations relative to surface seawater.

Air samples were pumped continuously at ~ 6 L min^{-1} through 0.63 cm ID Synflex tubing (Motion Industries, TX) mounted on the railing on the top of flying bridge and running to the laboratory. Surface seawater (about 4 m below the sea surface) was pumped into the Weiss-type equilibrator at 15 L min^{-1}. Equilibrator headspace and ambient air were alternately sampled every 6 minutes using a stream select valve. The sample stream passed through a 20 μL sampling loop after being dehumidified by a Nafion dryer (Permapure Inc). The Nafion dryer and the 20 μL sampling loop were

flushed with the sample air at a rate of 25 mL min^{-1} for 90 seconds before injection into the GC/FID, which was equipped with a 15 m long, 32 μm ID GS-GasPro column (1 m pre-column and 14 m main-column) with nitrogen carrier gas. Prior to the cruise, a series of standard mixtures (C_1 - C_3) ranging from 0 – 1000 ppm (parts per million) were made using two known concentration standards (15 ppm and 1000 ppm) from Scott Specialty Gases. Standards with methane concentrations at 0.09 (± 0.01) ppm, 1.09 (± 0.02) ppm, 1.69 (± 0.02) ppm and 2.88 (± 0.06) ppm were also calibrated against a whole air tank, which was calibrated to the NOAA-04 methane scale. The standards with methane concentrations at 0.09 – 2.88 ppm were used to create a standard curve to calibrate the instrument. Higher concentration standards 15 (± 1.5) ppm, 503 (± 25) ppm, 1000 (± 50) ppm were also run and used as an alternate calibration curve when the measured concentration exceeded the lower calibration range. The precision of the system was determined from five standard injections. The precision for concentrations ≤ 3 ppm was 3 % for methane, 2 % for ethane and 3 % for propane. The precision for concentrations > 3 ppm was less than 1 % for methane, ethane and propane.

The sea surface temperature and salinity were continuously measured by a Conductivity Temperature Depth (CTD) sensor from Sea-Bird Electronics (SBE 19 plus) at the outflow of the equilibrator. Wind speeds and directions were continuously measured by an anemometer at a height of ~ 9 m above the sea level.

6.2.2. Equilibrator concentration correction

The equilibrator headspace technique has been used for the determination of the net sea-to-air fluxes of many dissolved gases including but not limited to halocarbons

[*Butler et al.*, 2007 and references therein; *Hu et al.*, 2010 and references therein], CO_2 [*Takahashi et al.*, 2009 and references therein] and methane [*Amouroux et al.*, 2002; *Bange et al.*, 1994, 1996, 1998; *Kourtidis et al.*, 2006; *Rhee et al.*, 2009] over the past 20 years.

Due to the different solubilities for different gases, the time needed for the trace gas concentration in the headspace to reach equilibrium with the incoming seawater is different for each trace gas. The headspace mass concentration, C_e, at a time, t, can be expressed with the following equation when the equilibrator vent flow, Q_v, is zero [*Johnson*, 1999].

$$C_e = (C_i - \frac{C_w}{\alpha})e^{-(t/\tau_1)} + \frac{C_w}{\alpha} \tag{6.1}$$

where, $\tau_1 = \frac{V_e}{Q_w \varepsilon \alpha}$; V_e is the volume of the headspace, 12.5 L; Q_w is the volumetric flow rate of the seawater, 15 L min^{-1}; ε is a dimensionless equilibrator coefficient, which is typically about 0.3 - 0.4 [*Johnson*, 1999]; α is the Oswald solubility coefficient; C_i is the initial mass concentration in the headspace and C_w is the mass concentration of the trace gas in the incoming seawater.

When the equilibrator vent flow, Q_v, is not zero, the air in the headspace is removed and replaced by the ambient air at a rate of Q_v. The trace gas concentration in the headspace can then be expressed by the following equation [*Johnson*, 1999].

$$C_e = \frac{\frac{C_w}{\alpha \tau_1}(1 - e^{-t/\tau_2}) + \frac{C_a}{\tau_v}(1 - e^{-t/\tau_2}) + \frac{C_i}{\tau_2}e^{-t/\tau_2}}{1/\tau_2} \tag{6.2}$$

where, $\tau_v = \dfrac{v_e}{Q_v}$ and $\dfrac{1}{\tau_2} = \dfrac{1}{\tau_1} + \dfrac{1}{\tau_v}$; C_a is the mass concentration of the trace gas in the

ambient air.

Under normal operating conditions, the equilibrator vent flow is zero except the duration when the instrument is flushing the dryer and sample loop (i.e. collecting the headspace air sample). Assuming the equilibrator vent flow is off for a period of t_1 (min) and on for a period of t_2 (min) at a rate of Q_v (ml min^{-1}), the trace gas concentration in the headspace at $t_1 + t_2$ can be expressed as:

$$C_e = \frac{\dfrac{C_w}{\alpha \tau_1}(1 - e^{-t_2/\tau_2}) + \dfrac{C_a}{\tau_v}(1 - e^{-t_2/\tau_2})}{1/\tau_2} + ((C_i - \frac{C_w}{\alpha})e^{-t_1/\tau_1} + \frac{C_w}{\alpha})e^{-t_2/\tau_2} \qquad (6.3)$$

Since the trace gas concentrations in the ambient air and in the equilibrator headspace were measured, C_a, C_i, and C_e are known. The trace gas concentration in seawater can be expressed as a function of C_a, C_i, and C_e (Equation 6.4).

$$C_w = \frac{C_e - \dfrac{\tau_2}{\tau_v}(1 - e^{-t_2/\tau_2})C_a - e^{-(\frac{t_1}{\tau_1} + \frac{t_2}{\tau_2})}C_i}{\dfrac{\tau_2(1 - e^{-t_2/\tau_2})}{\alpha \tau_1} + \dfrac{(1 - e^{-t_1/\tau_1})e^{-t_2/\tau_2}}{\alpha}} \qquad (6.4)$$

In this study, the vent flow, 25 ml min^{-1}, was only on for 2.5 min between two seawater measurements, resulting in only 1 % of difference in the C_w compared to the case without the vent flow. Given such a small effect, we can simplify equation (6.4) by assuming the vent flow is 0 during t_1 to t_2. Then τ_v is equal to 0, and τ_1 is equal to τ_2. Equation (6.4) can be expressed as:

$$C_w = \frac{C_e - C_i e^{-(\frac{t_1 - t_2}{\tau_1})}}{\frac{1 - e^{-(\frac{t_1 + t_2}{\tau_1})}}{\alpha}} \qquad (6.5)$$

In equations (6.1 – 6.5), it is assumed that the trace gas concentration in the seawater is constant during t_1 and t_2. However, in reality, this assumption may not be true especially when the ship speed is fast. Therefore, assuming the seawater concentration is constant during a very short time period (Δt) (i.e. < 1 second) and the seawater concentrations are $C_{w_1}, C_{w_2}, ..., C_{w_{n-1}}, C_{w_n}$ for each Δt ($n\Delta t = t_1 + t_2$), the trace gas concentration in the headspace can be expressed by:

$$C_e = (C_i - \frac{C_{w_1}}{\alpha})e^{-\frac{n\Delta t}{\tau_1}} + (\frac{C_{w_1} - C_{w_2}}{\alpha})e^{-\frac{(n-1)\Delta t}{\tau_1}} + (\frac{C_{w_2} - C_{w_3}}{\alpha})e^{-\frac{(n-2)\Delta t}{\tau_1}} + ... + (\frac{C_{w_{n-1}} - C_{w_n}}{\alpha})e^{-\frac{\Delta t}{\tau_1}} + \frac{C_{w_n}}{\alpha}$$

$$(6.6)$$

By substituting the C_e in equation (6.5) with equation (6.6), C_w can be expressed by:

$$C_w = \frac{1 - e^{-\Delta t/\tau_1}}{1 - e^{-n\Delta t/\tau_1}}(C_{w_1} e^{-\frac{n-1}{\tau_1}\Delta t} + C_{w_2} e^{-\frac{n-2}{\tau_1}\Delta t} + C_{w_3} e^{-\frac{n-3}{\tau_1}\Delta t} + ... + C_{w_{n-1}} e^{-\frac{1}{\tau_1}\Delta t} + C_{w_n}) \qquad (6.7)$$

Assuming $a_i = \frac{1 - e^{-\Delta t/\tau_1}}{1 - e^{-n\Delta t/\tau_1}} e^{-\frac{n-i}{\tau_1}\Delta t}$ ($i = 1, 2, 3, ..., n$), C_w can be rewritten as:

$$C_w = a_1 C_{w_1} + a_2 C_{w_2} + a_3 C_{w_3} + ... + a_{n-1} C_{w_{n-1}} + a_n C_{w_n} \qquad (6.8)$$

Therefore, the fractional contributions of the true seawater concentrations, $C_{w_1}, C_{w_2}, ..., C_{w_{n-1}}, C_{w_n}$, to the corrected seawater concentration (C_w) are $a_1, a_2, ..., a_{n-1}, a_n$. For the very soluble gases (i.e. CO_2, N_2O), $a_1, a_2, ..., a_{n-1}, a_n$ exponentially increase from 0 to 1 as a_1 goes to a_n, and C_w is more representative of an instantaneous incoming

seawater concentration. For the less soluble gases (i.e. CH_4, CO), $a_1, a_2, ..., a_{n-1}, a_n$ are close to $1/n$ and C_w is more representative of an average seawater concentration during the last $n\Delta t$ min. In this study, the seawater concentrations were calculated using equation (2.4), and they represent average seawater concentrations over a period of 12 min. As the ship speed was in a range of $0 - 4$ knots when sampling, 12 min represents a distance of $0 - 1480$ m.

6.2.3. Net sea-to-air flux calculation

The net sea-to-air flux (F) is calculated by:

$$F = k_w(C_w - \alpha C_a)$$ (6.9)

where, k_w is the gas transfer velocity (m d^{-1}) [*Sweeney et al.*, 2007], and C_w, C_a and α are defined above. The gas transfer velocity parameterization from *Sweeney et al.* [2007] is an improvement over the typical *Wanninkhof* [1992] parameterization since they closed the previous gap between field measurements [*Liss and Merlivat*, 1986; *Nightingale et al.*, 2000] and radiocarbon estimates [*Tans et al.*, 1990; *Wannninkhof*, 1992] on this parameter.

The gas transfer velocity (k_w) from *Sweeney et al.* [2007] is expressed as:

$$k_w = 0.27 u_{10}^2 (\frac{Sc}{660})^{-0.5}$$ (6.10)

where, Sc is the Schmidt Number of methane in seawater from *Wanninkhof* [1992] and u_{10} is the 10 m normalized wind speed (m s^{-1}) determined using the equation given by *Large and Pond* [1982].

6.3. Results

Atmospheric methane during this cruise ranged from 1.70 ppm to 4.01 ppm with a mean of 2.03 ppm (Figure 6.2a). The atmospheric methane fluctuated around a background concentration of 1.92 ppm during the occupation of the sites and transits except at the end of GC600 and the transit to GC185 (Figure 6.2a). The surface seawater methane concentrations ranged from 1.76 to 23.5 nmol L^{-1} at MC118, 1.76 to 11.9 nmol L^{-1} at GC600, and 1.72 to 4.48 nmol L^{-1} at GC185 (Table 6.1). The presence of ethane (Figure 6.2b) and propane (Figure 6.2c) in the surface seawater over the seep area (mainly at MC118 and GC 600) indicates a thermogenic contribution from the deepwater hydrocarbon seeps. The maximum methane concentration observed in surface seawater during this study, 156 nmol L^{-1}, was observed on year day (YD) 191 (10 July, 2009) on the continental shelf offshore from Louisiana (Figures 6.1 and 6.2a). The corresponding atmospheric methane concentrations reached 2.10 ppm due to the net sea-to-air flux (Figure 6.2a). Increased ethane and propane along with elevated salinity and decreased temperature (Figures 6.2b, c and d) suggest that the elevated methane in the surface seawater may be associated with upwelling of hydrocarbon enriched waters. A similar feature in the surface seawater was observed in the same region in June of 2010 during the Persistent Localized Underwater Methane Emission Study (PLUMES) [*Yvon-Lewis et al.*, 2011].

The methane saturation anomaly is defined as the percent difference between the partial pressures of methane in surface seawater and air. They ranged from -51.8 % to

Table 6.1. Mean atmospheric methane mixing ratios, seawater methane concentrations, saturation anomalies and net sea-to-air fluxes of methane at the three seep sites (ranges of values in parentheses).

Sites	Atmospheric CH$_4$ mixing ratio (ppm)	Seawater CH$_4$ concentration (nmol L^{-1})	Saturation anomaly (%)	Averaged wind speed (m s^{-1})	Flux (μmol m^{-2} d^{-1})	
					W92[a]	S07[b]
MC118	1.93 (1.71-2.62)	5.85 (1.76-23.5)	207 (-6.42-1196)	5.6	15.4 (-0.52-86.1)	12.8 (-0.45-75.0)
GC600	2.13 (1.72-3.83)	3.61 (1.76-11.9)	90.5 (-46.0-598)	5.3	5.41 (-4.19-34.9)	4.67 (-3.65-30.4)
GC185	1.81 (1.71-1.98)	2.41 (1.72-4.48)	39.6 (2.33-156)	4.0	1.25 (0.08-4.13)	1.07 (0.07-3.60)

[a] W92 refers to the flux calculated using the *Wanninkhof* [1992] gas transfer velocity parameterization;

[b] S07 refers to the flux calculated using the *Sweeney et al.* [2007] gas transfer velocity parameterization

7.43 X 10^3 % (Figure 6.2f). The calculated net sea-to-air fluxes ranged from -4.68 to 416 μmol m^{-2} d^{-1} (Figure 6.2f). The mean net sea-to-air flux at each of the three seep areas was 12.8 μmol m^{-2} d^{-1} (MC118), 4.67 μmol m^{-2} d^{-1} (GC600) and 1.07 μmol m^{-2} d^{-1} (GC185) (Table 6.1). To compare the results from this study to those from previous studies, we calculated the flux using the gas transfer velocity from *Wanninkhof* [1992] in addition to using the *Sweeney et al.* [2007] relationship described earlier. The calculated net sea-to-air methane fluxes from the deepwater hydrocarbon plume areas are one to two orders of magnitude lower than those from shallow water seep plume areas (Table 6.2; *Mau et al.*, 2007; *Schmale et al.*, 2005). For the deep water environment, the calculated fluxes from this study are in the same range as those determined from most previous studies (Table 6.2; *Reeburgh et al.*, 1991; *Schmale et al.*, 2005; *Yoshida et al.*, 2004; *Yvon-Lewis et al.*, 2011). However, they are three orders of magnitude lower than those reported by *Solomon et al.* [2009] who investigated the same region as the current study including one of the same identified seep sites.

6.4. Discussion

Based on the results above, four main issues will be addressed in the following discussion: 1) the source for the elevated atmospheric methane during the transit from GC600 to GC185; 2) the diffusive net sea-to-air fluxes of methane over three seep sites and the extrapolated total fluxes of methane over the deepwater seep area in the northern Gulf of Mexico; 3) potential causes for the large discrepancy between the results from this study and those reported by *Solomon et al.* [2009]; and 4) the impact of small areas of high methane concentration hotspots on our regional air-sea flux estimate if extremely

Table 6.2. Diffusive net sea-to-air fluxes of methane from different marine environments.

Location	Water Depth (m)	Flux (μmol m^{-2} d^{-1}) [a]	Reference
Deep water environments (> 200 m)			
Deepwater hydrocarbon plume area in the northern Gulf of Mexico	550 – 1250	-4.19 - 86.1	This study
Deepwater hydrocarbon plume area in the northern Gulf of Mexico	500 - 600	200 - 10,500	*Solomon et al.*, 2009
Plume area during the Deepwater Horizon oil spill	1500	-0.055 - 1.83	*Yvon-Lewis et al.*, 2011
Sorokin Trough and Dnepr Area in Black Sea	>200	40.6 - 49.2	*Schmale et al.*, 2005
Central Black Sea	>200	27	*Reeburgh et al.*, 2006
Sea of Okhotsk	>200	0.36 - 88	*Yoshida et al.*, 2004
Baltic and North Seas	>200	-6.6 - 13.89	*Bange et al.*, 1994
Aegean Sea	>200	1.81	*Bange et al.*, 1996
Northwestern Levantine Basin	>200	3.02	*Bange et al.*, 1996
Open Ocean in the Atlantic	>200	0.3	*Rhee et al.*, 2009
Open Ocean in the Pacific	>1000	0.9 - 3.5	*Tilbrook and Karl*, 1995
Shallow water environments (≤ 200 m)			
Coal Oil Point	<70	195	*Mau et al.*, 2007
Northwest Black Sea	<200	53	*Amouroux et al.*, 2002
Northwestern continental shelf of the Sea of Okhotsk	<200	0.47 - 11	*Yoshida et al.*, 2004
Shelf waters of Dnepr Area	<200	67	*Schmale et al.*, 2005
Coastal region of the Atlantic	<200	3.2	*Rhee et al.*, 2009

[a] Fluxes were calculated using the gas transfer velocity parameterization of *Wanninkhof* [1992].

high concentrations existed in the surface seawater over a deepwater hydrocarbon plume area and were missed in this study.

6.4.1. Elevated atmospheric methane

An area of elevated atmospheric methane with a maximum concentration of 4.01 ppm was observed on YD 197 (16 July) at GC600 (Figure 6.2a). The elevated atmospheric methane persisted for 19 hours and extended over 50 kilometers to the northwest of GC600 during the transit to GC185 (Figure 6.2a). Coincident elevated ethane and propane in the atmosphere suggest a thermogenic gas contribution (Figures 2.2b and 2.2c). The 24 h air-mass back-trajectories obtained from the NOAA Air Resources Laboratory (http://www.ready.noaa.gov/ready/open/hysplit4.html) show that the air masses with increased atmospheric methane came from the same region as those with background concentrations of 1.81 ppm (Figure 6.3), suggesting a localized source rather than long-range transport. Since the methane concentrations in the underlying seawater were close to a seawater background concentration of 2.40 nmol L^{-1} (Figure 6.2a), methane transport via diffusive sea-to-air gas exchange is not the source of these high atmospheric concentrations.

Although bubbles traveling over 1000 m from a deepwater seep site have been observed [*Greinert et al.*, 2006], whether or not they can reach the surface is still debated [*McGinnis et al.*, 2006; *Rehder et al.*, 2009]. In this study, to increase the atmospheric methane concentration to 4.01 ppm (3.25 ppm averaged over the area with elevated methane concentrations), there would need to be 3 X 10^5 mol d^{-1} of methane released to the atmosphere assuming a marine boundary layer height of 700 m (data
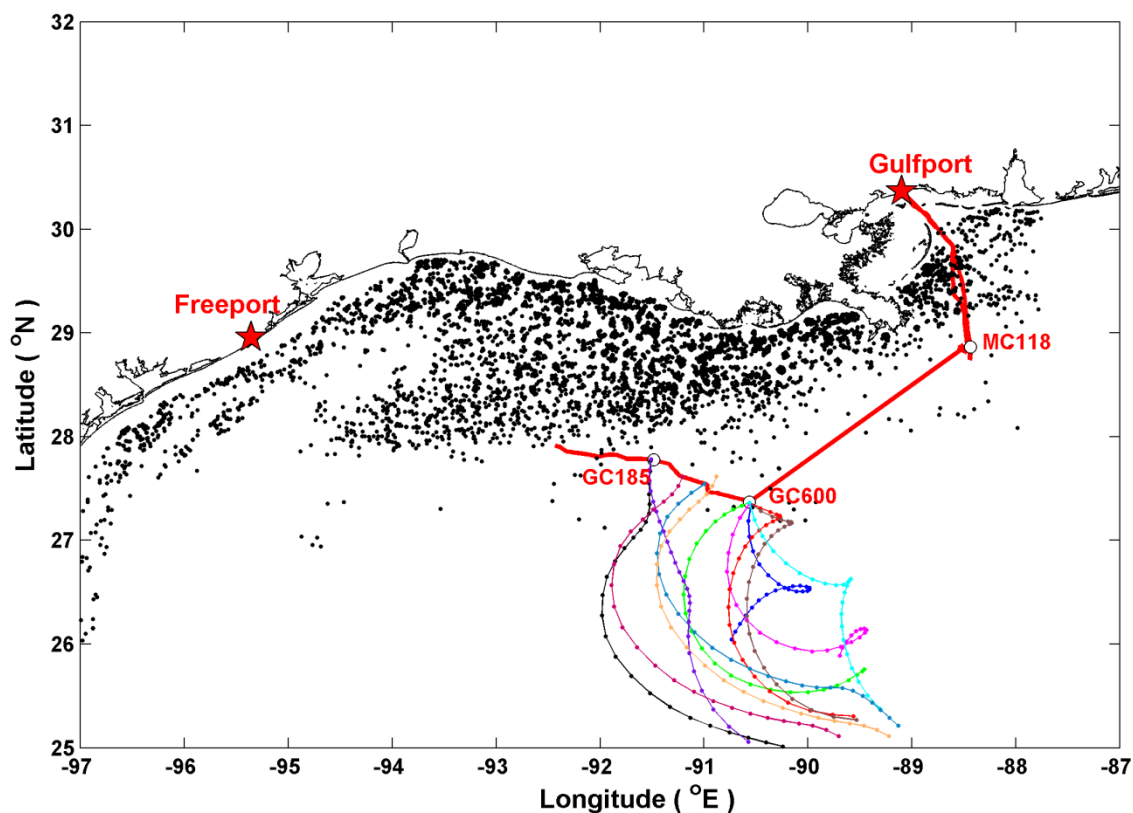
Figure 6.3. 24 hour back-trajectories of air masses (dot lines) and locations of oil platforms (black dots) in the northern Gulf of Mexico. Back-trajectories were downloaded from NOAA Air Resources Laboratory (http://www.ready.noaa.gov/ready/open/hysplit4.html) and platform locations are from MMS Gulf of Mexico regional database (http://www.gomr.mms.gov/homepg/pubinfo/repcat/arcinfo/index.html). White circles denote the locations of three seep sites. Red stars stand for the ports where the ship departed or arrived.
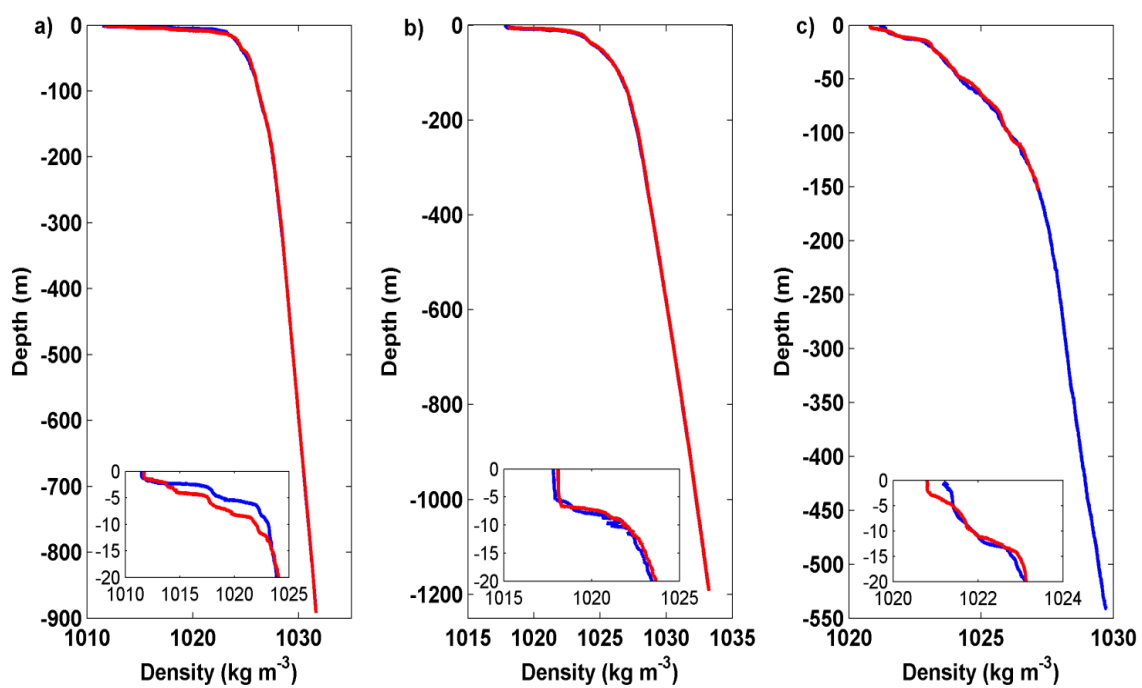
Figure 6.4. Vertical profiles of density at MC118 (a), GC600 (b) and GC185 (c). Red and blue lines stand for two randomly selected CTD casts from each site.

from http://ready.arl.noaa.gov/READYamet.php) and assuming that the elevated methane only spread out in a circle 100 m in diameter centered on the ship as it moved along the cruise track. It is not likely for direct methane transport via gas bubbles at GC600 to contribute such a large amount of methane to the atmosphere due to the strong pycnocline during the summer (Figure 6.4) and the 1200 m water depth at this site. While slicks were observed from the ship at this site along with intermittent oil droplets rising to the surface, surface water concentrations were 2.85 ± 0.73 (1 σ) nmol L^{-1}, suggesting that these droplets were not carrying high concentrations of methane. Since the observation of the elevated atmospheric methane to the northwest of GC600 does coincide with satellite data from 20 July showing very extensive oil slicks over this broad region of the Gulf, we could not completely exclude the possibility that methane could be transported inside of the oily bubbles to the atmosphere. However, we cannot provide an appropriate mechanism for this possibility.

Fugitive release to the atmosphere directly from oil platforms around GC600 is possible (Figure 6.3). Given the fact that no significantly elevated atmospheric methane concentrations were observed near the recovery ships during the Deepwater Horizon oil spill, which were flaring tremendous amounts of gas [*Yvon-Lewis et al.*, 2011], flaring itself is an unlikely source of methane to the atmosphere. Not flaring or accidentally releasing gas from the drilling oil platform during this time is not likely to be the explanation either based on the drilling records from the Drilling Rig OCEAN MONARCH (the rig close to GC600). A likely explanation could be an undetected leak from one or more of the nearby oil platforms.
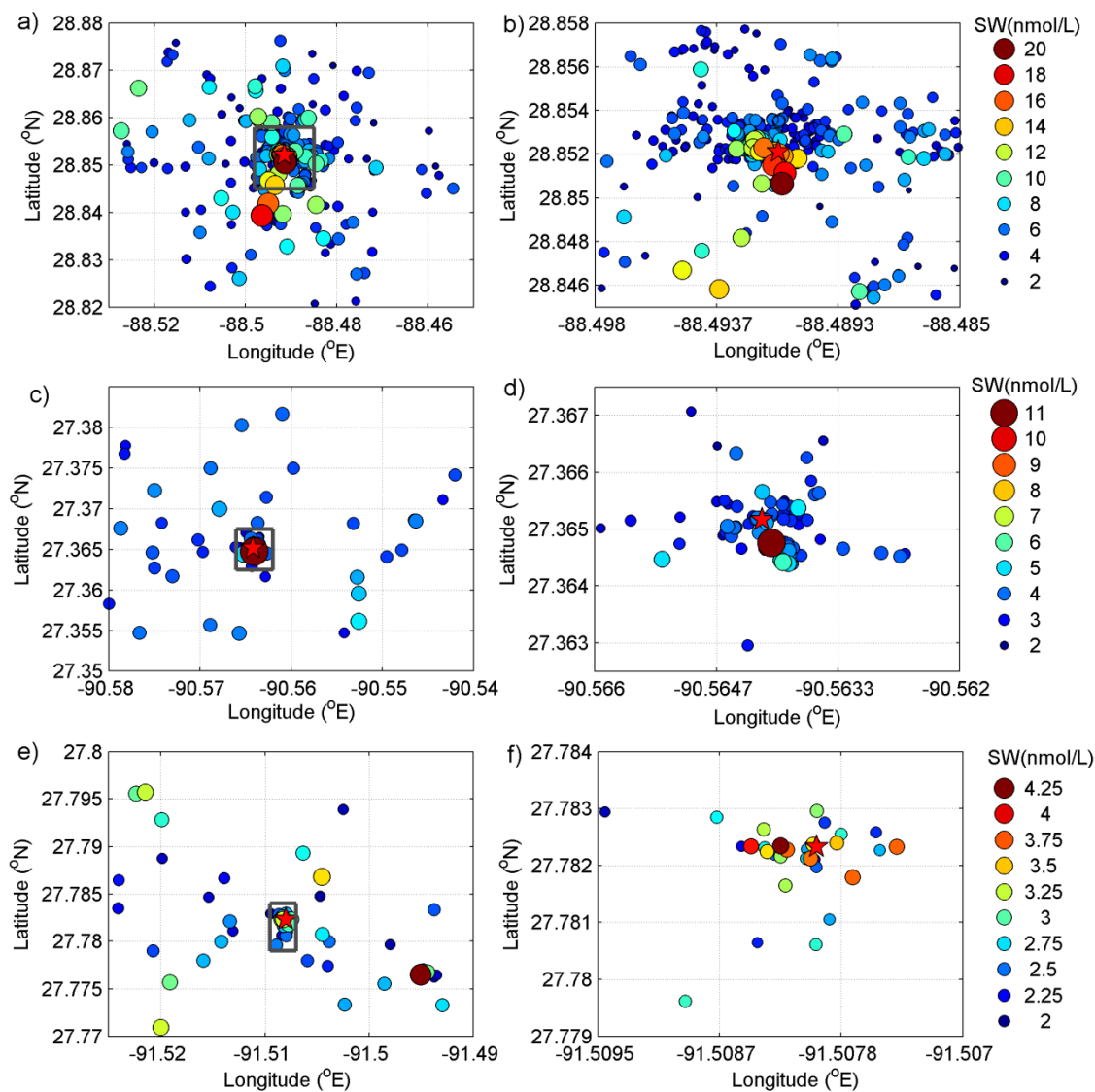
Figure 6.5. Methane concentrations in surface seawater at MC118 (a - b), GC600 (c - d) and GC185 (e - f). Grey rectangles in the lefthand panels indicate the blown-up regions, which are plotted in the righthand panels. Red stars indicate the locations of the seeps.
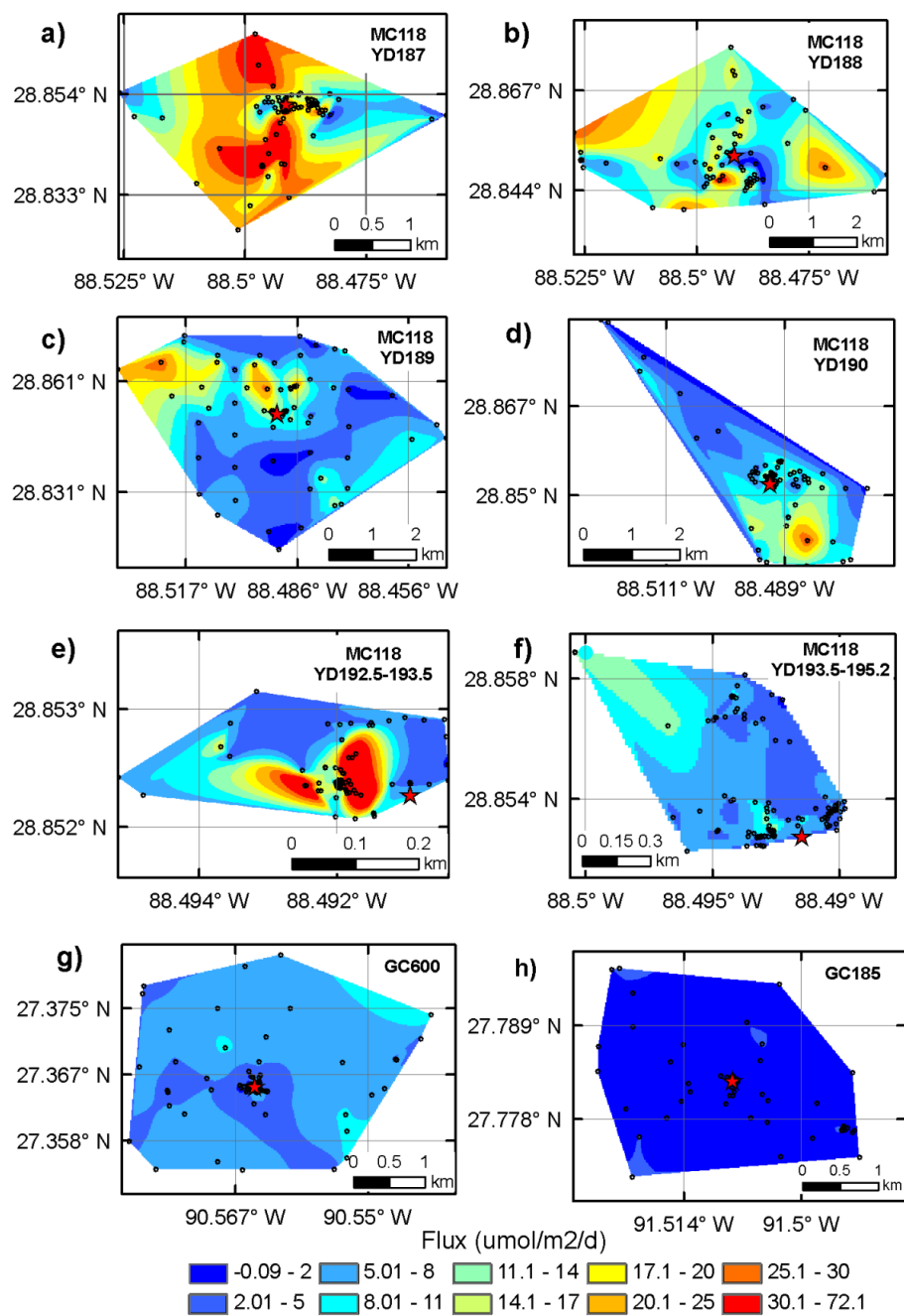
Figure 6.6. Contour plots of methane net sea-to-air fluxes at the three seep sites using natural neighbor. Red stars indicate the locations of the seeps. Black circles stand for the locations of the flux measurements.

6.4.2. Methane net sea-to-air fluxes over the seep area in the northern Gulf of Mexico

High spatial variability was observed in sea surface methane and net sea-to-air fluxes over the three seep areas (Figures 6.5 and 6.6). Overall, MC118 had higher sea surface methane concentrations and higher net sea-to-air fluxes than either GC600 or GC185 (Tables 6.1 and 6.3; Figures 6.5 and 6.6). GC600 is the oiliest site surveyed during this study. Although surfactants can inhibit bubble dissolution and enhance the methane transport, lower surface seawater methane concentrations and lower diffusive fluxes were observed than those at MC118. GC185 is the shallowest site occupied during this study. During a prior study at this site, a methane concentration of 608 nmol L^{-1} at a water depth of ~ 20 m was reported and used to determine a net sea-to-air flux of 3420 μmol m^{-2} d^{-1} in the plume area [*Solomon et al.*, 2009]. Therefore, higher methane concentrations in the air and sea surface as well as higher fluxes were anticipated. However, both the atmospheric methane and the sea surface (4 mbsl) methane were near background (Table 6.1). Spatial variability between sites is associated with characteristics of their geological and physical environment, e.g. seep intensity, oil-water ratio, water depth, currents, and mixed layer depth. Spatial variability within one seep site (Figure 6.5) is related with the rising angle of the bubbles and the directions of mid-depth and surface currents. High temporal variability within one seep site was also observed during our surface survey (Figures 6.2 and 6.6). The magnitudes of the fluxes and the elevated flux areal extent vary from day to day (Table 6.3; Figure 6.6). The temporal variability of methane fluxes could be due to changes in seepage rates,

Table 6.3. Mass fluxes over the survey area using different interpolation gridding methods. The boundaries for the gridded fluxes are shown in figure 6.6. The year day is abbreviated as YD.

Sites	Survey Area (km^2)	Area with fluxes ≥ 8 μmol m^{-2} d^{-1} (km^2)	Natural Neighbor		Inverse Distance Weighted		Krigging	
			Area weighted mean flux (μmol m^{-2} d^{-1})	Mass Flux (mol d^{-1})	Area weighted mean flux (μmol m^{-2} d^{-1})	Mass Flux (mol d^{-1})	Area weighted mean flux (μmol m^{-2} d^{-1})	Mass Flux (mol d^{-1})
MC118								
YD 187	15.15	14.00	19.8	300	21.5	326	23.2	352
YD 188	16.27	13.91	13.2	215	12.0	195	11.3	183
YD 189	34.64	12.31	7.82	271	8.68	301	9.11	316
YD 190	8.530	3.430	7.75	66.1	8.70	74.2	8.82	75.2
YD 192.5 - 193.5	0.06155	0.03014	12.1	0.744	15.5	0.954	18.7	1.15
YD 193.5 -195.2	0.5318	0.0055	6.98	3.71	6.36	3.38	6.23	3.31
GC600	8.571	0.407	6.05	51.9	5.53	47.4	5.26	45.1
GC185	6.686	0.000	1.02	6.85	1.03	6.86	1.00	6.69

currents, wind speeds, surface wave action, etc. [*Clark et al.*, 2003, 2010; *Greinert et al.*, 2006; *Leifer and Boles*, 2005; *Leifer et al.*, 2006; *Quigley et al.*, 1999].

The daily methane mass flux distribution for each survey area was determined by interpolation using natural neighbor, inverse distance weighted interpolation, and krigging (Table 6.3). The three different interpolation methods do not produce significantly different fluxes. Since the natural neighbor method produced a smoother shape, we chose this algorithm as our main interpolation method for plotting the mass flux distribution over the seep sites. Due to the high temporal and spatial variability of the methane fluxes within and between sites, it is difficult to extrapolate the observed net sea-to-air fluxes to other periods or to other hydrocarbon seeps (Figures 6.5 and 6.6). However, we can approximate the upper limit of the diffusive net sea-to-air flux of methane from the deepwater hydrocarbon seeps in the northern Gulf of Mexico under normal conditions (i.e. no mud volcanoes or submarine earthquake) by assigning the highest daily flux determined in this study, 300 mol d^{-1} (per seep site), to other deepwater hydrocarbon seeps in this region. Large uncertainty exists in the number of active seeps in the northern Gulf of Mexico. Geophysical anomalies generated by seeps in the geologic past exceed 5000 possible sites [*Frye*, 2008] whereas preliminary results for seeps detected by remote sensing (see the detailed method in *Garcia-Pineda et al.* [2010]) suggest a maximum number of active vents about 1500. Assuming that each of the 1500 - 5000 seeps in the northern Gulf of Mexico has daily net sea-to-air flux of 300 mol d^{-1} and they persistently emit methane to the atmosphere at the same rate over a one-year period, the total diffusive net sea-to-air flux from deepwater hydrocarbon seeps in

the northern Gulf of Mexico is about 3 - 9 Gg yr^{-1}. Compared with the total annual emission of methane to the atmosphere, 5.8 X 10^5 Gg yr^{-1} [*Denman et al.*, 2007], the contribution of the net diffusive sea-to-air flux from deepwater hydrocarbon seeps in the northern Gulf of Mexico is insignificant to the atmospheric methane budget.

6.4.3. Explanation for flux discrepancy

The three orders of magnitude methane flux discrepancy between this study and that reported by *Solomon et al.* [2009] is mainly attributable to the surface seawater methane values used in the flux equation (Equation 6.9). The "surface" seawater methane concentrations reported in *Solomon et al.* [2009] were in the range of 57.1 − 1609 nmol L^{-1} while the methane concentrations in this study ranged from 1.72 − 23.5 nmol L^{-1}. Although we cannot exclude the possibility of temporal variability, we can evaluate the methodological differences between these two studies. How each study defines a "surface" sampling depth is a key factor that bears consideration. In the present study, seawater was continuously sampled from ~ 4 m water depth within the mixed layer as the ship was moving. Mean mixed layer depths were 4.8 m (0 − 28.8 m; median: 3.5 m; 32 CTD casts) at MC118, 4.9 m (4.2 − 5.5 m; 2 CTD casts) at GC 600, and 2.1 m (1.4 − 2.6 m; 3 CTD casts) at GC185 (Figure 6.4). When determining the air-sea flux using the air-sea concentration gradient, the dissolved concentrations must be measured as close to the surface as possible. By contrast, the shallowest sample collected in *Solomon et al.* [2009] was around 20 m. Their temperature and salinity profiles (see supplementary materials in *Solomon et al.* [2009]) do not display a mixed layer depth

below 20 m. Therefore, the "surface" water value they used to calculate methane fluxes were not diagnostic of true surface water values.

A contributing but minor factor to the differences in net sea-to-air fluxes reported in the two studies involves the atmospheric methane concentrations used in the flux calculation. *Solomon et al.* [2009] used an averaged atmospheric methane concentration for their flux calculations, while the atmospheric mixing ratios were measured once every 12 minutes locally during the current study. Atmospheric methane ranged from 1.70 ppm to 4.01 ppm over the seep sites during the current study. At times, the atmospheric methane concentrations were over twice the average background concentration. In some places during the occupation of GC600, the surface ocean acted as a sink for atmospheric methane and would have been misinterpreted as a source to the atmosphere if average atmospheric methane concentrations were used in the flux calculations. Fluxes of methane from the ocean to the atmosphere or other incidental hydrocarbon emissions could result in perturbations to the local atmospheric methane concentrations, and these perturbations should be accounted for in the calculation of the flux.

6.4.4. Impact of small area high concentration hotspots on the regional air-sea flux

To determine if the regional air-sea flux results from continuous air-sea measurements are more representative than discrete measurements, we investigate whether the technique used in this study could have missed a high methane concentration hotspot that is large enough to impact the overall flux from the plume area. To address this possibility, the sensitivity of the corrected seawater concentration (C_w) to

the size and concentration of a potential hotspot is determined using equation (6.7). We assumed 1) that any corrected seawater concentration $\geq$ 4 nmol L^{-1} (twice the background concentration) indicated an observable hotspot; and 2) that the ship left a background concentration of 2 nmol L^{-1} and immediately crossed a methane hotspot with a concentration ranging from 4 to 1609 nmol L^{-1} (the highest 20 m value reported by *Solomon et al.* [2009]). Under these conditions, a surface hotspot with a concentration of 1609 nmol L^{-1} is observable for a hotspot with a diameter $\geq$ 2 m when the ship speed is 4 knots (e.g. when the ship is conducting coarse surveys) (Figures 6.7a and 6.7c), and a diameter $\geq$ 5 cm when the ship speed is 0.1 knots (e.g. when the ship was holding a station) (Figures 6.7b and 6.7d). As the concentration of the hotspot decreases, the hotspot size required for unequivocal detection would exponentially increase (Figure 6.7).

Since the corrected seawater concentration (C_w) is close to an average concentration over 12 min (see equation 6.7), it averages out the high and low seawater concentrations. Here, we will assess the possible impact of missed hotspots along the survey track. Assuming the three seep sites only contain hotspots with methane concentrations of 1609 nmol L^{-1} and waters with background concentrations of 2 nmol L^{-1}, the possible sizes of the missed hotspots can be determined by equation (6.7) using the actual ship speeds and the observed concentrations. The area of each possible missed hotspot ranges from 5.2×10^{-4} m^2 to 77 m^2 and the total area of missed hotpots in each of the three plume areas is 181 – 930 m^2 (MC118), 51 m^2 (GC600) and 20 m^2 (GC185), corresponding to fluxes of 0.80 – 5.16 mol d^{-1} (MC118), 0.24 mol d^{-1} (GC600) and 0.05
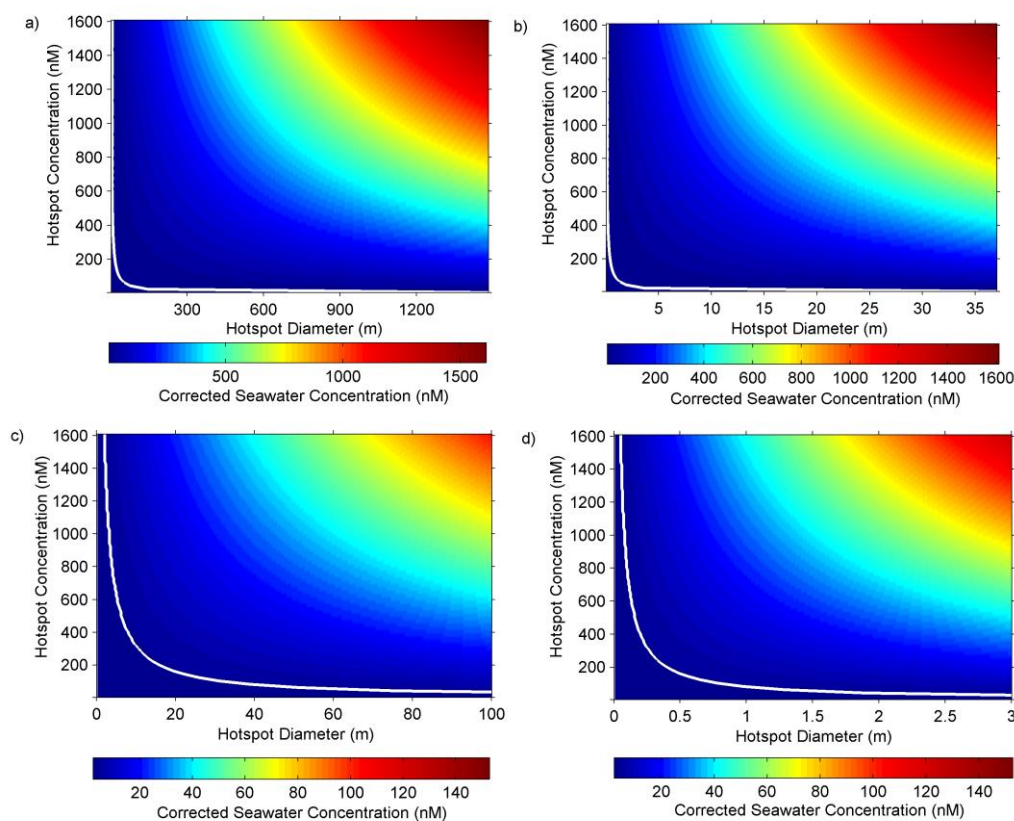
Figure 6.7. Corrected seawater methane concentrations (C_w) (colored contours) as a function of hotspot sizes (x-axis) and hotspot concentrations (y-axis). (a) A scenario when the ship crosses a hotspot with an infinite variety of sizes and concentrations from a background concentration of 2 nmol L^{-1} at a ship speed of 4 knots (e.g. when ship is doing coarse survey). (b) A scenario when the ship crosses a hotspot with an infinite variety of sizes and concentrations from a background concentration of 2 nmol L^{-1} at a ship speed of 0.1 knots (e.g. when ship is holding station). (c) is an expansion of (a) and (d) is an expansion of (b). White lines indicate 4 nmol L^{-1} contours, our defined boundary for an observable hotspot signal. Any concentration or size condition to the right and above the white line meets the criteria for being a detectable hotspot.

Table 6.4. The integrated net mass flux of methane from each survey area each day and the total potential mass flux from hotspots at those sites.

Sites	Survey Area (km^2)	Mass Flux [a] (mol d^{-1})	Total Hotspot Area (km^2)	Hotspots Mass Flux [b] (mol d^{-1})
MC118				
YD 187	15.15	300	0.930 x 10^{-3}	5.16
YD 188	16.27	215	0.238 x 10^{-3}	1.34
YD 189	34.64	271	0.444 x 10^{-3}	1.82
YD 190	8.53	66.1	0.181 x 10^{-3}	0.82
YD 192.5 - 193.5	0.062	0.74	0.597 x 10^{-3}	4.66
YD 193.5 -195.2	0.53	3.71	0.181 x 10^{-3}	0.80
Mean		142		2.43
GC600	8.57	51.9	0.051 x 10^{-3}	0.24
GC185	6.69	6.85	0.020 x 10^{-3}	0.05

[a] Integrated mass flux using natural neighbor. [b] The total methane flux from hotspots assuming relatively small areas of hotspots exist on the survey tracks.

mol d^{-1} (GC185) (Table 6.4). The mean flux over each plume area resulting from hotspots that might have been missed using the current survey technique accounts for only 1.7 % (MC118), 0.5 % (GC600) and 0.7 % (GC185) of the integrated regional flux (Table 6.4).

Another potential limitation of the survey technique used in this study is the possibility that hotspots between the survey tracks were never sampled. Since the extremely high surface water methane concentrations reported in *Solomon et al.* [2009] were from GC185, we use this site to investigate the impact of missed hotspots between the survey tracks. Assuming that either the missed hotspots or our sampling pattern were randomly distributed throughout the survey area, we estimate the probability that a hotspot was completely missed. For each surface water measurement, the probability (*P*) that a hotspot was missed is calculated as a function of the total integrated hotspot area (A_h) and the total survey area (A; 6.686 km^2) of GC185.

$$P = (A - A_h) / A \qquad (6.11)$$

Since we sampled 71 times, the probability that the hotspot was completely missed on all 71 measurements is P^{71}. This calculation clearly shows that as the area of the hotspot increases, the probability that it was missed rapidly decreases (Figure 6.8). While there is an increased probability that a relatively small total integrated hotspot area was missed, this relatively small area leads to a relatively small flux from hotspots. Interestingly, even if we assume a background flux of 50 times the observed value for GC185, a total integrated hotspot area of only 1.92 % of the survey area is necessary to produce a daily flux similar to our "background" observations. And for a hotspot area of
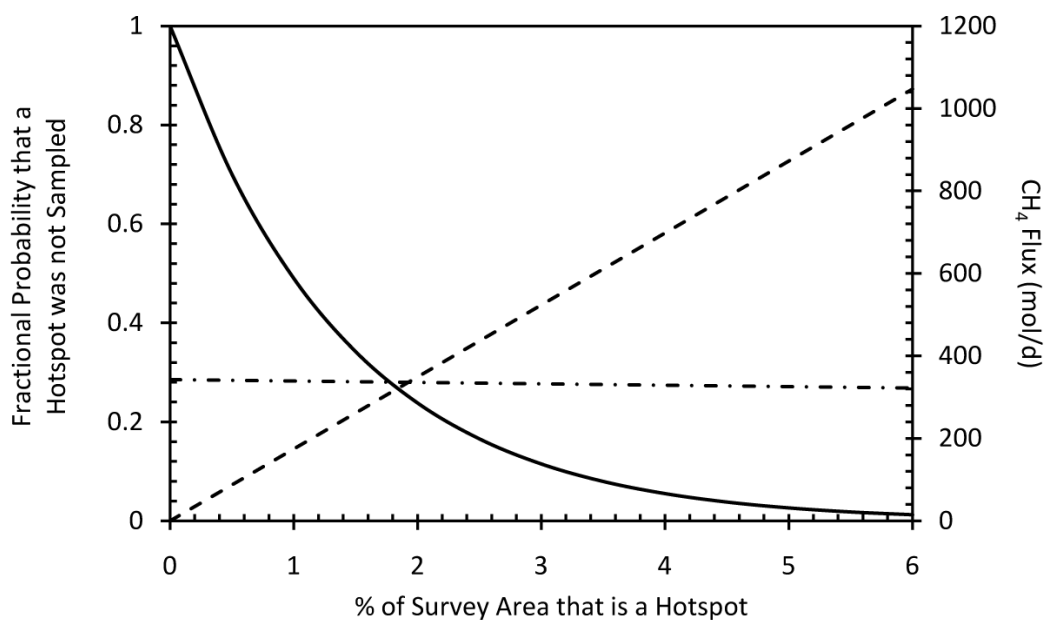
Figure 6.8. Hotspots potentially missed between sampled locations at GC185 as a function of assumed total hotspot area. Probability that a hotspot was missed during the survey ($n = 71$) (solid line). CH_4 flux from the total integrated hotspot area (dashed line). CH_4 flux from the fifty-times the background (i.e. non-hotspot) area at GC185 (dashed-dotted line).

1.92 %, there is only a 25 % chance that hotspots covering this total integrated area were missed during our sampling campaign.

6.5. Conclusions

Elevated methane concentrations in surface seawater were observed, and elevated net sea-to-air methane fluxes were determined at three seep sites (MC118, GC 600 and GC185) in the northern Gulf of Mexico. The net sea-to-air methane fluxes ranged from - 4.19 μmol m^{-2} d^{-1} to 86.1 μmol m^{-2} d^{-1} over the deepwater hydrocarbon plume areas, agreeing with most previous studies. Variations in the atmospheric methane concentrations suggest the need for measuring atmospheric methane concentration when assessing the net sea-to-air fluxes. High temporal and spatial variability in the methane fluxes was observed over the three seep areas. Extrapolating the highest flux from this study to other deepwater hydrocarbon seeps in the northern Gulf of Mexico suggests that diffusive net sea-to-air fluxes from deepwater hydrocarbon seeps in the northern Gulf of Mexico is an insignificant source to atmospheric methane. However, the elevated air concentrations on GC600 require about 3 X 10^5 mol d^{-1} of methane released in this area. This tremendous methane source could not be characterized during this study.

Three orders of magnitude of discrepancy exist between the results from this study and those reported in *Solomon et al.* [2009] for the estimation of the diffusive net sea-to-air flux of methane from deepwater hydrocarbon seeps in the northern Gulf of Mexico. The large discrepancy between these two studies is mainly attributed to the different concentrations observed and the depths of those concentrations. The concentrations reported here are all from within or close to the surface mixed layer and

appropriate for use in air-sea flux calculations. However, assuming that extremely high methane concentrations existed as relatively small hotspots in the surface seawater over deepwater hydrocarbon seep area, the impact of those hotspots on the regional diffusive air-sea flux would be small.

7. SUMMARY AND CONCLUSIONS

The coastal ocean is supersaturated with CH_3Br and CH_3Cl [*Hu et al.*, 2010; *Lobert et al.*, 1995; *Moore et al.*, 1996; *Sturrock et al.*, 2003]. Contributions of CH_3Br and CH_3Cl from the coastal ocean to the atmosphere are not well studied. GOMECC (section 2) represents the first large-scale coastal study for CH_3Br and CH_3Cl. Results from this study indicate higher CH_3Br and CH_3Cl production rates in surface coastal seawater than those in surface open ocean [*Hu et al.*, 2010]. Extrapolating emissions of CH_3Br and CH_3Cl from the GOMECC study to the global coastal area yields 1.4 (0.5 - 3.6) Gg yr^{-1} and 50 (19 – 98) Gg yr^{-1} for the global coastal emissions of CH_3Br and CH_3Cl. There are some problems for simple global extrapolation, e.g., the extrapolated emissions may be biased by regional in-situ wind speed or regional production rate. To overcome this problem, we developed coastal saturation anomaly – (SST, wind speed) relationship for CH_3Cl and estimated the global oceanic emission using the 1° x 1° gridded model (see section 4), which was 50 ($\pm$ 17) Gg yr^{-1}. For CH_3Br, since the atmospheric mixing ratios are declining and the surface saturation anomalies of CH_3Br keep changing, it is not possible to develop any empirical relationship between saturation anomalies of CH_3Br and SST or wind speed that is valid during the decline of atmospheric CH_3Br. Therefore, I applied the mean production rate calculated from the GOMECC and HalocAST study to the global coastal oceanic area, and calculated the emission rates using climatological wind speed. Results suggest that the calculated global emission would be 4.6 ($\pm$ 1.5) Gg yr^{-1} for CH_3Br. Coastal ocean removes CH_3Br

and CH$_3$Cl both chemically and biologically [*Elliott and Rowland*, 1995; *King and Saltzman*, 1997; *Tokarczyk et al.*, 2003]. The total aquatic degradation rates in coastal ocean for CH$_3$Br and CH$_3$Cl are higher than those in open ocean [*King and Saltzman*, 1997; *Tokarczyk and Saltzman*, 2001; *Tokarczyk et al.*, 2001; *Tokarczyk et al.*, 2003; *Tokarczyk et al.*, 2003]. Calculated global coastal oceanic degradation rates for CH$_3$Br and CH$_3$Cl using 1° x 1° gridded model (see *Hu et al.* [Submitted] for the method) are about 0.8 ($\pm$ 0.3) Gg yr^{-1} (at the end of non-QPS phaseout) and 35 ($\pm$ 10) Gg yr^{-1}. The net fluxes of CH$_3$Br and CH$_3$Cl from the coastal ocean to the atmosphere are about 3.8 ($\pm$1.2) (at the end of non-QPS phaseout) Gg yr^{-1} and 15 ($\pm$7) Gg yr^{-1}. This suggests that the coastal ocean does contribute to the "missing sources" of CH$_3$Br and CH$_3$Cl.

Lobert et al. [1995] first established a global oceanic net sink of -12.6 Gg yr^{-1} for atmospheric CH$_3$Br. Their results were then supported by many subsequent field observations. In 2002, a key saturation anomaly-SST relationship [*King et al.*, 2002] was developed to calculate global net sea-to-air fluxes of CH$_3$Br before the atmospheric CH$_3$Br phase-down. The implementation of *Montreal Protocol on Substances That Deplete the Ozone Layer* and its amendments resulted in the phaseout of fumigation - non-QPS uses of CH$_3$Br. Sixteen years after that first cruise reported by *Lobert et al.* [1995, 1996], saturation anomalies of CH$_3$Br were determined in the same region to assess the oceanic saturation state as the non-QPS phaseout nears completion (section 3). Our findings show for the first time that saturation anomalies of CH$_3$Br over large areas have become more positive than those observed 16 years ago, which supports our hypothesis II. The global net sea-to-air flux in 2010 was estimated at 3 Gg yr^{-1},

indicating that the ocean has become a net small source for atmospheric CH_3Br. This is a dramatic shift in the view of the ocean in the budget of atmospheric CH_3Br. The change in the saturation state indicates that the saturation anomaly - SST relationship used by modelers for oceanic methyl bromide became invalid once the atmospheric CH_3Br phase-down began. Our results also highlight the need to separate the emission from uptake by the ocean when determining the budget of atmospheric traces gases with oceanic sources and sinks. In addition, we demonstrated that there was no significant change in the annual oceanic production rate and the biological oceanic uptake rate constant over the past 16 years.

The ocean is one of the major sources for atmospheric CH_3Cl next to the tropical terrestrial source and biomass burning. Total efflux of CH_3Cl from warm waters (annual mean SST $\geq 12^oC$) to the atmosphere was estimated at $380 - 500$ Gg yr^{-1} [*Clerbaux and Cunnold et al.*, 2007] whereas total influx from the atmosphere to cold waters (annual mean SST $< 12^oC$) was estimated at $93 - 145$ Gg yr^{-1} [*Moore*, 2000] previously. The shortcomings on the prior estimates include limited field data, lacking of salinity dependence in the solubility expression and use of old parameterization on the gas exchange coefficient. Section four represents our efforts to improve the estimate on the oceanic budget of CH_3Cl. We measured solubilities of CH_3Cl in both fresh water and seawater at temperatures from $0\ ^oC$ to $40\ ^oC$ and improved the solubility parameterization by including salinity dependence. We also developed seasonal saturation anomaly as a function of sea surface temperature and wind speed using data from ten different cruises. Including all of these improvements along with the updated

gas transfer velocity from *Sweeney et al.* [2007], the global net sea-to-air flux of CH_3Cl was estimated at 335 (210 – 480) Gg yr^{-1}. In addition, we estimated the emissions and uptake rates of CH_3Cl from the global ocean with spatial resolution of 1° x 1°. Emissions and uptake rates in warm waters are about 540 (± 170) Gg yr^{-1} and 170 (± 50) Gg yr^{-1} whereas they are about 150 (±45) Gg yr^{-1} and 200 (± 60) Gg yr^{-1} in cold waters. Our results support our hypothesis III that both warm waters and cold waters play a dual role in atmospheric budget of CH_3Cl.

Numerous studies were conducted to quantify sources and sinks of atmospheric methyl bromide and methyl chloride since the 1990s. However, the atmospheric budgets of methyl bromide and methyl chloride remain imbalanced. In section five, we examined the linkage of the "missing sources" between CH_3Cl and CH_3Br using a "top-down" two-box model. Results suggest that the "missing sources" of CH_3Cl and CH_3Br are likely to share the same origin. Part of their "missing sources" is likely from the tropical terrestrial ecosystems. This demonstrates that part of hypothesis IV is true. Because the "unknown emissions" (total terrestrial emissions + the imbalance in the atmospheric budget) of CH_3Cl and CH_3Br share the same origin, we constrained the emission rate of fumigation – non-QPS emissions assuming that the "unknown emissions" of CH_3Br have the same trend as those of CH_3Cl. Using the derived "unknown emissions" and the emission ratio of fumigation – non-QPS emissions, we predicted the new steady-state of CH_3Br under three different scenarios (assuming only eliminating fumigation – non-QPS emissions; assuming eliminating all the fumigation emissions; and assuming removing all the anthropogenic sources). Results suggest that, if eliminating all the anthropogenic

sources, the atmospheric CH_3Br is likely to drop to the pre-industrial level and the ocean will become a more significant source for atmospheric CH_3Br.

Combining results from sections two to five, it suggests that the total oceanic emissions of CH_3Br and CH_3Cl account for 29 % and 15 % in the total natural emissions of CH_3Br and CH_3Cl whereas the ocean contributes 23 % and 7.5 % to the global sinks of CH_3Br and CH_3Cl. As a conclusion, the ocean is both a source and a sink for the atmospheric CH_3Br and CH_3Cl but it plays a more important role in the atmospheric CH_3Br budget than that in the atmospheric CH_3Cl budget.

Gas hydrates are the largest methane reservoir. Whether gas hydrates, especially the deepwater gas hydrates, contribute significantly to the atmospheric methane budget is uncertain. Section six presents our study in the northern Gulf of Mexico during HYFLUX. Continuous air-sea flux measurements of methane were made with high spatial and temporal resolution. Results suggest that methane fluxes to the atmosphere from deepwater hydrocarbon seeps in the northern Gulf of Mexico were insignificant to atmospheric methane budget [*Hu et al.*, 2012]. We also estimated methane fluxes from possibly missed methane hotspots over deepwater hydrocarbon plume area. Results suggest that fluxes from high methane-concentration hotspots are unlikely to contribute significantly to total regional methane flux. Another subsequent study was conducted in the same region to quantify methane sea-to-air fluxes during the Deepwater Horizon oil spill [*Yvon-Lewis et al.*, 2011], which simulated rapid clathrate decomposing condition. The amount of methane transported to the atmosphere during this event was small. Most methane emitted from the wellhead was dissolved at ~1100 m [*Valentine et al.*, 2010;

Yvon-Lewis et al., 2011] and oxidized overtime [*Kessler et al.*, 2011]. Combining results from all these studies suggest that the deepwater hydrocarbon sources are not likely to contribute significantly to the atmospheric methane budget. They also reject our hypothesis V.

REFERENCES

Alvain, S., C. Moulin, Y. Dandonneau, and F. M. Bréon (2005), Remote sensing of phytoplankton groups in case 1 waters from global SeaWiFS imagery, *Deep Sea Research Part I: Oceanographic Research Papers*, *52*(11), 1989-2004, doi: 10.1016/j.dsr.2005.06.015.

Alvain, S., C. Moulin, Y. Dandonneau, and H. Loisel (2008), Seasonal distribution and succession of dominant phytoplankton groups in the global ocean: A satellite view, *Global Biogeochem. Cycles*, 22(3), GB3001, doi: 10.1029/2007gb003154.

Amouroux, D., G. Roberts, S. Rapsomanikis, and M. O. Andreae (2002), Biogenic gas (CH4, N2O, DMS) emission to the atmosphere from near-shore and shelf waters of the north-western Black Sea, *Estuarine, Coastal and Shelf Science*, *54*(3), 575-587.

Andreae, M. O., and P. Merlet (2001), Emission of trace gases and aerosols from biomass burning, *Global Biogeochem. Cycles*, 15(4), 955-966, doi: 10.1029/2000gb001382.

Antajan, E., M. J. Chretiennot-Dinet, C. Leblanc, M. H. Daro, and C. Lancelot (2004), 19'-hexanoyloxyfucoxanthin may not be the appropriate pigment to trace occurrence and fate of Phaeocystis: the case of P-globosa in Belgian coastal waters, *J. Sea Res.*, 52(3), 165-177.

Baker, J. M., C. E. Reeves, P. D. Nightingale, S. A. Penkett, S. W. Gibb, and A. D. Hatton (1999), Biological production of methyl bromide in the coastal waters of the North Sea and open ocean of the northeast Atlantic, *Mar. Chem.*, 64(4), 267-285.

Baker, J. M., C. E. Reeves, S. A. Penkett, L. M. Cardenas, and P. D. Nightingale (1998), An estimate of the global emissions of methyl bromide from automobile exhausts, *Geophys. Res. Lett.*, 25(13), 2405-2408.

Bange, H. W., U. H. Bartell, S. Rapsomanikis, and M. O. Andreae (1994), Methane in the Baltic and North Seas and a Reassessment of the Marine Emissions of Methane, *Global Biogeochem. Cycles*, 8(4), 465-480.

Bange, H. W., S. Dahlke, R. Ramesh, L. A. Meyer-Reil, S. Rapsomanikis, and M. O. Andreae (1998), Seasonal study of methane and nitrous oxide in the coastal waters of the southern Baltic Sea, Estuarine, *Coastal and Shelf Science*, 47(6), 807-817.

Bange, H. W., S. Rapsomanikis, and M. O. Andreae (1996), The Aegean Sea as a source of atmospheric nitrous oxide and methane, *Mar. Chem.*, 53(1-2), 41-49.

Bertram, F. J., and J. B. Kolowich (2000), A study of methyl bromide emissions from automobiles burning leaded gasoline using standardized vehicle testing procedures, *Geophys. Res. Lett.*, 27(9), 1423-1426, doi: 10.1029/1999gl011008.

Blei, E., C. J. Hardacre, G. P. Mills, K. V. Heal, and M. R. Heal (2010), Identification and quantification of methyl halide sources in a lowland tropical rainforest, *Atmospheric Environment*, 44(8), 1005-1010.

Blough, N. V., and R. Del Vecchio (2002), Chromophoric DOM in the coastal environment, in Biogeochemistry of Marine Dissolved Organic Matter, edited by D. Hansell and C. Carlson, pp. 509 - 546, *Academic Press*, New York.

Boswell, R., and T. S. Collett (2011), Current perspectives on gas hydrate resources, *Energy & Environmental Science*, 4(4), 1206-1215.

Brainerd, K. E., and M. C. Gregg (1995), Surface mixed and mixing layer depths, *Deep Sea Research Part I: Oceanographic Research Papers*, 42(9), 1521-1543.

Butler, J. H. (1994), The potential role of the ocean in regulating atmospheric CH3Br, *Geophys. Res. Lett.*, 21(3), 185-188.

Butler, J. H. (2000), Atmospheric chemistry: Better budgets for methyl halides?, *Nature*, 403(6767), 260-261.

Butler, J. H., D. B. King, J. M. Lobert, S. A. Montzka, S. A. Yvon-Lewis, B. D. Hall, N. J. Warwick, D. J. Mondeel, M. Aydin, and J. W. Elkins (2007), Oceanic distributions and emissions of short-lived halocarbons, *Global Biogeochem. Cycles*, 21, GB1023, doi:1010.1029/2006GB002732.

Butler, J. H., and J. M. Rodriguez (1996), Mehyl bromide in the atmosphere, in The Methyl Bromide Issue, edited by C. Bell, N. Price and B. Chakrabarti, London: John Wiley and Sons, Ltd.

Butler, J. H., M. Battle, M. L. Bender, S. A. Montzka, A. D. Clarke, E. S. Saltzman, C. M. Sucher, J. P. Severinghaus, and J. W. Elkins (1999), A record of atmospheric halocarbons during the twentieth century from polar firn air, *Nature*, 399(6738), 749-755.

Butler, J. H., J. W. Elkins, T. M. Thompson, B. D. Hall, T. H. Swanson, and V. Koropalov (1991), Oceanic Consumption of CH3CCl3: Implications for Tropospheric OH, *J. Geophys. Res.*, 96(D12), 22347-22355.

Chen, N., T. S. Bianchi, and J. M. Bland (2003), Implications for the role of pre- versus post-depositional transformation of chlorophyll-a in the Lower Mississippi River and Louisiana shelf, *Mar. Chem.*, 81(1-2), 37-55.

Chen, T., D. R. Blake, J. P. Lopez, and F. S. Rowland (1999), Estimation of global vehicular methyl bromide emissions: Extrapolation from a case study in Santiago, Chile, *Geophys. Res. Lett.*, 26(3), 283-286, doi: 10.1029/1998gl900214.

Clark, J. F., I. Leifer, L. Washburn, and B. P. Luyendyk (2003), Compositional changes in natural gas bubble plumes: observations from the Coal Oil Point marine hydrocarbon seep field, *Geo-Mar. Lett.*, 23, 187-193.

Clark, J. F., L. Washburn, and K. Schwager Emery (2010), Variability of gas composition and flux intensity in natural marine hydrocarbon seeps, *Geo-Mar. Lett.*, 30(3), 379-388.

Clerbaux, C., D. M. Cunnold, J. Anderson, A. Engel, P. J. Fraser, et al. (2007), Chapter 1: Long-Lived Compounds, in Scientific Assessment of Ozone Depletion: 2006, edited by C. A. Ennis, World Meteorological Organization, Global Ozone Research and Monitoring Project-Report No. 50.

Cox, M. L., P. J. Fraser, G. A. Sturrock, S. T. Siems, and L. W. Porter (2004), Terrestrial sources and sinks of halomethanes near Cape Grim, Tasmania, *Atmospheric Environment*, 38(23), 3839-3852, doi:10.1016/j.atmosenv.2004.03.050.

Cynar, F. J., and A. A. Yayanos (1991), Enrichment and Characterization of a Methanogenic Bacterium from the Oxic Upper Layer of the Ocean, *Curr. Microbiol.*, 23(2), 89-96.

de Angelis, M. A., and C. Lee (1994), Methane Production during Zooplankton Grazing on Marine-Phytoplankton, *Limnol. Oceanogr.*, 39(6), 1298-1308.

De Bruyn, W. J., and E. S. Saltzman (1997a), Diffusivity of methyl bromide in water, *Mar. Chem.*, 57(1-2), 55-59.

De Bruyn, W. J., and E. S. Saltzman (1997b), The solubility of methyl bromide in pure water, 35%. sodium chloride and seawater, *Mar. Chem.*, 56(1-2), 51-57.

Denman, K. L., G. Brasseur, A. Chidthaisong, P. Ciais, P. M. Cox, R. E. Dickinson, D. Hauglustaine, C. Heinze, E. Holland, D. Jacob, U. Lohmann, S. Ramachandran, P. L. da Silva Dias, S. C. Wofsy, and X. ZHang (2007), Couplings Between Changes in the Climate System an Biogeochemistry, in Climate Change 2007: *The Physical Science Basis*. Contribution of Working Group I to the Fourth Assessment Report of the Intergovernmental Panel on Climate Change, edited by

S. Solomon, D. Qin, M. Manning, Z. Chen, M. Marquis, K. B. Averyt, M. Tignor and H. L. Miller, Cambridge University Press, Cambridge, United Kingdom and New York, NY, USA.

Dimmer, C. H., P. G. Simmonds, G. Nickless, and M. R. Bassford (2001), Biogenic fluxes of halomethanes from Irish peatland ecosystems, *Atmospheric Environment*, 35(2), 321-330.

Ehhalt, D., M. Prather, F. Dentener, R. Derwent, E. Dlugokencky, E. Holland, I. Isaksen, J. Katima, V. Kirchhoff, P. Matson, P. Midgley, and M. Wang (2001), Atmospheric Chemistry and Greenhouse Gases, in Climate Change 2001: *The Scientific Basis*. Contribution of Working Group I to the Third Assessment Report of the Intergovernmental Panel on Climate Change, edited by J. T. Houghton, et al., Cambridge University Press, Cambridge, U. K.

Elliott, S., and F. S. Rowland (1993), Nucleophilic substitution rates and solubilities for methyl halides in seawater, *Geophys. Res. Lett.*, 20(11), 1043-1046.

Elliott, S., and F. S. Rowland (1995), Methyl halide hydrolysis rates in natural waters, *J. Atmos. Chem.*, 20(3), 229-236.

Emery, W. J., and R. E. Thomson (2001), Data Analysis Methods in Physical Oceanography, Elservier, Amsterdam - London - New York - Oxford - Paris - Shannon - Tokyo.

Erickson, D. J., III (1993), A Stability Dependent Theory For Air-Sea Gas Exchange, *J. Geophys. Res.*, 98(C5), 8471-8488.

Fahey, D., and M. Hegglin (2011), Twenty Questions and Answer About the Ozone Layer: 2010 Update, in Scientific Asessment of Ozone Depletion: 2010, edited, World Meteorological Organization, Geneva, Switzerland.

Feely, R. A., R. Wanninkhof, D. A. Hansell, M. F. Lamb, D. Greeley, and K. Lee (2002), Water column CO2 measurements during the Gas Ex-98 expedition, in Gas Transfer at Water Surfaces, edited, pp. 173-180, AGU, Washington, DC.

Food and Agriculture Organization of the United Nations (FAO) (2010), Global Forest Resources Assessment Rep., Rome.

Forster, P. and V. Ramaswamy, et al. (2007), Chapter 2: Changes in Atmospheric Constituents and in Radiative Forcing, in Climate Change 2007: *The Physical Science Basis*. Contribution of Working Group I to the Fourth Assessment Report of the Intergovernmental Panel on Climate Change, edited by S. Solomon, D. Qin, M. Manning, Z. Chen, M. Marguis, K. B. Averyt, Tignor M.

and H. L. Miller, Cambridge University Press, Cambridge, United Kingdom and New York, NY, USA.

Frye, M. (2008), Preliminary Evaluation of in-Place Gas Hydrate Resources: Gulf of Mexico Outer Continental Shelf, MMS Report 2008-004 (US Department of Interior, Minerals Management Service, 2008).

Garcia-Pineda, O., I. MacDonald, B. Zimmer, B. Shedd and H. Roberts (2010), Remote-sensing evaluation of geophysical anomaly sites in the outer continental slope, northern Gulf of Mexico, *Deep-Sea Res. II*, 57, 1859 – 1869.

Garrido, J. L., and M. Zapata (1998), Detection of new pigments from Emiliania Huxleyi (primnesiophyceae) by high-performance liquid chromatography, liquid chromatography-mass spectrometry, visible spectroscopy, and fast atom bombardment mass spectrometry, *J. Phycol.*, 34(1), 70-78.

Gebhardt, S., A. Colomb, R. Hofmann, J. Williams, and J. Lelieveld (2008), Halogenated organic species over the tropical South American rainforest, *Atmos. Chem. Phys.*, 8(12), 3185-3197, doi:10.5194/acp-8-3185-2008.

Goericke, R., S. L. Strom, and M. A. Bell (2000), Distribution and Sources of Cyclic Pheophorbides in the Marine Environment, *Limnol. Oceanogr.*, 45(1), 200-211.

Greinert, J., Y. Artemov, V. Egorov, M. De Batist, and D. McGinnis (2006), 1300-m-high rising bubbles from mud volcanoes at 2080 m in the Black Sea: Hydroacoustic characteristics and temporal variability, *Earth Planetary Sci. Lett.*, 244(1-2), 1-15.

Groszko, W., and R. M. Moore (1998), Ocean-atmosphere exchange of methyl bromide: NW Atlantic and Pacific Ocean studies, *J. Geophys. Res.*, 103(D13), 16737-16741.

Hayduk, W., and H. Laudie (1974), Prediction of diffusion coefficients for nonelectrolytes in dilute aqueous solutions, *AIChE Journal*, 20(3), 611-615.

Head, E. J. H., B. T. Hargrave, and D. V. S. Rao (1994), Accumulation of a Pheophorbide a-Like Pigment in Sediment Traps During Late Stages of a Spring Bloom: A Product of Dying Algae?, *Limnol. Oceanogr.*, 39(1), 176-181.

Hornafius, J. S., D. Quigley, and B. P. Luyendyk (1999), The world's most spectacular marine hydrocarbon seeps (Coal Oil Point, Santa Barbara Channel, California): Quantification of emissions, *J. Geophys. Res.*, 104(C9), 20703-20711.

Houweling, S., F. Dentener, and J. Lelieveld (2000), Simulation of preindustrial atmospheric methane to constrain the global source strength of natural wetlands, *J. Geophys. Res.*, 105(D13), 17243-17255.

Hu, L., S. A. Yvon-Lewis, J. D. Kessler, and I. R. MacDonald (2012), Methane fluxes to the atmosphere from deepwater hydrocarbon seeps in the northern Gulf of Mexico, *J. Geophys. Res.*, 117, C01009, doi:10.1029/2011JC007208.

Hu, L., S. A. Yvon-Lewis, J. H. Butler, J. M. Lobert and D. B. King (submitted), An improved oceanic budget of methyl chloride, J. *Geophys. Res.*

Hu, L., S. A. Yvon-Lewis, Y. Liu, J. E. Salisbury, and J. E. O'Hern (2010), Coastal emissions of methyl bromide and methyl chloride along the eastern Gulf of Mexico and the east coast of the United States, *Global Biogeochem. Cycles*, 24, GB1007, doi:10.1029/2009GB003514.

Hu, L., S. A. Yvon-Lewis, Y. Liu, and T. S. Bianchi (submitted), The ocean in near equilibrium with atmospheric methyl bromide, *Global Biogeochem. Cycles*.

IPCC (Intergovernmental Panel on Climate Change) (2001), Climate Change 2001 - The Scientific Basis, edited by J. T. H. e. al., p. 881, Cambridge Univ. Press, Cambridge, UK.

Jeffrey, S. W., R. G. C. Mantoura, and S. W. Wright (1997), Phytoplankton pigments in oceanography, United Nations Educational Scientific and Cultural Organization, Paris.

Johnson, J. E. (1999), Evaluation of a seawater equilibrator for shipboard analysis of dissolved oceanic trace gases, *Analytica Chimica Acta*, 395(1-2), 119-132.

Keene, W. C., M. A. K. Khalil, D. J. Erickson, III, A. McCulloch, T. E. Graedel, J. M. Lobert, M. L. Aucott, S. L. Gong, D. B. Harper, G. Kleiman, P. Midgley, R. M. Moore, C. Seuzaret, W. T. Sturges, C. M. Benkovitz, V. Koropalov, L. A. Barrie, and Y. F. Li (1999), Composite global emissions of reactive chlorine from anthropogenic and natural sources: Reactive Chlorine Emissions Inventory, *J. Geophys. Res.*, 104(D7), 8429-8440.

Keppler, F., D. B. Harper, T. Röckmann, R. M. Moore, and J. T. G. Hamilton (2005), New insight into the atmospheric chloromethane budget gained using stable carbon isotope ratios, *Atmos. Chem. Phys.*, 5(9), 2403-2411.

Kessler, J. D., W. S. Reeburgh, J. Southon, R. Seifert, W. Michaelis, and S. C. Tyler (2006), Basin-wide estimates of the input of methane from seeps and clathrates to the Black Sea, *Earth Planetary Sci. Lett.*, 243(3-4), 366-375.

Kessler, J. D., D. L. Valentine, M. C. Redmond, M. Du, E. W. Chan, S. D. Mendes, E. W. Quiroz, C. J. Villanueva, S. S. Shusta, L. M. Merra, S. A. Yvon-Lewis and T. C. Weber (2011), A Persistent Oxygen Anomaly Reveals the Fate of Spilled Methane in the Deep Gulf of Mexico, *Science*, 331(6015), 312-315, doi: 10.1126/science.1199697.

Khalil, M. A. K., and R. A. Rasmussen (1999), Atmospheric methyl chloride, *Atmospheric Environment*, 33(8), 1305-1321.

Khalil, M. A. K., and R. A. Rasmussen (2000), Soil-Atmosphere exchange of radiatively and chemically active gases, *Environmental Science and Pollution Research*, 7(2), 79-82, doi: doi:10.1065/espr2000.04.021.

Khalil, M. A. K., R. M. Moore, D. B. Harper, J. M. Lobert, D. J. Erickson, V. Koropalov, W. T. Sturges, and W. C. Keene (1999), Natural emissions of chlorine-containing gases: Reactive Chlorine Emissions Inventory, *J. Geophys. Res.*, 104(D7), 8333-8346.

King, D. B., and E. S. Saltzman (1997), Removal of methyl bromide in coastal seawater: Chemical and biological rates, *J. Geophys. Res.*, 102(C8), 18715-18721.

King , D. B., J. H. Butler, S. A. Montzka, S. A. Yvon-Lewis, and J. W. Elkins (2000), Implications of methyl bromide supersaturations in the temperate North Atlantic Ocean, *J. Geophys. Res.*, 105(D15), 19763-19769.

King, D. B., J. H. Butler, S. A. Yvon-Lewis, and S. A. Cotton (2002), Predicting oceanic methyl bromide saturation from SST, *Geophys. Res. Lett.*, 29(24), 2199, doi:2110.1029/2002GL016091.

Kossina, E. (1921), Die Tiefen des Weltmeeres, Veroff. N. F., A. Geogr. - Naturwiss. Reihe, 9, 70.

Kourtidis, K., I. Kioutsioukis, D. F. McGinnis, and S. Rapsomanikis (2006), Effects of methane outgassing on the Black Sea atmosphere, *Atmos. Chem. Phys.*, 6, 5173-5182.

Large, W. G., and S. Pond (1982), Sensible and latent heat flux measurements over the ocean, *J. Phys. Oceanogr.*, 12, 464-482.

Le Treut, H., R. Somerville, U. Cubasch, Y. Ding, C. Mauritzen, A. Mokssit, T. Peterson, and M. Prather (2007), Historical Overview of Climate Change, in Climate Change 2007: *The physical Science Basis*. Contribution of Working Group I to the Fourth Assessment Report of the Intergovernmental Panel on Climate Change, edited by S. Solomon, D. Qin, M. Manning, Z. Chen, M.

Marqis, K. B. Averyt, M. Tignor and H. L. Miller, Cambridge University Press, Cambridge, United Kingdom and New York, NY, USA.

Lee-Taylor, J. M., and E. A. Holland (2000), Litter decomposition as a potential natural source of methyl bromide, *J. Geophys. Res.*, 105(D7), 8857-8864.

Lee-Taylor, J. M., G. P. Brasseur, and Y. Yokouchi (2001), A preliminary three-dimensional global model study of atmospheric methyl chloride distributions, *J. Geophys. Res.*, 106(D24), 34221-34233, doi: 10.1029/2001jd900209.

Lee-Taylor, J. M., and K. R. Redeker (2005), Reevaluation of global emissions from rice paddies of methyl iodide and other species, *Geophys. Res. Lett.*, 32, L15801. doi: 0.1029/2005gl022918.

Leifer, I., B. P. Luyendyk, J. Boles, and J. F. Clark (2006), Natural marine seepage blowout: Contribution to atmospheric methane, *Global Biogeochem. Cycles*, 20, GB3008, doi:3010.1029/2005GB002668.

Leifer, I., and I. MacDonald (2003), Dynamics of the gas flux from shallow gas hydrate deposits: interaction between oily hydrate bubbles and the oceanic environment, *Earth Planet. Sci. Lett.*, 210(3-4), 411-424.

Leifer, I., and J. Boles (2005), Measurement of marine hydrocarbon seep flow through fractured rock and unconsolidated sediment, *Marine and Petroleum Geology*, 22(4), 551-568.

Li, H.-J., Y. Yokouchi, H. Alkimoton, and Y. Narita (2001), Distribution of methyl chloride, methyl bromide and methyl iodide in the marine boundary air over the western Pacific and southeastern Indian Ocean, *Geochemical Journal*, 35(2), 137 - 145.

Liss, P. S., and L. Merlivat (1986), Air-sea gas exchange rates: Introduction and synthesis, in The Role of Air-Sea Exchange in Geochemical Cycling, edited by P. Buat-Menard, pp. 113 – 127, Springer, New York.

Llewellyn, C. A., and S. W. Gibb (2000), Intra-class variability in the carbon, pigment and biomineral content of prymnesiophytes and diatoms, *Mar Ecol-Prog Ser*, 193, 33-44.

Lobert, J. M., J. H. Butler, L. S. Geller, S. A. Yvon, S. A. Montzka, R. C. Myers, A. D. Clarke, and J. W. Elkins (1996), BLAST94: Bromine Latitudinal Air/Sea Transect 1994, Report on oceanic measurements of methyl bromide and other compounds, NOAA Tech. Memo. ERL CMDL.

Lobert, J. M., J. H. Butler, S. A. Montzka, L. S. Geller, R. C. Myers, and J. W. Elkins (1995), A Net Sink for Atmospheric CH3Br in the East Pacific Ocean, *Science*, 267(5200), 1002-1005.

Lobert, J. M., W. C. Keene, J. A. Logan, and R. Yevich (1999), Global chlorine emissions from biomass burning: Reactive Chlorine Emissions Inventory, *J. Geophys. Res.*, 104(D7), 8373-8389.

Low, J. C., N. Y. Wang, J. Williams, and R. J. Cicerone (2003), Measurements of ambient atmospheric C_2H_5Cl and other ethyl and methyl halides at coastal California sites and over the Pacific Ocean, *J. Geophys. Res.*, 108(D19), 4608.

Mabey, W., and T. Mill (1978), Critical review of hydrolysis of organic compounds in water under envrionmental conditions, *J. Phys. Chem.* Ref. Data 7(2), doi:10.1063/1061.555572.

Manley, S. L., N.-Y. Wang, M. L. Walser, and R. J. Cicerone (2007), Methyl halide emissions from greenhouse-grown mangroves, *Geophys. Res. Lett.*, 34(1), L01806, doi:10.1029/2006GL027777

Matthews, E. (1983), Global Vegetation and Land Use: New High-Resolution Data Bases for Climate Studies, *Journal of Climate and Applied Meteorology*, 22(3), 474-487, doi: 10.1175/1520-0450(1983)022<0474:gvalun>2.0.co;2.

Mau, S., D. L. Valentine, J. F. Clark, J. Reed, R. Camilli, and L. Washburn (2007), Dissolved methane distributions and air-sea flux in the plume of a massive seep field, Coal Oil Point, California, *Geophys. Res. Lett.*, 34, L22603, doi:22610.21029/22007GL031344.

McAnulla, C., I. R. McDonald, and J. C. Murrell (2001), Methyl chloride utilising bacteria are ubiquitous in the natural environment, *FEMS Microbiology Letters*, 201(2), 151-155, doi: doi:10.1016/s0378-1097(01)00256-7.

McCulloch, A., M. L. Aucott, C. M. Benkovitz, T. E. Graedel, G. Kleiman, P. M. Midgley, and Y.-F. Li (1999), Global emissions of hydrogen chloride and chloromethane from coal combustion, incineration and industrial activities: Reactive Chlorine Emissions Inventory, *J. Geophys. Res.*, 104(D7), 8391-8403.

McGinnis, D. F., J. Greinert, Y. Artemov, S. E. Beaubien, and A. Wüest (2006), Fate of rising methane bubbles in stratified waters: How much methane reaches the atmosphere?, *J. Geophys. Res.*, 111, C09007, doi:09010.01029/02005JC003183.

Mead, M. I., M. A. H. Khan, G. Nickless, B. R. Greally, D. Tainton, T. Pitman, and D. E. Shallcross (2008b), Leaf cutter ants: a possible missing source of biogenic halocarbons, *Environmental Chemistry*, 5(1), 5-10.

Mead, M. I., I. R. White, G. Nickless, K.-Y. Wang, and D. E. Shallcross (2008a), An estimation of the global emission of methyl bromide from rapeseed (Brassica napus) from 1961 to 2003, *Atmos. Environ.*, 42(2), 337-345.

Meehl, G. A., T. F. Stocker, W. D. Collins, P. Friedlingstein, A. T. Gaye, J. M. Gregory, A. Kitoh, R. Knutti, J. M. Murphy, A. Noda, S. C. B. Raper, I. G. Watterson, A. J. Weaver and Z.-C. Zhao (2007), Global Climate Projections, In: Climate Change 2007: *The Physical Science Basis*. Contribution of Working Group I to the Fourth Assessment Report of the Intergovernmental Panel on Climate Change, edited by Solomon, S., D. Qin, M. Manning, Z. Chen, M. Marquis, K. B. Averyt, M. Tignor and H. L. Miller, Cambridge University Press, New York, USA.

Menard, H. W., and S. M. Smith (1966), Hypsometry of Ocean Basin Provinces, *J. Geophys. Res.*, 71(18), 4305 - 4325.

Midgley, P. M., and A. McCulloch (1995), The production and global distribution of emissions to the atmosphere of 1,1,1-trichloroethane (methyl chloroform), *Atmospheric Environment*, 29(14), 1601-1608, doi: 10.1016/1352-2310(95)00078-d.

Millero, F. J. (1974), Seawater as a multicomponent electrolyte solution, in The Sea, edited by E. D. Goldberg, Wiley, New York.

Montzka, S. A., P. J. Fraser et al, J. H. Butler, P. S. Connell, D. M. Cunnold, J. S. Daniel, R. G. Derwent, et al., (2003), Controlled substances and other sources gases, in Chapter 5 in Scientific Assessment of Ozone Depletion: 2002, edited, Global Ozone Research and Monitoring Project - Report No. 47, World Meterological Organization, Geneva.

Montzka, S. A., S. Reimann, A. Engel, K. Krüger, S. O'Doherty, et al. (2011), Ozone-Depleting Substances (ODSs) and Related Chemiscals, in Scientific Assessment of Ozone Depletion 2010, edited by A. R. Ravishankara, pp. 1-108, World Meteorol. Organ., Geneva.

Montzka, S. A., J. H. Butler, B. D. Hall, D. J. Mondeel, and J. W. Elkins (2003), A decline in tropospheric organic bromine, *Geophys. Res. Lett.*, 30(15), 1826, doi:10.1029/2003GL017745.

Moore, R. M. (2000), The solubility of a suite of low molecular weight organochlorine compounds in seawater and implications for estimating the marine source of methyl chloride to the atmosphere, *Chemosphere - Global Change Science*, 2(1), 95-99.

Moore, R. M., C. E. Geen, and V. K. Tait (1995), Determination of Henry's Law constants for a suite of naturally occurring halogenated methanes in seawater, *Chemosphere*, 30(6), 1183-1191.

Moore, R. M., W. Groszko, and S. J. Niven (1996), Ocean-atmosphere exchange of methyl chloride: Results from NW Atlantic and Pacific Ocean studies, *J. Geophys. Res.*, 101(C12), 28529-28538.

Nightingale, P. D., P. S. Liss, and P. Schlosser (2000), Measurements of air-sea gas transfer during an open ocean algal bloom, *Geophys. Res. Lett.*, 27, 2117 – 2120.

Penkett, S. A., J. H. Butler, M. J. Kurylo, C. E. Reeves, J. M. Rodriguez, H. Singh, D. Toohey, and R. F. Weiss (1994), Methyl Bromide, in Scientific Assessment of Ozone Depletion: 1994, edited by C. A. Ennis, World Meterorological Organization, Global Ozone Research and Monitoring Project -Report No. 37, Geneva, Switzerland.

Prinn, R. G., et al. (2005), Evidence for variability of atmospheric hydroxyl radicals over the past quarter century, *Geophys. Res. Lett.*, 32(7), L07809, doi: doi:10.1029/2004gl022228.

Quigley, D. C., J. Scott Hornafius, B. P. Luyendyk, R. D. Francis, J. Clark, and L. Washburn (1999), Decrease in natural marine hydrocarbon seepage near Coal Oil Point, California, associated with offshore oil production, *Geology*, 27(11), 1047-1050.

Ramaswamy, V., O. Boucher, J. Haigh, D. Hauglustaine, J. Haywood, G. Myhre, T. Nakajima, G. Shi, and S. Solomon (2001), Radiative forcing of climate change in Climate Change 2001: The Scientific Basis, Contribution of Working Group I to the Third Assessment Report of the Intergovernmental Panel on Climate Change, edited by J. T. Houghton, et al., pp. 349-416, Cambridge Univ. Press., Cambridge, U. K.

Reeburgh, W. S. (2007), Oceanic Methane Biogeochemistry, *Chem. Rev.*, 107, 486-513.

Reeburgh, W. S., S. C. Tyler, and J. Carroll (2006), Stable carbon and hydrogen isotope measurements on Black Sea water-column methane, *Deep-Sea Res Pt II: Tropical Studies in Oceanography*, 53(17-19), 1893-1900.

Reeburgh, W. S., B. B. Ward, S. C. Whalen, K. A. Sandbeck, K. A. Kilpatrick, and L. J. Kerkhof (1991), Black-Sea Methane Geochemistry, *Deep-Sea Res.*, 38, S1189-S1210.

Reeves, C. E. (2003), Atmospheric budget implications of the temporal and spatial trends in methyl bromide concentration, *J. Geophys. Res.*, 108(D11), 4343.

Rehder, G., P. W. Brewer, E. T. Peltzer, and G. Friederich (2002), Enhanced lifetime of methane bubble streams within the deep ocean, *Geophys. Res. Lett.*, 29(15), doi:10.1029/2001GL013966.

Rehder, G., I. Leifer, P. G. Brewer, G. Friederich, and E. T. Peltzer (2009), Controls on methane bubble dissolution inside and outside the hydrate stability field from open ocean field experiments and numerical modeling, *Mar. Chem.*, 114(1-2), 19-30.

Rhee, T. S., A. J. Kettle, and M. O. Andreae (2009), Methane and nitrous oxide emissions from the ocean: A reassessment using basin-wide observations in the Atlantic, *J. Geophys. Res.*, 114, D12304, doi:12310.11029/12008JD011662.

Rhew, R. C. (2011), Sources and sinks of methyl bromide and methyl chloride in the tallgrass prairie: Applying a stable isotope tracer technique over highly variable gross fluxes, *J. Geophys. Res.*, 116(G3), G03026, doi: 10.1029/2011jg001704.

Rhew, R. C., and T. Abel (2007), Measuring Simultaneous Production and Consumption Fluxes of Methyl Chloride and Methyl Bromide in Annual Temperate Grasslands, *Environmental Science & Technology*, 41(22), 7837-7843, doi: 10.1021/es0711011.

Rhew, R. C., M. Aydin, and E. S. Saltzman (2003), Measuring terrestrial fluxes of methyl chloride and methyl bromide using a stable isotope tracer technique, *Geophys. Res. Lett.*, 30(21), 2103, doi: 10.1029/2003gl018160.

Rhew, R. C., C. Chen, Y. A. Teh, and D. Baldocchi (2010), Gross fluxes of methyl chloride and methyl bromide in a California oak-savanna woodland, *Atmospheric Environment*, 44(16), 2054-2061, doi: 10.1016/j.atmosenv.2009.12.014.

Rhew, R. C., B. R. Miller, M. K. Vollmer, and R. F. Weiss (2001), Shrubland fluxes of methyl bromide and methyl chloride, *J. Geophys. Res.*, 106(D18), 20875-20882, doi:10.1029/2001jd000413.

Rhew, R. C., B. R. Miller, and R. F. Weiss (2000), Natural methyl bromide and methyl chloride emissions from coastal salt marshes, *Nature*, 403(6767), 292-295.

Rhew, R. C., Y. A. Teh, and T. Abel (2007), Methyl halide and methane fluxes in the northern Alaskan coastal tundra, *J. Geophys. Res.*, 112, G02009,doi:02010.01029/02006JG000314, doi: 10.1029/2006jg000314.

Saemundsdottir, S., and P. A. Matrai (1998), Biological Production of Methyl Bromide by Cultures of Marine Phytoplankton, *Limnol. Oceanogr.*, 43(1), 81-87.

Saito, T., and Y. Yokouchi (2006), Diurnal variation in methyl halide emission rates from tropical ferns, *Atmospheric Environment*, 40(16), 2806-2811.

Saito, T., and Y. Yokouchi (2008), Stable carbon isotope ratio of methyl chloride emitted from glasshouse-grown tropical plants and its implication for the global methyl chloride budget, *Geophys. Res. Lett.*, 35(8), L08807, doi: 10.1029/2007gl032736.

Saito, T., Y. Yokouchi, Y. Kosugi, M. Tani, E. Philip, and T. Okuda (2008), Methyl chloride and isoprene emissions from tropical rain forest in Southeast Asia, *Geophys. Res. Lett.*, 35(19), L19812, doi: 10.1029/2008gl035241.

Saltzman, E. S., M. Aydin, W. J. De Bruyn, D. B. King, and S. A. Yvon-Lewis (2004), Methyl bromide in preindustrial air: Measurements from an Antarctic ice core, *J. Geophys. Res.*, 109, D05301, doi:05310.01029/02003JD004157.

Sander, S. P., D. M. Golden, M. J. Kurylo, G. K. Moortgat, P. H. Wine, et al. (2006), Chemical kinetics and photochemical data for use in Atmospheric Studies: Evaluation Number 15, edited, JPL publication 06-2, Pasadena, CA: Jet Propulsion Laboratory, NASA.

Scarratt, M. G., and R. M. Moore (1996), Production of methyl chloride and methyl bromide in laboratory cultures of marine phytoplankton, *Mar. Chem.*, 54(3-4), 263-272.

Scarratt, M. G., and R. M. Moore (1998), Production of methyl bromide and methyl chloride in laboratory cultures of marine phytoplankton II, *Mar. Chem.*, 59(3-4), 311-320.

Schauffler, S. M., E. L. Atlas, D. R. Blake, F. Flocke, R. A. Lueb, J. M. Lee-Taylor, V. Stroud, and W. Travnicek (1999), Distributions of brominated organic compounds in the troposphere and lower stratosphere, *J. Geophys. Res.*, 104(D17), 21513-21535.

Schauffler, S. M., L. E. Heidt, W. H. Pollock, T. M. Gilpin, J. F. Vedder, S. Solomon, R. A. Lueb, and E. L. Atlas (1993), Measurements of halogenated organic compounds near the tropical tropopause, *Geophys. Res. Lett.*, 20(22), 2567-2570.

Schmale, O., J. Greinert, and G. Rehder (2005), Methane emission from high-intensity marine gas seeps in the Black Sea into the atmosphere, *Geophys. Res. Lett.*, 32, L07609, doi:07610.01029/02004GL021138.

Schoemann, V., S. Becquevort, J. Stefels, W. Rousseau, and C. Lancelot (2005), Phaeocystis blooms in the global ocean and their controlling mechanisms: a review, *J. Sea Res.,* 53(1-2), 43-66.

Shorter, J. H., C. E. Kolb, P. M. Crill, R. A. Kerwin, R. W. Talbot, M. E. Hines, and R. C. Harriss (1995), Rapid degradation of atmospheric methyl bromide in soils, *Nature*, 377(6551), 717-719.

Singh, H. B., L. J. Salas, and R. E. Stiles (1983), Methyl Halides in and Over the Eastern Pacific (40°N-32°S), *J. Geophys. Res.*, 88(C6), 3684-3690.

Solomon, E. A., M. Kastner, I. R. MacDonald, and I. Leifer (2009), Considerable methane fluxes to the atmosphere from hydrocarbon seeps in the Gulf of Mexico, *Nat. Geosci.*, 2(8), 561-565.

Spivakovsky, C. M., et al. (2000), Three-dimensional climatological distribution of tropospheric OH: Update and evaluation, *J. Geophys. Res.*, 105(D7), 8931-8980, doi: doi:10.1029/1999jd901006.

Sturrock, G. A., C. E. Reeves, G. P. Mills, S. A. Penkett, C. R. Parr, A. McMinn, G. Corno, N. W. Tindale, and P. J. Fraser (2003), Saturation levels of methyl bromide in the coastal waters off Tasmania, *Global Biogeochem. Cycles*, 17(4), 1101, doi:10.1029/2002GB002024.

Sweeney, C., E. Gloor, A. R. Jacobson, R. M. Key, G. McKinley, J. L. Sarmiento, and R. Wanninkhof (2007), Constraining global air-sea gas exchange for CO2 with recent bomb 14C measurements, *Global Biogeochem. Cycles*, 21, GB2015, doi: 2010.1029/2006GB002784.

Takahashi, T., S. C. Sutherland, R. Wanninkhof, C. Sweeney, R. A. Feely, D. W. Chipman, B. Hales, G. Friederich, F. Chavez, C. Sabine, A. Watson, D. C. E. Bakker, U. Schuster, N. Metzl, H. Yoshikawa-Inoue, M. Ishii, T. Midorikawa, Y. Nojiri, A. Körtzinger, T. Steinhoff, M. Hoppema, J. Olafsson, T. S. Arnarson, B. Tilbrook, T. Johannessen, A. Olsen, R. Bellerby, C. S. Wong, B. Delille, N. R. Bates, and H. J. W. de Baar (2009), Climatological mean and decadal change in surface ocean pCO2, and net sea-air CO2 flux over the global oceans, *Deep Sea Research Part II: Topical Studies in Oceanography*, 56(8-10), 554-577.

Tans, P. P., I. Y. Fung, and T. Takahashi (1990), Observational constraints on the global atmospheric CO$_2$ budget, *Science*, 247, 1431 – 1438.

Thomas, V. M., J. A. Bedford, and R. J. Cicerone (1997), Bromine emissions from leaded gasoline, *Geophys. Res. Lett.*, 24(11), 1371-1374, doi: 10.1029/97gl01243.

Tilbrook, B. D., and D. M. Karl (1995), Methane sources, distributions and sinks from California coastal waters to the oligotrophic North Pacific Gyre, *Mar. Chem.*, 49(1), 51-64.

Tokarczyk, R., and E. S. Saltzman (2001), Methyl bromide loss rates in surface waters of the North Atlantic Ocean, Caribbean Sea, and eastern Pacific Ocean (8°-45°N), *J. Geophys. Res.*, 106(D9), 9843-9851.

Tokarczyk, R., K. D. Goodwin, and E. S. Saltzman (2001), Methyl bromide loss rate constants in the north Pacific Ocean, *Geophys. Res. Lett.*, 28(23), 4429-4432.

Tokarczyk, R., K. D. Goodwin, and E. S. Saltzman (2003b), Methyl chloride and methyl bromide degradation in the Southern Ocean, *Geophys. Res. Lett.*, 30(15), 1808, doi:10.1029/2003GL017459.

Tokarczyk, R., E. S. Saltzman, R. M. Moore, and S. A. Yvon-Lewis (2003a), Biological degradation of methyl chloride in coastal seawater, *Global Biogeochem. Cycles*, 17(2), 1057, doi:10.1029/2002GB001949.

United Nations Environment Programme (UNEP) (2007), 2006 Report of the Methyl Bromide Technical Options Committee 2006 Assessment, coordinated by M. Pizano, I. Porter, M. Marcotte, M. Besri, and J. Banks, Naribi, Kenya.

Valentine, D. L., J. D. Kessler, M. C. Redmond, S. D. Mendes, M. B. Heintz, C. Farwell, L. Hu, F. S. Kinnaman, S. A. Yvon-Lewis, M. Du, E. W. Chan, F. G. Tigreros and C. J. Villanueva (2010), Propane Respiration Jump-Starts Microbial Response to a Deep Oil Spill, *Science*, 330(6001), 208 - 211, doi: 10.1126/science.1196830.

van der Werf, G. R., J. T. Randerson, L. Giglio, G. J. Collatz, M. Mu, P. S. Kasibhatla, D. C. Morton, R. S. DeFries, Y. Jin, and T. T. van Leeuwen (2010), Global fire emissions and the contribution of deforestation, savanna, forest, agricultural, and peat fires (1997–2009), *Atmos. Chem. Phys.*, 10(23), 11707-11735, doi:10.5194/acp-10-11707-2010.

Varner, R. K., P. M. Crill, and R. W. Talbot (1999a), Wetlands: A potentially significant source of atmospheric methyl bromide and methyl chloride, *Geophys. Res. Lett.*, 26(16), 2433-2435, doi:10.1029/1999gl900587.

Varner, R. K., P. M. Crill, R. W. Talbot, and J. H. Shorter (1999b), An estimate of the uptake of atmospheric methyl bromide by agricultural soils, *Geophys. Res. Lett.*, 26(6), 727-730, doi:10.1029/1999gl900071.

Vernet, M., B. G. Mitchell, E. Sakshaug, G. Johnsen, R. Iturriaga, and P. Wassmann (1996), Evidence for a novel pigment with in vivo absorption maximum at 708 nm associated with Phaeocystis cf pouchetii blooms, *Mar. Ecol. Prog. Ser.*, 133(1-3), 253-262.

Wanninkhof, R. (1992), Relationship between wind speed and gas exchange over the ocean, *J. Geophys. Res.*, 97(C5), 7373-7382.

Warner, M. J., and R. F. Weiss (1985), Solubilities of chlorofluorocarbons 11 and 12 in water and seawater, *Deep Sea Research Part A. Oceanographic Research Papers*, 32(12), 1485-1497.

Warwick, N., J. Pyle, and D. Shallcross (2006), Global Modelling of the Atmospheric Methyl Bromide Budget, *J. Atmos. Chem.*, 54(2), 133-159, doi:10.1007/s10874-006-9020-3.

Watling, R., and D. B. Harper (1998), Chloromethane production by wood-rotting fungi and an estimate of the global flux to the atmosphere, *Mycol. Res.*, 102(7), 769-787.

Weiss, R. F. (1970), The solubility of nitrogen, oxygen and argon in water and seawater, *Deep-Sea Res.*, 17(4), 721-735.

Weiss, R. F., and B. A. Price (1980), Nitrous oxide solubility in water and seawater, *Mar. Chem.*, 8(4), 347-359.

Welschmeyer, N. A., and C. J. Lorenzen (1985), Chlorophyll Budgets - Zooplankton Grazing and Phytoplankton Growth in a Temperate Fjord and the Central Pacific Gyres, *Limnol. Oceanogr.*, 30(1), 1-21.

World Meteorological Organization (WMO) (2003), Scientific assessment of ozone depletion: 2002, Global Ozone Research and Monitoring Project - Report No. 44.

World Meteorological Organization (WMO) (2007), Scientific Assessment of Ozone Depletion: 2006, Global Ozone Research and Monitoring Project - Report No. 50.

World Meteorological Organization (WMO) (2011), Scientific Assessment of Ozone Depletion: 2010, Global Ozone Research and Monitoring Project - Report No. 52.

Wright, S. W., S. W. Jeffrey, R. F. C. Mantoura, C. A. Llewellyn, T. Bjoernland, D. Repeta, and N. Welschmeyer (1991), Improved HPLC method for the analysis of chlorophylls and carotenoids from marine phytoplankton, *Mar. Ecol. Prog. Ser.*, 77, 183-196.

Wuebbles, D. J., and K. Hayhoe (2002), Atmospheric methane and global change, *Earth-Science Reviews*, 57(3-4), 177-210.

Xiao, X., R. G. Prinn, P. G. Simmonds, L. P. Steele, P. C. Novelli, J. Huang, R. L. Langenfelds, S. O'Doherty, P. B. Krummel, P. J. Fraser, L. W. Porter, R. F. Weiss, P. Salameh, and R. H. J. Wang (2007), Optimal estimation of the soil uptake rate of molecular hydrogen from the Advanced Global Atmospheric Gases Experiment and other measurements, *J. Geophys. Res.*, 112, D07303, doi:10.1029/2006JD007241.

Yagi, K., J. Williams, N.-Y. Wang, and R. J. Cicerone (1995), Atmospheric Methyl Bromide (CH3Br) from Agricultural Soil Fumigations, *Science*, 267(5206), 1979-1981, doi:10.1126/science.267.5206.1979.

Yevich, R., and J. A. Logan (2003), An assessment of biofuel use and burning of agricultural waste in the developing world, *Global Biogeochem. Cycles*, 17, doi: 10.1029/2002gb001952.

Yokouchi, Y., M. Ikeda, Y. Inuzuka, and T. Yukawa (2002), Strong emission of methyl chloride from tropical plants, *Nature*, 416(6877), 163-165.

Yokouchi, Y., T. Saito, C. Ishigaki, and M. Aramoto (2007), Identification of methyl chloride-emitting plants and atmospheric measurements on a subtropical island, *Chemosphere*, 69(4), 549-553.

Yoshida, Y., Y. Wang, T. Zeng, and R. Yantosca (2004), A three-dimensional global model study of atmospheric methyl chloride budget and distributions, *J. Geophys. Res.*, 109, D24309, doi:10.1029/2004JD004951.

Yvon, S. A., and J. H. Butler (1996), An improved estimate of the oceanic lifetime of atmospheric CH_3Br, *Geophys. Res. Lett.*, 23(1), 53-56.

Yvon-Lewis, S. A., and J. H. Butler (1997), The potential effect of oceanic biological degradation on the lifetime of atmospheric CH_3Br, *Geophys. Res. Lett.*, 24(10), 1227-1230.

Yvon-Lewis, S. A., and J. H. Butler (2002), Effect of oceanic uptake on atmospheric lifetimes of selected trace gases, *J. Geophys. Res.*, 107(D20), 4414, doi:4410.1029/2001JD001267.

Yvon-Lewis, S. A., L. Hu, and J. Kessler (2011), Methane flux to the atmosphere from the Deepwater Horizon oil disaster, *Geophys. Res. Lett.*, 38, L01602, doi:01610.01029/02010GL045928.

Yvon-Lewis, S. A., D. B. King, R. Tokarczyk, K. D. Goodwin, E. S. Saltzman, and J. H. Butler (2004), Methyl bromide and methyl chloride in the Southern Ocean, *J. Geophys. Res.*, 109(C02008), doi:10.1029/2003JC001809.

Yvon-Lewis, S. A., E. S. Saltzman, and S. A. Montzka (2009), Recent trends in atmospheric methyl bromide: analysis of post-Montreal Protocol variability, *Atmos. Chem. Phys.*, 9(16), 5963-5974.

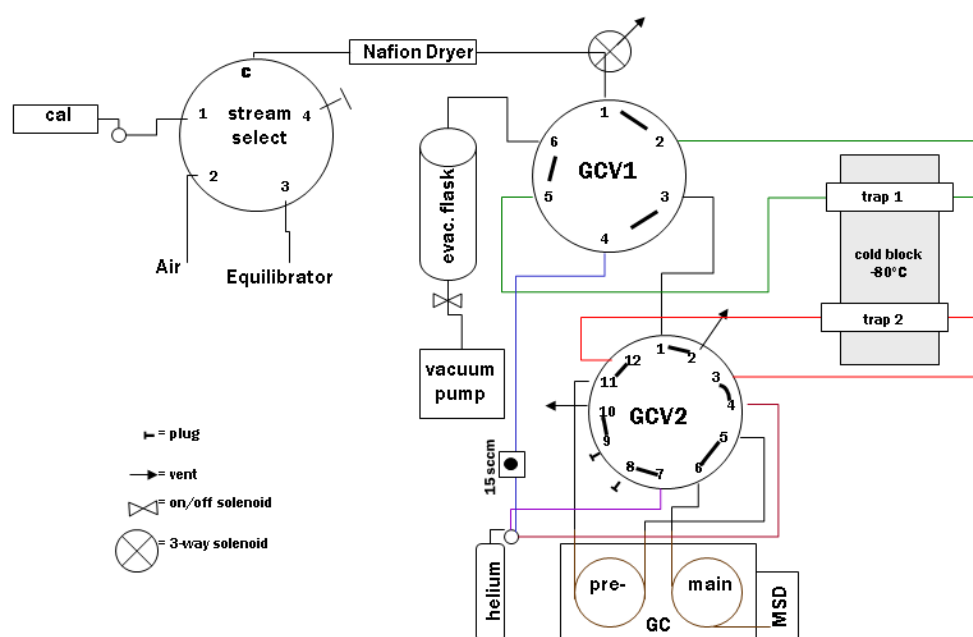**APPENDIX A**

THE ANALYTICAL SYSTEM FOR AIR AND SURFACE SEAWATER

MEASUREMENTS FOR HALOCARBONS DURING GOMECC

Concentrations of 26 halocarbon compounds (CH_3Cl, CH_3Br, HCFC-22, CFC-12, HCFC-142, C_2H_5Cl, H-1211, CFC-11, C_5H_8, DMS, CH_3I, CH_3NO_3, CFC-113, CH_2BrCl, $CHCl_3$, $CH_3CH_2NO_3$, CH_3CCl_3, CCl_4, i-$C_3H_7NO_3$, n-$C_3H_7NO_3$, CH_2Br_2, C_2HCl_3, $CHBrCl_2$, $CHClBr_2$, $CHBr_3$, and C_2Cl_4) in the air and surface seawater were measured with an automated gas chromatograph (Agilent 6890N) and mass spectrometer (Agilent 5973N) (GC-MS) equipped with a "Weiss"-type equilibrator (20 L). Air samples were pumped continuously at ~ 6 L min^{-1} through 0.63 cm ID Synflex tubing (Motion Industries, TX). Surface seawater was continuously flowing through the equilibrator at 15 L min^{-1}. The ratio of the headspace and seawater volumes was about 2:1. Gases in surface seawater were constantly equilibrating with gases in the equilibrator headspace for ~ 80 min. Air or gas in the equilibrator was alternately sampled to our analytical system through a nafion drier (Figure A1). The collected gas sample passed through a Unibeads 1S packed trap (3.175 mm OD, 1.6 mm ID) (Trap 1) at -80 ºC and into a calibrated, evacuated stainless steel flask (3 L) (Figure A1). Halocarbon compounds were trapped in the Unibeads 1S packed trap. The change in flask pressure and the flask temperature were recorded electronically. The pressure in the flask was used to determine the exact volume of the whole air sample that was collected. After GC valve #1 (GCV1) was switched from "load" to "transfer", the primary trap

(trap 1) would be flash heated at 200 ºC for 3 min, which allowed the sample to be focused in the second Unibeads 1S packed trap (1.59 mm OD, 0.5 mm ID) (trap 2) at -80 ºC. When GC valve #2 (GCV2) was switched from "backflush" to "inject", the second trap was flash heated at 200 ºC for 3 min and the sample was then injected into the GC column (0.25 mm ID x 5 m pre- and 55 m main, DB-VRX; J&W). The pre-column (4 m) was backflushed at 10 min after injection to prevent the entry of heavier compounds into the main column (56 m). The temperature of the GC was programmed with settings shown in Table A1 and the head pressure of the carrier gas (He) for the GC column was set to 24.5 psi.

Table A1. Temperature program in the halocarbon GC instrument.

	Ramp Rate (^{o}C min^{-1})	Temperature (^{o}C)	Hold (min)
Step 1	-	30	5
Step 2	35	100	3
Step 3	45	220	7

Figure A1. Schematic diagram of the automated analytical system for air and surface seawater measurements for halocarbons.
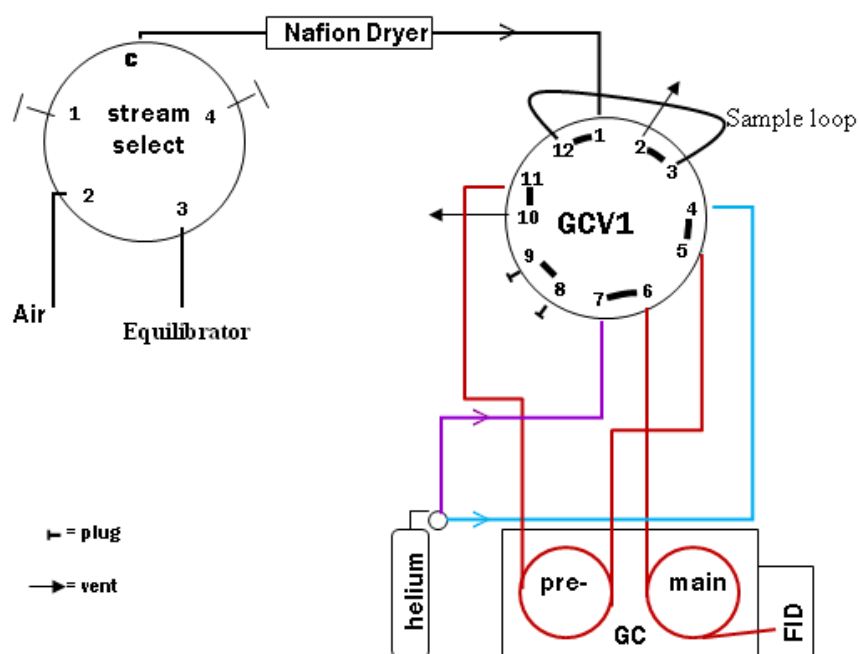
APPENDIX B

THE ANALYTICAL SYSTEM FOR AIR AND SURFACE SEAWATER

CONCENTRATION MEASUREMENTS FOR HYDROCARBONS DURING

HYFLUX

Concentrations of C_1 - C_3 hydrocarbons in the air and surface seawater were measured with an automated gas chromatograph and flame ionization detector (GC/FID, Agilent 6850) equipped with a "Weiss"-type equilibrator (20 L). Air samples were pumped continuously at $\sim$ 6 L min^{-1} through 0.63 cm ID Synflex tubing (Motion Industries, TX). Surface seawater was continuously flowing through the equilibrator at 15 L min^{-1}. The ratio of the headspace and seawater volumes was about 2:1. Air or gas in the equilibrator was alternately sampled to our analytical system every 6 minutes with a stream select valve. The sample stream passed through a 20 μL sampling loop after being dehumidified by a Nafion dryer (Permapure Inc) (Figure B1). The Nafion dryer and the 20 μL sampling loop were flushed with the sample air at a rate of 25 mL min^{-1} for 90 seconds before injection into the GC/FID, which was equipped with a 15 m long, 32 μm ID GS-GasPro column (1 m pre-column and 14 m main-column) with nitrogen carrier gas. The temperature of the GC oven was programmed (Table B1) and the head pressure of the GC column was set at 6.5 psi.

Table B1. Temperature program in the hydrocarbon GC instrument.

	Ramp Rate (^{o}C min^{-1})	Temperature (^{o}C)	Hold (min)
Step 1	-	40	1
Step 2	40	80	1

Figure B1. Schematic diagram of the automated analytical system for air and surface seawater concentration measurements for hydrocarbons.

APPENDIX C

THE COMBINED ANALYTICAL SYSTEM FOR AIR AND SURFACE

SEAWATER CONCENTRATION MEASUREMENTS FOR HALOCARBONS

AND HYDROCARBONS DURING HALOCAST

The analytical system used during HalocAST is a combined system according to the analytical systems described in Appendices A and B. Concentrations of 20 halocarbon compounds (CH_3Cl, CH_3Br, HCFC-22, CFC-12, HCFC-142, C_2H_5Cl, H-1211, CFC-11, CH_3I, CFC-113, CH_2BrCl, $CHCl_3$, CH_3CCl_3, CCl_4, CH_2Br_2, C_2HCl_3, $CHBrCl_2$, $CHClBr_2$, $CHBr_3$, and C_2Cl_4) along with methane in the air and surface seawater were measured with an automated GC- (MS/FID) system (the model of GC/FID: Agilent 6850; the model of MS: Agilent 5975) equipped with a "Weiss"-type equilibrator (20 L) (Figure C1). Air samples were pumped continuously at ~ 6 L min^{-1} through 0.63 cm ID Synflex tubing (Motion Industries, TX). Surface seawater was continuously flowing through the equilibrator at 15 L min^{-1}. The ratio of the headspace and seawater volumes was about 2:1. Air and gas in the equilibrator were alternately sampled to our analytical system every ~ 40 minutes using a stream select valve. The sample stream passed through a Nafion dryer and a 20 μL sampling loop (Figure C1). Halocarbons were then trapped in the cryotraps at - 80 ^{o}C whereas the gas sample in the 20 μL sampling loop was injected into the GC/FID. The temperature program of the GC oven was optimized for methane analysis after injecting the 20 μL sample to the GC/FID. The settings for the GC oven, the head pressure of the carrier gas (N_2) and the

lengths of pre- and main columns (GS-GasPro column) were described in Appendix B. Once the methane run was completed and the temperature of the GC oven dropped to 35 ^{o}C, halocarbons in the sample were focused at trap 2. By heating up trap 2 to 200 ^{o}C and turning GC valve #3 (GCV3) from "backflash" to "inject", halocarbons were injected into the narrow bore DB-VRX column (I.D. 0.18 mm; length: 40 m (pre-column: 3 m; main column: 27 m); film: 1.0 μm). Head pressure of the carrier gas (He) was set to 34 psi and the temperature program of the GC oven was shown in Table C1. GCV3 was switched to "backflush" in 12 min after halocarbons were injected into the GC.

Table C1. Temperature program for the halocarbon analysis in the combined halocarbon

and hydrocarbon instrument.

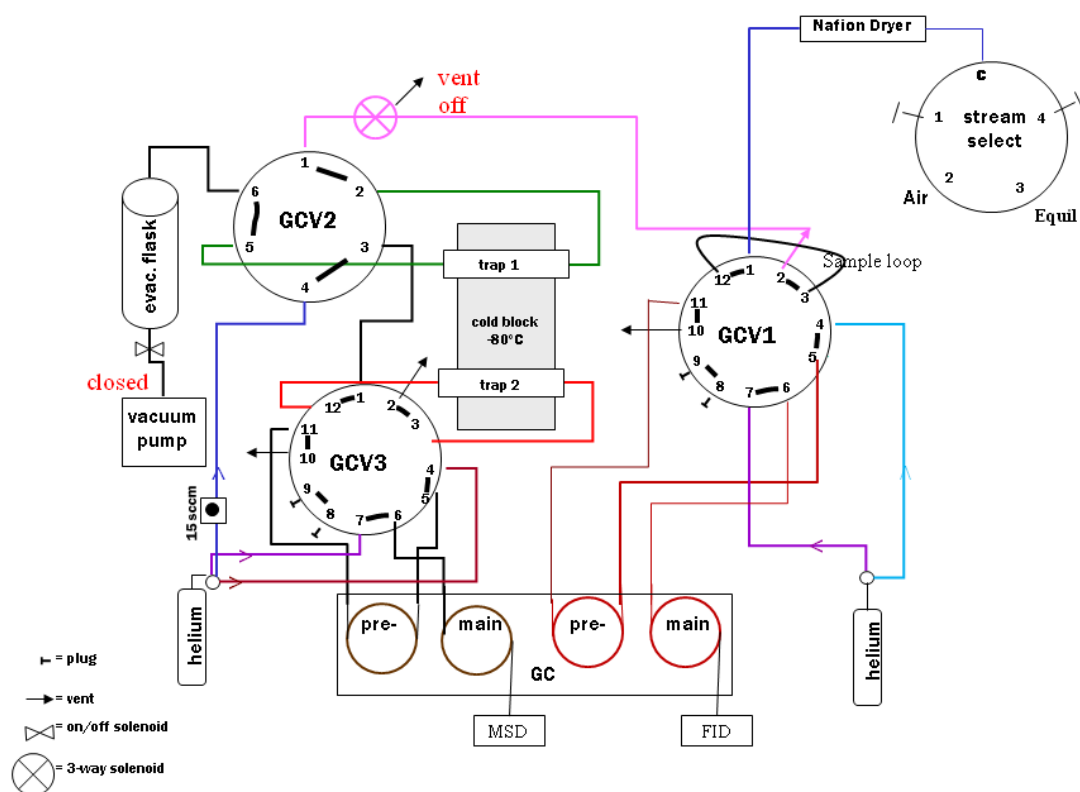|	Ramp Rate (^{o}C min^{-1})	Temperature (^{o}C)	Hold (min)
Step 1	-	35	4.7
Step 2	35	100	3
Step 3	30	220	7

Figure C1. Schematic diagram of the analytical system for air and surface seawater

concentration analysis for both hydrocarbons and halocarbons.

APPENDIX D

THE ANALYTICAL SYSTEM FOR HALOCARBON DEPTH-PROFILE

MEASUREMENTS

Depth profile samples were collected from Niskin bottles with 100 mL ground glass syringes and loaded to volume calibrated bulbs connected to purge valve #2 (PV2) (a Valco loop selection valve (VICI Metronics, TX) with 34 ports and 16 positions) (Figure D1). All the water samples were stored in the bulbs at 5 ^{o}C until they were analyzed within 12 hours. When PV2 was switched from "load" to "inject", humidified helium or nitrogen would push the water sample into a sparger at 144 ml min^{-1} (Figure D1). Gases in the water sample were carried by helium or nitrogen into the primary trap (trap 1) through purge valves (PV3 and PV1) and two nafion driers (Figure D1). The second part of this system is the same as the surface saturation-anomaly instrument described in Appendix A.
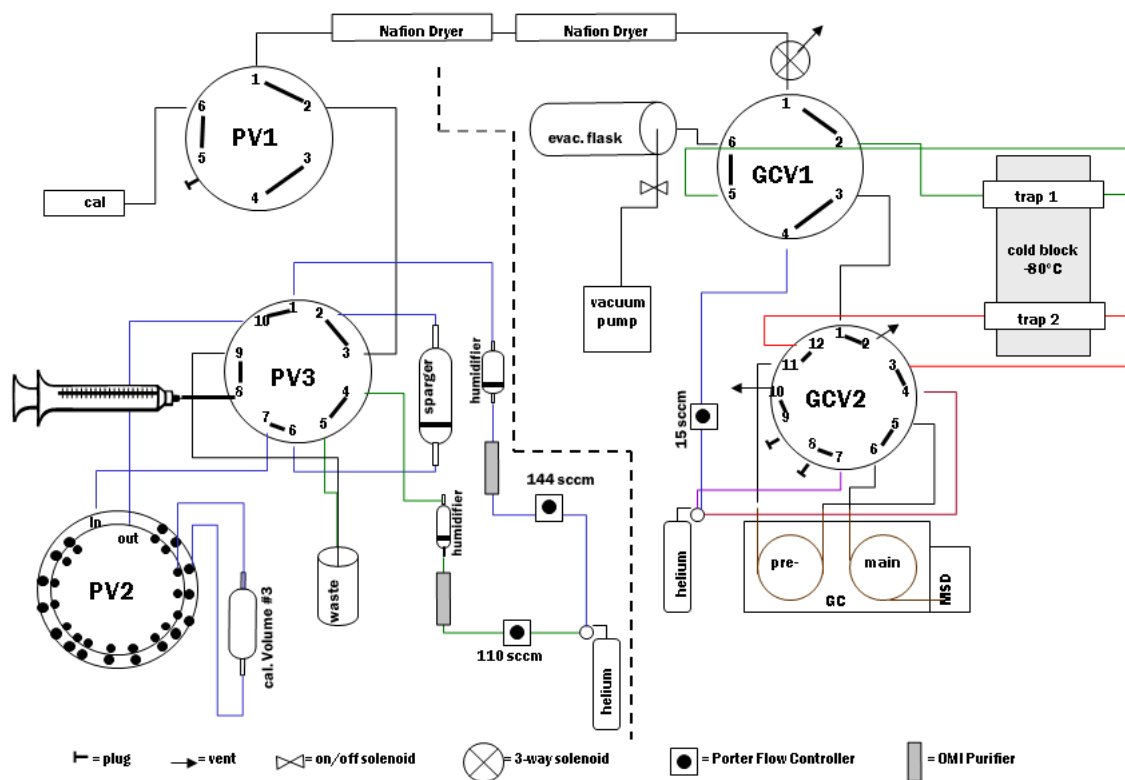
Figure D1. Schematic diagram of the halocarbon depth-profile instrument.

APPENDIX E

THE ANALYTICAL SYSTEM FOR ^{13}C-LABELED METHYL BROMIDE

CONCENTRATION MEASUREMENTS

Biological degradation rate constant measurements of CH_3Br with a stable isotope incubation technique (Section 3) involve periodically monitoring $^{13}CH_3Br$ concentration in incubated seawater samples. Analysis of $^{13}CH_3Br$ concentration in seawater samples was conducted with an analytical system shown in Figure E1, which was modified based on the depth-profile instrument (Figure D1). About 25 ml of incubated seawater was loaded into a volume calibrated bulb. The seawater sample was then pushed into a sparger along with 10 μL known concentration of CD_3Br (25 ppm) at 144 ml min^{-1}. $^{13}CH_3Br$ and CD_3Br were purged by N_2 into the cryotrap and GC-MS system described in Appendices A, C and D.

Concentrations of $^{13}CH_3Br$ were determined by signals of masses (m/z) 97 and 99 [e.g., *Tokarczyk and Saltzman*, 2001]. The signal of mass 97 was derived from both $^{13}CH_3{}^{81}Br$ and $CD_3{}^{79}Br$ whereas mass 99 was entirely contributed by $CD_3{}^{81}Br$. Since CD_3Br was used as an internal standard, the CD_3Br 97/99 remained constant among different runs. However, the concentration of $^{13}CH_3Br$ kept decreasing during the incubation due to the chemical and biological degradation, resulting in a decline in the ratio of peak areas of 97/99. Using the ratio of peak areas of 97/99 and the known concentration of CD_3Br, we can calculate the concentration of $^{13}CH_3Br$ for each run. The

precision of $^{13}CH_3Br$ concentration measurements, 0.3 %, was determined by multiple injections from aliquants of MilliQ water spiked with $^{13}CH_3Br$.

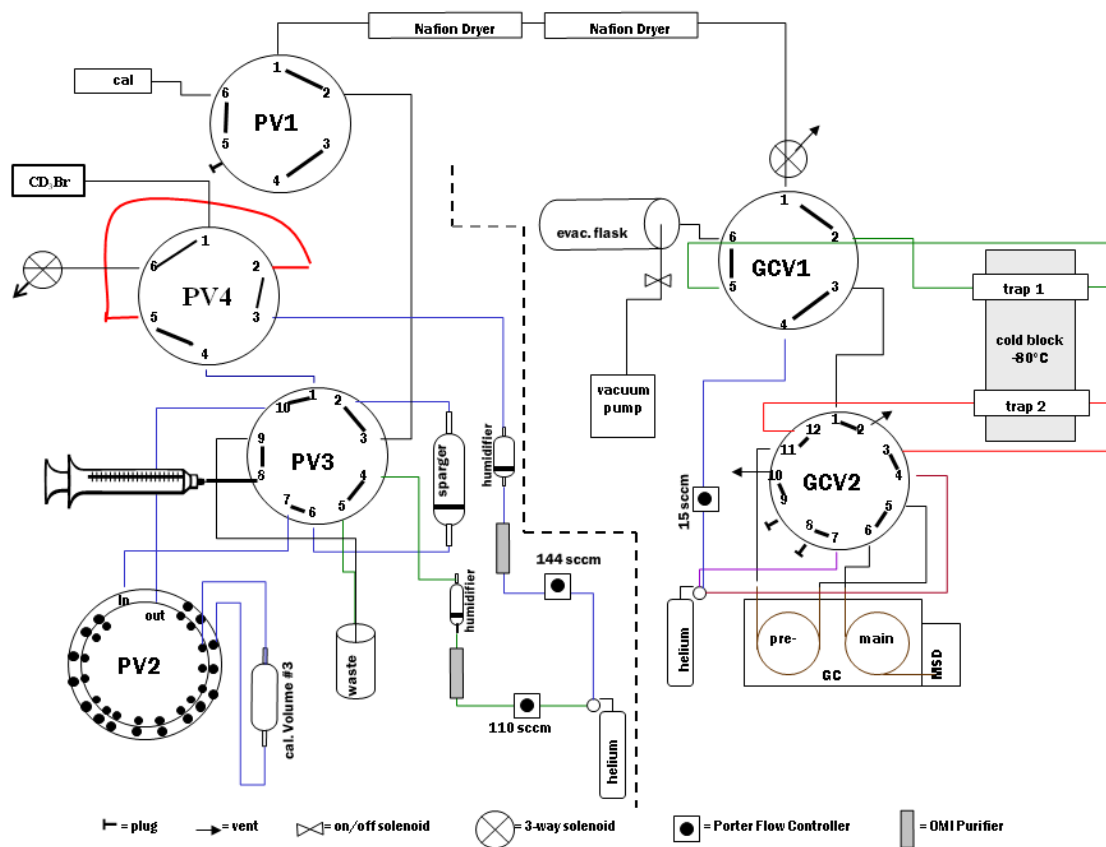**Figure E1.** Schematic diagram of the instrumentation for $^{13}CH_3Br$ concentration measurements.

VITA

Name: Lei Hu

Address: Department of Oceanography, Texas A&M University, 3146 TAMU, College Station, TX 77843

Email Address: leihutx@gmail.com

Education: B.A., Chemistry, Ocean University of China, 2007

Ph.D., Oceanography, Texas A&M University, 2012

Selected Peer-Reviewed Publications:

Hu, L., S. A. Yvon-Lewis, J. H. Butler, J. M. Lobert and D. B. King (submitted), An improved oceanic budget of methyl chloride, *J. Geophys. Res.*

Hu, L., S. A. Yvon-Lewis, Y. Liu, and T. S. Bianchi (submitted), The ocean in near equilibrium with atmospheric methyl bromide, *Global Biogeochem. Cycles*.

Hu, L., S. A. Yvon-Lewis, J. D. Kessler, and I. R. MacDonald (2012), Methane fluxes to the atmosphere from deepwater hydrocarbon seeps in the northern Gulf of Mexico, *J. Geophys. Res.*, 117, C01009, doi:10.1029/2011JC007208.

Hu, L., S. A. Yvon-Lewis, Y. Liu, J. E. Salisbury, and J. E. O'Hern (2010), Coastal emissions of methyl bromide and methyl chloride along the eastern Gulf of Mexico and the east coast of the United States, *Global Biogeochem. Cycles*, 24, GB1007, doi:10.1029/2009GB003514.

Valentine, D. L., J. D. Kessler, M. C. Redmond, S. D. Mendes, M. B. Heintz, C. Farwell, L. Hu, F. S. Kinnaman, S. A. Yvon-Lewis, M. Du, E. W. Chan, F. Garcia Tigreros, and C. J. Villanueva (2010), Propane respiration jump-starts microbial response to a deep oil spill, *Science*, 330, 208, doi: 10.1126/science.1196830.

Yvon-Lewis, S. A., L. Hu, and J. Kessler (2010), Methane flux to the atmosphere from the Deepwater Horizon oil disaster, *Geophs. Res. Lett.*, 38, L01602, doi: 10.1029/2010GL045928.